NUREG/CR-4667, Vol. 27
ANL-99/11

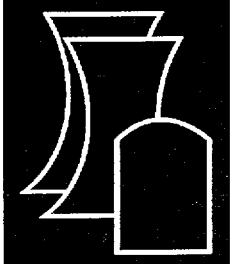

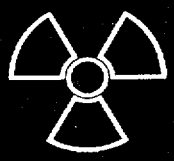

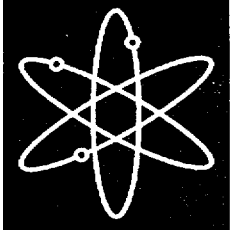

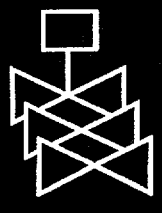

Environmentally Assisted Cracking in Light Water Reactors

Semiannual Report
July 1998 – December 1998

Argonne National Laboratory

U.S. Nuclear Regulatory Commission
Office of Nuclear Regulatory Research
Washington, DC 20555-0001

AVAILABILITY NOTICE

Availability of Reference Materials Cited in NRC Publications

NRC publications in the NUREG series, NRC regulations, and *Title 10, Energy,* of the *Code of Federal Regulations,* may be purchased from one of the following sources:

1. The Superintendent of Documents
   U.S. Government Printing Office
   P.O. Box 37082
   Washington, DC 20402–9328
   <http://www.access.gpo.gov/su_docs>
   202–512–1800

2. The National Technical Information Service
   Springfield, VA 22161–0002
   <http://www.ntis.gov/ordernow>
   703–487–4650

The NUREG series comprises (1) brochures (NUREG/BR-XXXX), (2) proceedings of conferences (NUREG/CP-XXXX), (3) reports resulting from international agreements (NUREG/IA-XXXX), (4) technical and administrative reports and books [(NUREG-XXXX) or (NUREG/CR-XXXX)], and (5) compilations of legal decisions and orders of the Commission and Atomic and Safety Licensing Boards and of Office Directors' decisions under Section 2.206 of NRC's regulations (NUREG-XXXX).

A single copy of each NRC draft report is available free, to the extent of supply, upon written request as follows:

Address: Office of the Chief Information Officer
Reproduction and Distribution
Services Section
U.S. Nuclear Regulatory Commission
Washington, DC 20555–0001
E–mail: <DISTRIBUTION@nrc.gov>
Facsimile: 301–415–2289

A portion of NRC regulatory and technical information is available at NRC's World Wide Web site:

<http://www.nrc.gov>

All NRC documents released to the public are available for inspection or copying for a fee, in paper, microfiche, or, in some cases, diskette, from the Public Document Room (PDR):

NRC Public Document Room
2120 L Street, N.W., Lower Level
Washington, DC 20555–0001
<http://www.nrc.gov/NRC/PDR/pdr1.htm>
1–800–397–4209 or locally 202–634–3273

Microfiche of most NRC documents made publicly available since January 1981 may be found in the Local Public Document Rooms (LPDRs) located in the vicinity of nuclear power plants. The locations of the LPDRs may be obtained from the PDR (see previous paragraph) or through:

<http://www.nrc.gov/NRC/NUREGS/SR1350/V9/lpdr/html>

Publicly released documents include, to name a few, NUREG-series reports; *Federal Register* notices; applicant, licensee, and vendor documents and correspondence; NRC correspondence and internal memoranda; bulletins and information notices; inspection and investigation reports; licensee event reports; and Commission papers and their attachments.

Documents available from public and special technical libraries include all open literature items, such as books, journal articles, and transactions, *Federal Register* notices, Federal and State legislation, and congressional reports. Such documents as theses, dissertations, foreign reports and translations, and non-NRC conference proceedings may be purchased from their sponsoring organization.

Copies of industry codes and standards used in a substantive manner in the NRC regulatory process are maintained at the NRC Library, Two White Flint North, 11545 Rockville Pike, Rockville, MD 20852–2738. These standards are available in the library for reference use by the public. Codes and standards are usually copyrighted and may be purchased from the originating organization or, if they are American National Standards, from—

American National Standards Institute
11 West 42nd Street
New York, NY 10036–8002
<http://www.ansi.org>
212–642–4900

NUREG/CR-4667, Vol. 27
ANL-99/11

Environmentally Assisted Cracking in Light Water Reactors

Semiannual Report
July 1998 – December 1998

Manuscript Completed: October 1999
Date Published: October 1999

Prepared by
O.K. Chopra, H.M. Chung, E.E. Gruber,
T.F. Kassner, W.E. Ruther, W.J. Shack,
J.L. Smith, W.K. Soppet, R.V. Strain

Argonne National Laboratory
9700 South Cass Avenue
Argonne, IL 60439

M.B. McNeil, NRC Project Manager

Prepared for
Division of Engineering Technology
Office of Nuclear Regulatory Research
U.S. Nuclear Regulatory Commission
Washington, DC 20555-0001
NRC Job Code W6610

Previous Documents in Series

Environmentally Assisted Cracking in Light Water Reactors Semiannual Report
April—September 1985, NUREG/CR-4667 Vol. I, ANL-86-31 (June 1986).
October 1985—March 1986, NUREG/CR-4667 Vol. II, ANL-86-37 (September 1987).
April—September 1986, NUREG/CR-4667 Vol. III, ANL-87-37 (September 1987).
October 1986—March 1987, NUREG/CR-4667 Vol. IV, ANL-87-41 (December 1987).
April—September 1987, NUREG/CR-4667 Vol. V, ANL-88-32 (June 1988).
October 1987—March 1988, NUREG/CR-4667 Vol. 6, ANL-89/10 (August 1989).
April—September 1988, NUREG/CR-4667 Vol. 7, ANL-89/40 (March 1990).
October 1988—March 1989, NUREG/CR-4667 Vol. 8, ANL-90/4 (June 1990).
April—September 1989, NUREG/CR-4667 Vol. 9, ANL-90/48 (March 1991).
October 1989—March 1990, NUREG/CR-4667 Vol. 10, ANL-91/5 (March 1991).
April—September 1990, NUREG/CR-4667 Vol. 11, ANL-91/9 (May 1991).
October 1990—March 1991, NUREG/CR-4667 Vol. 12, ANL-91/24 (August 1991).
April—September 1991, NUREG/CR-4667 Vol. 13, ANL-92/6 (March 1992).
October 1991—March 1992, NUREG/CR-4667 Vol. 14, ANL-92/30 (August 1992).
April—September 1992, NUREG/CR-4667 Vol. 15, ANL-93/2 (June 1993).
October 1992—March 1993, NUREG/CR-4667 Vol. 16, ANL-93/27 (September 1993).
April—September 1993, NUREG/CR-4667 Vol. 17, ANL-94/26 (June 1994).
October 1993—March 1994, NUREG/CR-4667 Vol. 18, ANL-95/2 (March 1995).
April—September 1994, NUREG/CR-4667 Vol. 19, ANL-95/25 (September 1995).
October 1994—March 1995, NUREG/CR-4667 Vol. 20, ANL-95/41 (January 1996).
April—December 1995, NUREG/CR-4667 Vol. 21, ANL-96/1 (July 1996).
January 1996—June 1996, NUREG/CR-4667 Vol. 22, ANL-97/9 (June 1997).
July 1996—December 1996, NUREG/CR-4667 Vol. 23, ANL-97/10 (October 1997).
January 1997—June 1997, NUREG/CR-4667 Vol. 24, ANL-98/6 (April 1998).
July 1997—December 1997, NUREG/CR-4667 Vol. 25, ANL-98/18 (September 1998).
January 1998—June 1998, NUREG/CR-4667 Vol. 26, ANL-98/30 (December 1998).

Environmentally Assisted Cracking in Light Water Reactors Semiannual Report July 1998–December 1998

by

O. K. Chopra, H. M. Chung, E. E. Gruber, T. F. Kassner,
W. E. Ruther, W. J. Shack, J. L. Smith, W. K. Soppet, and R. V. Strain

Abstract

This report summarizes work performed by Argonne National Laboratory on fatigue and environmentally assisted cracking (EAC) in light water reactors from July 1998 to December 1998. Topics that have been investigated include (a) environmental effects on fatigue S–N behavior of primary pressure boundary materials, (b) irradiation–assisted stress corrosion cracking of austenitic stainless steels (SSs), and (c) EAC of Alloys 600 and 690. Fatigue tests have been conducted to determine the crack initiation and crack growth characteristics of austenitic SSs in LWR environments. Procedures are presented for incorporating the effects of reactor coolant environments on the fatigue life of pressure vessel and piping steels. Slow-strain-rate tensile tests and posttest fractographic analyses were conducted on several model SS alloys irradiated to ≈0.3 and 0.9 x 10^{21} n·cm^{-2} (E > 1 MeV) in helium at 289°C in the Halden reactor. The results have been used to determine the influence of alloying and impurity elements on the susceptibility of these steels to irradiation–assisted stress corrosion cracking. Fracture toughness J–R curve tests were also conducted on two heats of Type 304 SS that were irradiated to ≈0.3 x 10^{21} n·cm^{-2} in the Halden reactor. Crack–growth–rate tests have been conducted on compact–tension specimens of Alloys 600 and 690 under constant load to evaluate the resistance of these alloys to stress corrosion cracking in LWR environments.

Contents

Figures

Tables

Executive Summary

Environmental Effects on Fatigue Strain-versus-Life (S–N) Behavior of Primary Pressure Boundary Materials

The ASME Boiler and Pressure Vessel Code provides rules for the construction of nuclear power plant components. Appendix I to Section III of the Code specifies design fatigue curves for structural materials. However, the effects of light water reactor (LWR) coolant environments are not explicitly addressed by the Code design curves. Recent test data illustrate potentially significant effects of LWR environments on the fatigue resistance of carbon and low–alloy steels and austenitic stainless steels (SSs). Under certain loading and environmental conditions, fatigue lives of carbon and low–alloy steels can be a factor of ≈70 lower in an LWR environment than in air. These results raise the issue of whether the design fatigue curves in Section III are appropriate for the intended purpose.

To establish the effects of various material, loading, and environmental parameters on the fatigue lives of carbon and low–alloy steels and austenitic SSs, existing fatigue S–N data have been analyzed and summarized. Two approaches have been proposed for incorporating the effects of LWR environments into ASME Section III fatigue evaluations: (a) develop new design fatigue curves for LWR applications, and (b) use a fatigue life correction factor to account for environmental effects. The latter is referred as F_{en} method. Both methods of evaluating fatigue lives are based on statistical models that have been developed at Argonne National Laboratory for estimating fatigue lives of carbon and low–alloy steels and austenitic SSs in LWR environments. The environmentally adjusted design fatigue curves provide allowable cycles for fatigue crack initiation in LWR coolant environments. The design curves for carbon and low–alloy steels, as well as those for austenitic SSs maintain the margin of 20 on life provided in the ASME Code design fatigue curves. However, to be consistent with the current ASME Code curves, the margin on stress is 2 for carbon and low–alloy steels and 1.5 for austenitic SSs.

In the F_{en} method, environmental effects on life are estimated from the statistical models but the correction is applied to fatigue lives estimated from the current Code design curves. Therefore, estimates of fatigue lives that are based on the two methods may differ because of differences in the ASME mean curve and the best-fit curve to existing fatigue data. The existing fatigue S–N data indicate that the current Code design curve for carbon steels (CSs) is comparable to the statistical–model curve for low–alloy steels (LASs), but it is somewhat conservative at stress levels <500 Mpa, when compared with the statistical–model curve for CSs. Consequently, usage factors based on the F_{en} method would be comparable to those based on the environmentally adjusted design fatigue curves for LASs and would be somewhat higher for CSs.

For austenitic SSs, the ASME mean curve and consequently the current Code design fatigue curve are nonconservative in air when compared with the statistical–model curve and a corresponding design curve, i.e., it predicts longer fatigue lives than the best-fit curve to the existing S–N data. Consequently, before adjusting for the conservatism in the design curves, usage factors that are based on the F_{en} method would be lower than those determined from design fatigue curves based on the Argonne results.

Fatigue tests have also been conducted to determine the crack initiation and crack growth characteristics of austenitic SSs in air and LWR environments. Results of fatigue tests that examine the influence of reactor environment on the formation and growth of short cracks in Type 304 SS are presented. Crack lengths as a function of fatigue cycles were determined in air and water environments. The results indicate that, at the same fraction of life, the crack lengths are longer in water than in air. The crack growth rates (CGRs) in water are greater than those in air, and the CGRs in PWR water are greater than those in high-dissolved oxygen (DO) water. The decrease in fatigue life of austenitic SSs in LWR water is primarily caused by the effects of environment on the growth of short cracks that are <500 μm deep. The results from the present study are not consistent with the slip dissolution model for enhanced CGRs in LWR environments. Oxide film rupture strengths and/or H_2 evolution most likely play a greater role than slip dissolution in these environments.

Irradiation-Assisted Stress Corrosion Cracking of Austenitic Stainless Steels

Slow-strain-rate tensile (SSRT) tests in simulated boiling water reactor (BWR) water (DO ≈8 ppm) were conducted on 16 model austenitic SS alloys that were irradiated at 288°C in He in the Halden boiling heavy-water reactor to a fluence of $\approx 0.3 \times 10^{21}$ n·cm^{-2} (E > 1 MeV) and on nine alloys that were irradiated to a fluence of $\approx 0.9 \times 10^{21}$ n·cm^{-2} (E > 1 MeV). Fractographic analysis by scanning electron microscopy was conducted to determine the susceptibility of these alloys to irradiation-assisted stress corrosion cracking (IASCC), as manifested by the degree of transgranular and intergranular fracture. Heat-to-heat variations in ductility and susceptibilities to intergranular and transgranular stress corrosion cracking (IGSCC and TGSCC) were very significant. This finding suggests that heat-to-heat variation in CGR could also be large.

After irradiation to the lower fluence, a high-purity heat of Type 316L SS with a very low concentration of Si exhibited the highest susceptibility to IGSCC. A Type 304 SS alloy with a high concentration of O exhibited very deleterious effects from water after irradiation and even in the unirradiated state. This observation is consistent with previous studies of an irradiated BWR neutron absorber tubes and core shroud welds which suggested that high O concentration in steels is conducive to greater susceptibility to IGSCC. Susceptibilities to TGSCC of the 16 alloys at $\approx 0.3 \times 10^{21}$ n·cm^{-2} (E > 1 MeV) could be correlated well in terms of N and Si concentrations. All alloys that contained <100 wppm N and <1.0 wt.% Si were susceptible, whereas all alloys that contained >100 wppm N or >1.0 wt.% Si were relatively resistant to TGSCC. Because practically all commercial heats of Type 304 or 304L SSs contain >100 wppm, N this means that, to delay the onset of and increase resistance to IASCC, it is helpful to ensure a certain minimum concentration of Si in steels. Results of initial tests on alloys irradiated to a fluence of $\approx 0.9 \times 10^{21}$ n·cm^{-2} (E > 1 MeV) were consistent with the finding that a low level of Si (<0.5 wt.%) is conducive to relatively higher susceptibility to IASCC. Silicon atoms exert profound effects on irradiation-induced hardening. A high concentration of Si is conducive to less hardening and a lower number density of Frank loops. The beneficial effect of high concentrations of Cr was very significant, that is, alloys that contained <15.5 wt.% Cr exhibited relatively higher susceptibility to IASCC, whereas an alloy that contained >21 wt.% Cr exhibited relatively lower susceptibility than other alloys irradiated under similar conditions.

Susceptibility to IASCC appears to be influenced by many alloying and impurity elements in a complex manner. More conclusive evidence for the observed effects will be provided by the

more complete data that will be obtained from the whole test matrix including the materials irradiated to higher fluences.

Fracture toughness J–R curve tests have been conducted on two heats of Type 304 SS that were irradiated to a fluence of ≈0.3 x 10^{21} n cm^{-2} (E > 1 MeV) at ≈288°C in a He environment in the Halden boiling heavy–water reactor. The tests were performed on 1/4–T compact tension (CT) specimens in air at 288°C, crack extensions were determined by both DC potential and elastic unloading compliance techniques. Neutron irradiation at 288°C to 0.3 x 10^{21} n cm^{-2} decreased the fracture toughness of both heats. The commercial heat C19 exhibited fracture toughness that is superior to the fracture toughness of the laboratory heat L20. The values of fracture toughness J_{ic} are ≥500 kJ/m^2 for C19 and ≈60 kJ/m^2 for L20.

Environmentally Assisted Cracking of Alloys 600 and 690 in Simulated LWR Water

To evaluate the resistance of Alloys 600 and 690 to environmentally assisted cracking (EAC) in LWR coolant environment, fracture-mechanics CGR tests were conducted in air and water environments on CT specimens of several heats of these alloys in annealed and in annealed and thermally treated conditions. A statistical analysis of the results was used to develop correlations for predicting CGRs of the materials as a function of stress intensity, load ratio, and DO levels. However, because the experimental data were obtained for only a single rise time, i.e., frequency, alternate forms for the correlations have also been developed which can be used to extrapolate the results to other rise times. Experiments are planned to verify the predictions of the correlation for the effect of rise time.

The CGRs in the low–C heat of Alloy 600 do not appear to be sensitive to either heat treatment or DO level, whereas the CGRs in the high–C heats show a strong environmental enhancement in high–DO environments. The results are inconclusive for the high–C Alloy 600 in low–DO environments. Alloy 690 shows only a modest environmental enhancement in the low–DO environments; environmental effects appear to be independent of the loading conditions as long as $CGR_{air} \geq 10^{-11}$ s^{-1}. The CGRs in Alloy 690 in high–DO show some environmental enhancement for loading conditions that correspond to low CGRs in air.

Constant load crack growth rate tests have also been conducted on CT specimens of Alloys 600 and 690 in high–DO water at temperatures between 200 and 320°C. The growth rates for the hot–worked Alloy 600 are a factor of ≈5 higher than those for the hot–worked + thermally treated Alloy 600. The addition of sulfate increased the CGRs of both alloys by a factor of 3–7. The Alloy 690 specimens show little dependence of K on growth rates; the CGRs range between ≈2 x 10^{-12} and 6 x 10^{-12} m/s, values that may be below the sensitivity of the crack–monitoring system. The results indicate that for Alloy 600, the CGRs increase slightly with increasing K.

Acknowledgments

The authors thank W. F. Burke, T. M. Galvin, J. Tezak, R. W. Clark, and D. R. Perkins for their contributions to the experimental effort. This work is sponsored by the Office of Nuclear Regulatory Research, U.S. Nuclear Regulatory Commission, under Job Code W6610; Program Manager: Dr. M. B. McNeil.

1 Introduction

The U.S. Nuclear Regulatory Commission (NRC) and its predecessor, the U.S. Atomic Energy Commission, have conducted research programs that address the aging of reactor components. The results of the research have been used to evaluate and establish regulatory guidelines to ensure acceptable levels of reliability for light water reactor (LWR) components. The products of this program have been technical reports, methodologies for evaluating licensee submittals, and other inputs to the regulatory process. The results have led to the resolution of regulatory issues, as well as to the development, validation, and improvement of regulations and regulatory guides. The present research on the effects of simulated reactor coolant environments on cracking of reactor components was initiated to resolve the remaining critical technical issues related to cracking phenomena in LWR components. Initially, this project addressed cracking of boiling water reactor (BWR) pipes. Subsequently, in response to requests from the NRC Division of Nuclear Reactor Regulation (NRR) for assistance in dealing with developing cracking problems in aging reactors, the focus shifted to other problems in environmentally assisted cracking (EAC) of LWR components.

The overall objective of this program is to provide data and physical models to be used by the NRC staff in assessing environmentally assisted degradation of primary pressure boundary components in LWRs. The research is divided into five tasks:

(a) *Environmental effects on fatigue, crack growth, and stress corrosion cracking*
Fatigue and EAC of piping, pressure vessels, and core components in LWRs are important concerns during plant operation and for extended reactor lifetimes. The degradation processes in U.S. reactors include fatigue, intergranular stress corrosion cracking (IGSCC), and propagation of fatigue or stress corrosion cracks that initiate in the weld-sensitized heat-affected zones of stainless steel (SS) components. Occurrences of mechanical–vibration– and thermal–fluctuation–induced fatigue failures in LWR plants have also been documented. The objective of this task is to improve fatigue design curves and assess the additivity of fatigue damage in piping and vessel steels under load histories that are typical of LWR components. The results of this work will be used to assess industry fatigue evaluations that are related to license renewal.

(b) *Component vulnerability to irradiation-assisted stress corrosion cracking*
Irradiation–assisted stress corrosion cracking (IASCC) of in–core components in both BWRs and pressurized water reactors (PWRs) is becoming a more common problem as reactors age. The general pattern of the observed failures indicates that, as nuclear plants age and neutron fluence increases, many apparently nonsensitized austenitic materials become susceptible to intergranular failure by IASCC. Some of these failures have been reported for components that are subjected to relatively low or negligible stress levels, e.g., control–blade sheaths and handles and instrument dry tubes of BWRs. Although most failed components can be replaced, it would be very difficult or impractical to replace some safety–significant structural components, such as the BWR top guide, core plate, and shroud. The objective of this task is to provide data and models that are needed to assess industry analyses of the likelihood of degradation and failure of core internal components that are due to IASCC, and to evaluate licensee submissions that are related to inspection and remediation.

(c) *Cracking of nickel alloy components of LWR primary systems*
Internal components of reactor vessels are made of Ni-based alloys, e.g., Alloys 600, X750, and 182, which are susceptible to IGSCC. The causes and mechanisms of this cracking are not adequately understood, and the uncertainty is increased when licensee submissions are evaluated for factors such as damage accumulation and inspection intervals. The objective of this task is to provide technical data on the effects of cracks in Ni-alloy components on the residual life, inspection, and repair of the component. The results will be used to support NRR staff assessments of industry crack-growth models, and potential detection and mitigation measures.

(d) *Analysis of postweld heat treatment processes and validation of flaw acceptance criteria*
The objective of this task is to evaluate the effect of postweld heat treatment on long-term resistance to environmental cracking by assessing sensitization and other microstructural changes. This evaluation will provide the NRC with insights for use in reviewing licensee submittals.

(e) *Assessment of industry crack-growth models*
This task has two objectives. The first is to perform an independent evaluation of industry models that are used to establish inspection intervals and repair criteria. The second objective is to perform more detailed analyses of flaw acceptance criteria.

Research during this six-month reporting period has focused on fatigue of austenitic SSs, fracture toughness J-R curve tests in air, and IASCC during slow-strain-rate tensile (SSRT) tests (in simulated BWR water) of SS specimens that were irradiated to fluence levels of ≈0.3 and 0.9 x 10^{21} n·cm^{-2} (E > 1 MeV) at 288°C in the Halden reactor, and EAC of Alloys 600 and 690 in high-purity (HP) oxygenated water.

2 Environmental Effects on Fatigue Strain-versus-Life (S–N) Behavior of Primary Pressure Boundary Materials

Experience with operating nuclear power plants worldwide reveals that many failures can be attributed to fatigue; examples include piping components, nozzles, valves, and pumps.[1-3] In most cases, these failures have been associated with thermal loading that is due to thermal stratification or thermal striping, or with mechanical loading that is due to vibratory loading. Significant thermal loadings due to flow stratification were not included in the original design basis analysis. The effects of these loadings may also have been aggravated by corrosion effects that are due to exposure to high-temperature aqueous environments. Fatigue cracks have been observed in pressurizer surge lines in PWRs (NRC Bulletin No. 88-11), and in feedwater lines connected to nozzles of pressure vessels in BWRs and steam generators in PWRs (NRC IE Bulletin, 79-13; NRC Information Notice 93-20). These cracks have been attributed to corrosion fatigue (NRC IE Bulletin, 79-13) or strain-induced corrosion cracking[4] caused by cyclic loading that is due to thermal stratification during start-up (hot standby) and shut-down periods.

2.1 Methods for Incorporating Effects of LWR Coolant Environment into ASME Code Fatigue Evaluations (O. K. Chopra and W. J. Shack)

Cyclic loadings on a structural component occur because of changes in the mechanical and thermal loadings as the system goes from one set of pressure, temperature, moment, and

force loading to any other load set. For each pair of load sets, an individual fatigue usage factor is determined by the ratio of the number of cycles anticipated during the lifetime of the component to the allowable cycles. Figures I-9.1 through I-9.6 of Appendix I to Section III of the ASME Boiler and Pressure Vessel Code[5] specify fatigue design curves that define the allowable number of cycles as a function of applied stress amplitude. The cumulative usage factor (CUF) is the sum of the individual usage factors, and Section III of the ASME Code requires that the CUF at each location not exceed 1.

The Code design fatigue curves were based on strain-controlled tests of small polished specimens at room temperature in air. In most studies, the fatigue life of a test specimen is defined as the number of cycles for the tensile stress to drop 25% from its peak value, which corresponds to an ≈3-mm-deep crack. Consequently, fatigue life N represents the number of cycles required to initiate a crack ≈3 mm deep. The best-fit curves to the experimental data were expressed in terms of the Langer equation[6] of the form

$$\varepsilon_a = B(N)^{-b} + A, \qquad (1)$$

where ε_a is strain amplitude and A, B, and b are parameters of the model. (Eq. 1 may be written in terms of stress amplitude S_a instead of strain amplitude ε_a, where stress amplitude is the product of strain amplitude and elastic modulus, i.e., $S_a = E\,\varepsilon_a$.) The design fatigue curves were obtained by decreasing the best-fit curves by a factor of 2 on stress or 20 on cycles, whichever was more conservative, at each point on the best-fit curve. As described in the Section III criteria document,[7] these factors were intended to account for the differences and uncertainties in relating the fatigue lives of laboratory test specimens to those of actual reactor components. The factor of 20 on cycles is the product of three subfactors: 2 for scatter of data (minimum to mean), 2.5 for size effects, and 4 for surface finish, atmosphere, etc. "Atmosphere" was intended to reflect the effects of an industrial environment rather than the controlled environment of a laboratory. The factors of 2 and 20 are not safety margins but rather conversion factors that must be applied to the experimental data to obtain reasonable estimates of the lives of actual reactor components; in a benign environment, some fraction of the factor actually represents a safety margin.

Subsection NB-3121 of Section III of the Code states that the data on which the fatigue design curves (Figs. I-9.1 through I-9.6) are based did not include tests in the presence of corrosive environments that might accelerate fatigue failure. Article B-2131 in Appendix B to Section III states that the owner's design specifications should provide information about any reductions to fatigue design curves that are required because of environmental conditions. Recent fatigue strain-vs.-life (S-N) data illustrate the potentially significant effects of LWR coolant environments on the fatigue resistance of carbon steels (CSs), low-alloy steels (LASs),[8-20] and austenitic SSs,[21-31] (Fig. 1).

A program is being conducted at Argonne National Laboratory to develop data and models for predicting the effects of environment on fatigue design curves of pressure vessel and piping steels. Fatigue tests are being conducted to obtain data under conditions that are not included in the existing fatigue data base and to establish the effects of various loading and environmental variables on the fatigue S-N behavior of pressure-boundary steels. The existing fatigue S-N data have been analyzed to establish the effects of various material, loading, and environmental parameters on the fatigue life of carbon and low-alloy steels and austenitic SSs; the results for carbon and low-alloy steels[18] and austenitic SSs have been

summarized.[31] Under certain environmental and loading conditions, fatigue lives of CSs can be a factor of 70 lower in the LWR environment than in air.[11,18–20] Therefore, the margins in the ASME Code may be less conservative than originally intended.

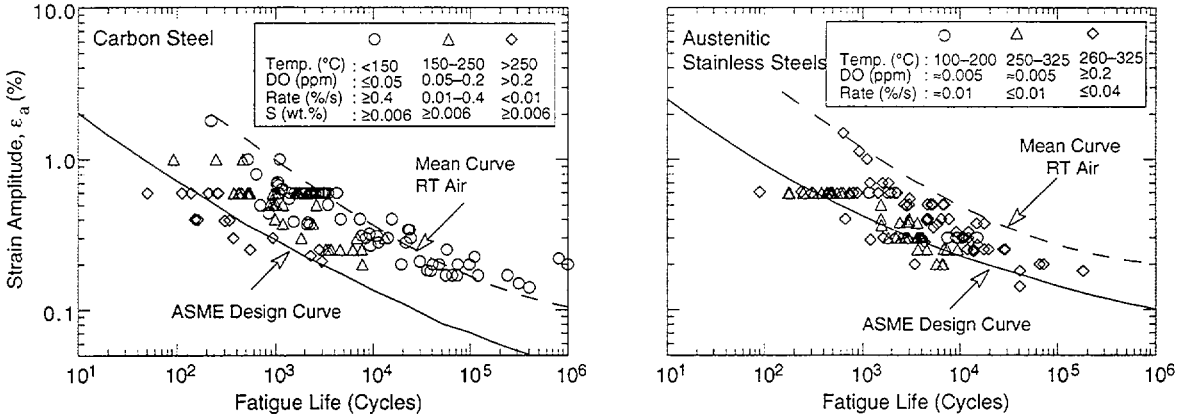

Figure 1. Fatigue S–N data for carbon steels and austenitic stainless steels in water

Two approaches have been proposed for incorporating the effects of LWR environments into ASME Section III fatigue evaluations: (a) develop new design fatigue curves for LWR applications, and (b) use a fatigue life correction factor to account for environmental effects. Both approaches are based on the existing fatigue S–N data in LWR environments, i.e., the best-fit curves to the experimental fatigue S–N data on LWR environments are used to obtain the design curves or fatigue life correction factor. As and when more data became available, the best-fit curves have been modified and updated to include the effects of various material, loading, and environmental parameters on fatigue life. Interim design fatigue curves that address environmental effects on fatigue life of carbon and low-alloy steels and austenitic SSs were first proposed by Majumdar et al.[32] Design fatigue curves based on a rigorous statistical analysis of the fatigue S–N data obtained in LWR environments were developed by Keisler et al.[33,34] Results of the statistical analysis have also been used to estimate the probability of fatigue cracking in reactor components.[33] The design curves and statistical models for estimating fatigue lives in LWR environments have recently been updated for carbon and low-alloy steels[18–20] and austenitic SSs.[30,31]

The alternative approach, proposed initially by Higuchi and Iida,[11] considers the effects of reactor coolant environments on fatigue life in terms of a fatigue life correction factor F_{en}, which is the ratio of the life in air to that in water. To incorporate environmental effects into the ASME Code fatigue evaluations, a fatigue usage for a specific load pair, based on the current Code design curves, is multiplied by the correction factor. Specific expressions for F_{en}, based on the statistical models[18–20,30,31,35] and on the correlations developed by the Environmental Fatigue Data Committee of Thermal and Nuclear Power Engineering Society of Japan,* have been proposed.

This report summarizes the data that are available on the effects of various material, loading, and environmental parameters on the fatigue lives of carbon and low-alloy steels and austenitic SSs. The two methods for incorporating the effects of LWR coolant environments

* M. Higuchi, presented at the Pressure Vessel Research Council Meeting, April, 1996, Orlando, FL.

into the ASME Code fatigue evaluations are presented. Differences between the methods and their significance on the design fatigue curves are discussed.

2.1.1 Fatigue S–N Data in LWR Environments

Carbon and Low–Alloy Steels

The fatigue life of both carbon and low–alloy steels is decreased significantly when five conditions are satisfied simultaneously, viz., strain amplitude, temperature, dissolved oxygen (DO) level in water, and S content of the steel are above a minimum level, and strain rate is below a threshold value. Although the microsturctures and cyclic–hardening behavior of CSs and LASs differ significantly, environmental degradation of fatigue life of these steels is very similar. For both steels, only moderate decrease in life (by a factor of <2) is observed when any one of the threshold conditions is not satisfied. The effects of the critical parameters on fatigue life and their threshold values are summarized below.

(a) *Strain.* A minimum threshold strain is required for environmentally assisted decrease in fatigue life of carbon and low–alloy steels.[18–20] The threshold value most likely corresponds to the rupture strain of the surface oxide film. Limited data suggest that the threshold value is ≈20% higher than the fatigue limit for the steel.

(b) *Strain Rate.* Environmental effects on fatigue life occur primarily during the tensile–loading cycle, and at strain levels greater than the threshold value required to rupture the surface oxide film. When any one of the threshold conditions is not satisfied, e.g., DO <0.05 ppm or temperature <150°C, the effects of strain rate are consistent with those in air, i.e., heats that are sensitive to strain rate in air, also show a decrease in life in water. When all other threshold conditions are satisfied, fatigue life decreases logarithmically with decreasing strain rate below 1%/s;[11,14] the effect of environment on life saturates at ≈0.001%/s.[18–20]

(c) *Temperature.* When other threshold conditions are satisfied, fatigue life decreases linearly with temperature above 150°C and up to 320°C.[10,11,14] Fatigue life is insensitive to temperatures below 150°C or when any other threshold condition is not satisfied.

(d) *Dissolved Oxygen in Water.* When other threshold conditions are satisfied, life decreases logarithmically with DO above 0.05 ppm; the effect saturates at ≈0.5 ppm DO.[10,14]

(e) *Sulfur Content of Steel.* Although S content and morphology are the most important parameters that determine susceptibility of CSs and LASs to fatigue crack growth in LWR environments, existing fatigue S–N data are inadequate to unequivocally establish the effect of S content on the fatigue life of these steels. When any one of the threshold conditions is not satisfied, environmental effects on life are minimal and relatively insensitive to changes in S content. When the threshold conditions are satisfied, i.e., high–temperature/high–DO water, the fatigue life of LASs decreases with increasing S content. Limited data suggest that the effects of environment on life saturate at a S content above 0.012 wt.%.[18] However, the fatigue life of CSs in high–temperature/ high–DO water seems to be insensitive to S content in the range of 0.002–0.015 wt.%.*

---

* M. Higuchi, presented at the Pressure Vessel Research Council Meeting, June, 1995, Milwaukee, WI.

Austenitic Stainless Steels

The fatigue life of austenitic SSs is decreased in LWR environments; the reduction in life depends on strain rate, level of DO in water, and temperature.[23-25,28-31] The effects of LWR environments on fatigue life of wrought materials are comparable for Types 304, 316, and 316NG SS. Although the fatigue lives of cast SSs are relatively insensitive to changes in ferrite content in the range of 12–28%,[23] the effects of loading and environmental parameters on the fatigue life of cast SSs differ somewhat. The significant results and threshold values of critical parameters are summarized below.

(a) *Strain.* A minimum threshold strain is required for environmentally assisted decrease in fatigue life of austenitic SSs. The threshold value most likely corresponds to the rupture strain of the surface oxide film. Limited data suggest that the threshold strain range is between 0.32 and 0.36%.[24,30]

(b) *Dissolved Oxygen in Water.* Environmental effects on fatigue life are more pronounced in low-DO, (<0.01 ppm DO) than in high-DO, (≥0.1 ppm DO) water.[23,30] The reduction in life is greater by a factor of ≈2 in a simulated PWR environment than in high-DO water. The fatigue lives of cast SSs are approximately the same in both high- or low-DO water and are comparable to those observed for wrought SSs in low-DO water.[30] Recent results indicate that, in high-DO water, the conductivity of water and the nature of the oxide film strongly affect the fatigue life of austenitic SSs.

(c) *Strain Rate.* Fatigue lives decrease with decreasing strain rate; the effect is greater in a low-DO PWR environment than in high-DO water. The results indicate that the strain rate below which effects of strain rate on fatigue life saturate may depend on both steel type and DO level. In low-DO environments, saturation strain rate appears to be at ≈0.0004%/s for Type 304 SS and somewhat higher for Type 316 SS.[24,30] Existing data are inadequate to define the saturation strain rate in high-DO water or that for cast SSs.

(d) *Temperature.* Existing data are inadequate to establish the functional form for the dependence of life on temperature. Limited data indicate that environmental effects on fatigue life are significant at temperatures above 250°C and minimal below 200°C.[24] At 250–330°C, fatigue life appears to be relatively insensitive to changes in temperature.

2.1.2 Mechanism of Fatigue Crack Initiation

The formation of surface cracks and their growth to an "engineering" size (3 mm deep) constitute the fatigue life of a material, which is represented by the fatigue S–N curves. Fatigue life has conventionally been divided into two stages: (a) initiation, expressed as the cycles needed to form microcracks on the surface; and (b) propagation, expressed as cycles needed to propagate the surface cracks to engineering size. The reduction in fatigue life in high-temperature water has often been attributed to easier crack initiation, because surface micropits that are present in high-temperature water act as stress raisers and provide preferred sites for the formation of fatigue cracks.[10] However, experimental data do not support this argument; the fatigue lives of carbon and low-alloy steel specimens that have been preoxidized at 288°C in high-DO water and then tested in air are identical to those of unoxidized specimens.[18,20] If the presence of micropits was responsible for the reduction in life, specimens that have been preexposed to high-DO water and tested in air should show a decrease in life. Also, the fatigue limit of these steels should be lower in water than in air.

Data obtained from specimens in high–DO water indicate that the fatigue limit is either the same as or ≈20% higher in water than in air.[18]

An alternative way to describe fatigue life considers fatigue life to be entirely composed of crack propagation.[36] In polycrystalline metals and alloys, the period during which surface cracks form is negligible; surface cracks, 10 μm or longer, form quite early in life.[37–41] The growth of these short fatigue cracks may be divided into three regimes: (a) an initial period, which is very sensitive to microstructure, involves growth of microstructurally small cracks (MSCs) and is characterized by a decelerating growth rate; (b) a final period of growth that can be predicted from fracture mechanics methodology and is characterized by an accelerating crack growth rate (CGR); and (c) a transition period that is controlled by a combination of the two regimes. Fatigue cracks that have grown so long that they show little or no influence of microstructure (i.e., greater than the critical length of MSCs) are called mechanically small cracks. The transition from an MSC to a mechanically small crack has been estimated to occur at a crack size ≈8 times the unit size of the microstructure, i.e., 100–150 μm. The reduction in life in LWR environments may arise from an increase in growth rates of cracks during the initial stage of MSC foprmation and shear crack growth and/or during the transition and final stage of tensile–crack growth.

The enhanced growth rates of long cracks in pressure vessel and piping steels in LWR environments have been attributed to either slip oxidation/dissolution[42] or hydrogen–induced cracking[43] mechanisms. Both mechanisms depend on the rates of oxide rupture, passivation, and liquid diffusion. Therefore, it is often difficult to differentiate between the two processes or to establish their relative contributions to crack growth in LWR environments.

Studies on crack initiation in smooth fatigue specimens indicate that the decrease in the fatigue life of carbon and low–alloy steels in LWR environments is caused primarily by the effects of environment on the growth of cracks that are <100 μm deep.[18,39] When compared with crack growth rates in air, growth rates in high–DO water are nearly two orders of magnitude greater for cracks that are <100 μm and one order of magnitude greater for cracks that are >100 μm. Metallographic examinations of test specimens indicate that, in high–DO water, surface cracks grow entirely as tensile cracks normal to the stress, whereas, in air or simulated PWR environments, they are at an angle of 45° to the stress axis.[39] Also, in CSs, cracks propagate across both ferrite and pearlite regions. These results indicate that growth of MSCs occurs by slip oxidation/dissolution.

In high–DO water, crack initiation in carbon and low–alloy steels may be explained as follows: (a) surface microcracks form quite early in fatigue life; (b) during cyclic loading, the protective oxide film is ruptured at strains greater than the fracture strain of surface oxides, and the microcracks grow by anodic dissolution of the freshly exposed surface to crack depths greater than the critical length of MSCs; and (c) these mechanically small cracks grow to engineering size, and their growth, which is characterized by accelerating rates, can be predicted by fracture mechanics methodology.

As discussed later in Section 2.2, studies on crack initiation in austenitic SSs yield similar results, i.e., that the decrease in fatigue life in LWR environments is caused primarily by the effects of environment on the growth of cracks that are <500 μm deep. However, fatigue lives that are lower in low–DO water than in high–DO water are difficult to reconcile in terms of the slip oxidation/dissolution mechanism. Also, austenitic SS specimens tested in LWR

environments show well-defined fatigue striations, indicating that mechanical factors and not the slip oxidation/dissolution process, are important.[30] The results indicate that environmentally assisted reduction in fatigue life of austenitic SSs is most likely caused by H-induced cracking.

2.1.3 Incorporating Environmental Effects into ASME Fatigue Evaluations

Two procedures are currently being proposed for incorporating effects of LWR coolant environments into the ASME Section III fatigue evaluations: (a) develop a new set of environmentally adjusted design fatigue curves[18,20,30,31] or (b) use fatigue life correction factor F_{en} to adjust the current ASME Code fatigue usage values for environmental effects.[20,31,35] For both approaches, the range and bounding values must be defined for key service parameters that influence fatigue life. It has been demonstrated that both approaches give similar results for carbon and low-alloy steels[18] but the results for austenitic SSs differ[31] because the existing ASME mean curve for SS in air is not consistent with the exiting fatigue S-N data.

Design Fatigue Curves

A set of environmentally adjusted design fatigue curves can be developed from the best-fit curves to the experimental data that were obtained in LWR environments by using the same procedure that has been used to develop the current ASME Code design fatigue curves. The best-fit experimental curves are first adjusted for the effect of mean stress by using the modified Goodman relationship

$$S'_a = S_a\left(\frac{\sigma_u - \sigma_y}{\sigma_u - S_a}\right) \qquad \text{for } S_a < \sigma_y, \tag{2a}$$

and

$$S'_a = S_a \qquad \text{for } S_a > \sigma_y, \tag{2b}$$

where S'_a = is the adjusted value of stress amplitude, and σ_y and σ_u are yield and ultimate strengths of the material, respectively. The design fatigue curves are then obtained by lowering the adjusted best-fit curve by a factor of 2 on stress or 20 on cycles, whichever is more conservative, to account for differences and uncertainties in fatigue life that are associated with material and loading conditions.

Statistical models that are based on the existing fatigue S-N data have been developed for estimating the fatigue lives of pressure vessel and piping steels in air and LWR environments.[18,20,30,31] In air at room temperature, the fatigue data for CSs are best represented by

$$\ln(N) = 6.564 - 1.975 \ln(\varepsilon_a - 0.113) \tag{3a}$$

and for LASs, by

$$\ln(N) = 6.627 - 1.808 \ln(\varepsilon_a - 0.151), \tag{3b}$$

where N is fatigue life of a smooth test specimen and ε_a is applied strain amplitude (%). In LWR environments, the fatigue data for CSs are best represented by

$$\ln(N) = 6.010 - 1.975 \ln(\varepsilon_a - 0.113) + 0.101\, S^*\, T^*\, O^*\, \dot{\varepsilon}^* \quad (4a)$$

and for LASs, by

$$\ln(N) = 5.729 - 1.808 \ln(\varepsilon_a - 0.151) + 0.101\, S^*\, T^*\, O^*\, \dot{\varepsilon}^*, \quad (4b)$$

where S^*, T^*, O^*, and $\dot{\varepsilon}^*$ are transformed S content, temperature, DO, and strain rate, respectively, defined as follows:

$$\begin{aligned} S^* &= S && (0 < S \le 0.015 \text{ wt.\%}) \\ S^* &= 0.015 && (S > 0.015 \text{ wt.\%}) \end{aligned} \quad (5a)$$

$$\begin{aligned} T^* &= 0 && (T < 150°C) \\ T^* &= T - 150 && (T = 150\text{–}350°C) \end{aligned} \quad (5b)$$

$$\begin{aligned} O^* &= 0 && (DO < 0.05 \text{ ppm}) \\ O^* &= \ln(DO/0.04) && (0.05 \text{ ppm} \le DO \le 0.5 \text{ ppm}) \\ O^* &= \ln(12.5) && (DO > 0.5 \text{ ppm}) \end{aligned} \quad (5c)$$

$$\begin{aligned} \dot{\varepsilon}^* &= 0 && (\dot{\varepsilon} > 1\%/s) \\ \dot{\varepsilon}^* &= \ln(\dot{\varepsilon}) && (0.001 \le \dot{\varepsilon} \le 1\%/s) \\ \dot{\varepsilon}^* &= \ln(0.001) && (\dot{\varepsilon} < 0.001\%/s). \end{aligned} \quad (5d)$$

The discontinuity in the value of O^* at 0.05 ppm DO is due to an approximation and does not represent a physical phenomenon. In air at room temperature, the fatigue data for Types 304 and 316 SS are best represented by

$$\ln(N) = 6.703 - 2.030 \ln(\varepsilon_a - 0.126), \quad (6a)$$

and for Type 316NG, by

$$\ln(N) = 7.422 - 1.671 \ln(\varepsilon_a - 0.126). \quad (6b)$$

In LWR environments, the fatigue data for Types 304 and 316 SS are best represented by

$$\ln(N) = 5.768 - 2.030 \ln(\varepsilon_a - 0.126) + T'\, \dot{\varepsilon}'\, O' \quad (7a)$$

and for Type 316NG, by

$$\ln(N) = 6.913 - 1.671 \ln(\varepsilon_a - 0.126) + T'\, \dot{\varepsilon}'\, O', \quad (7b)$$

where T', $\dot{\varepsilon}'$, and O' are transformed temperature, strain rate, and DO, respectively, defined as:

$$\begin{aligned} T' &= 0 && (T < 200°C) \\ T' &= 1 && (T \ge 200°C) \end{aligned} \quad (8a)$$

$$\begin{aligned} \dot{\varepsilon}' &= 0 && (\dot{\varepsilon} > 0.4\%/s) \\ \dot{\varepsilon}' &= \ln(\dot{\varepsilon}/0.4) && (0.0004 \le \dot{\varepsilon} \le 0.4\%/s) \\ \dot{\varepsilon}' &= \ln(0.0004/0.4) && (\dot{\varepsilon} < 0.0004\%/s) \end{aligned} \quad (8b)$$

$$\begin{aligned} O' &= 0.260 && (DO < 0.05 \text{ ppm}) \\ O' &= 0.172 && (DO \ge 0.05 \text{ ppm}). \end{aligned} \quad (8c)$$

The models are recommended for predicted fatigue lives of $\le 10^6$ cycles. As discussed in Section 2.1.1, recent data indicate that in high-DO water the conductivity of water and the nature of the oxide film have a strong effect on fatigue life of austenitic SSs. Only a moderate

decrease in fatigue life is observed in high-DO (≈0.8 ppm DO) high-purity (≤0.08 μS/cm) water at 288°C when the specimen is presoaked for ≈5 days to allow a stable surface oxide to develop and the steel electrochemical potential to stabilize. Consequently, estimates of fatigue life in High-DO water that are based on Eqs. 4–8 may be somewhat conservative. The stress-vs.-life curves are obtained from the strain-vs.-life curves, e.g., stress amplitude is the product of strain amplitude and elastic modulus. The room-temperature value for the elastic modulus is used in converting the curves.

The environmentally adjusted design fatigue curves were obtained by using the procedure that was used to develop the current ASME Code curves and the statistical models that are represented by Eqs. 3–7. The design fatigue curves for carbon and low-alloy steels and Types 304 and 316 austenitic SS in air and LWR environments are shown in Figs. 2–6. Because the fatigue life of Type 316NG is superior to that of Types 304 or 316 SS, Figs. 5 and 6 may be used conservatively for Type 316NG SS.

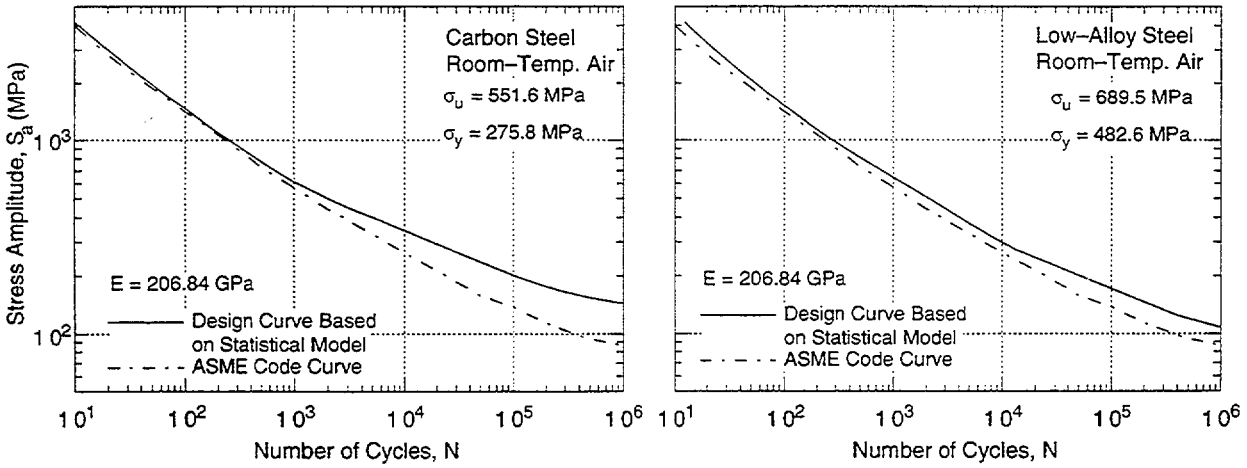

Figure 2. Design fatigue curves developed from statistical model for carbon and low-alloy steels in air at room temperature

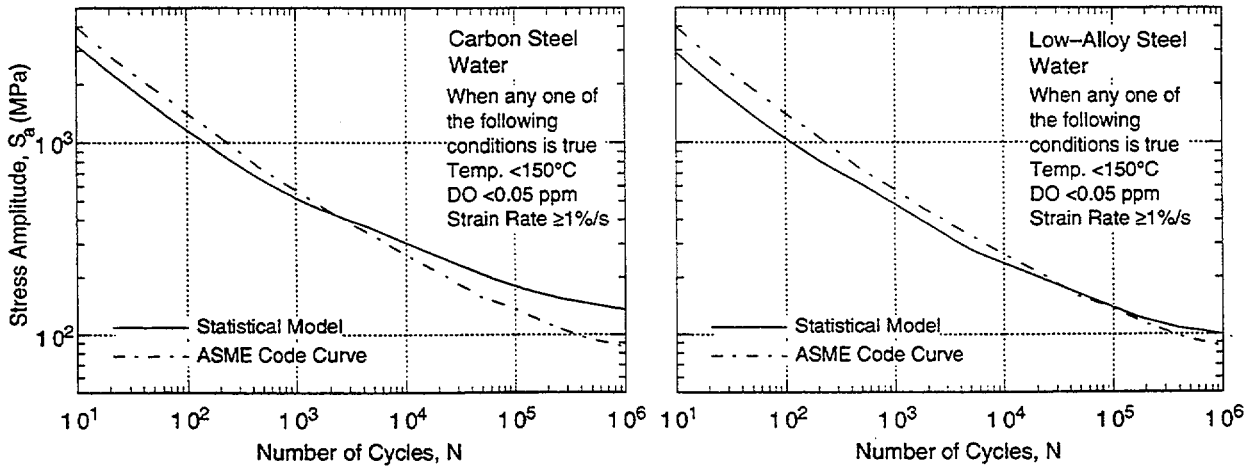

Figure 3. Design fatigue curves developed from statistical model for carbon and low-alloy steels under service conditions where one or more threshold values are not satisfied

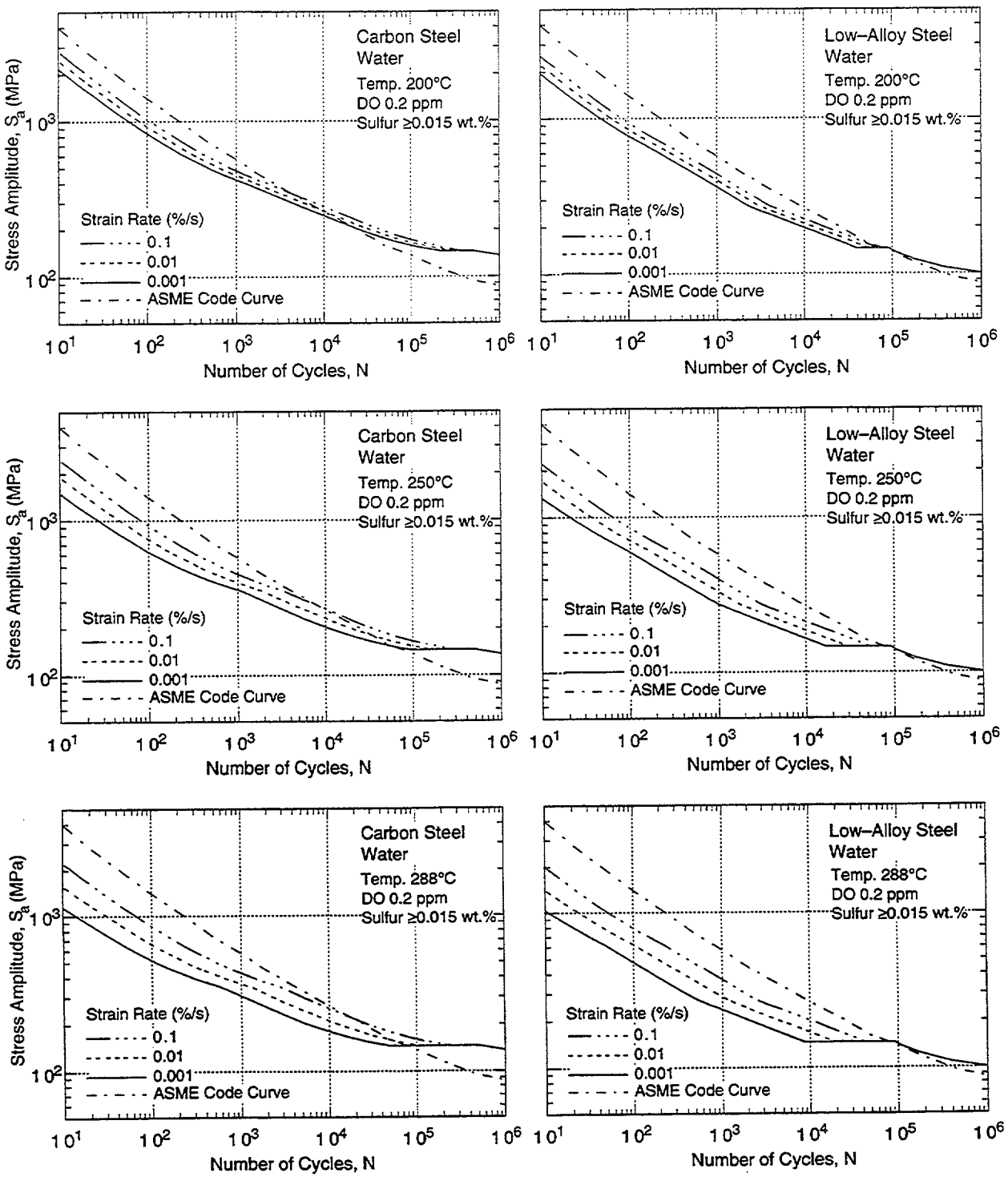

Figure 4. Design fatigue curves developed from statistical model for carbon and low-alloy steels under service conditions where all critical threshold values are satisfied

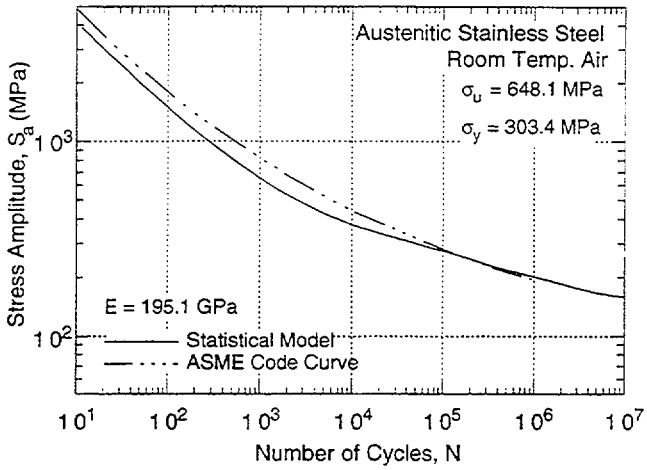

Figure 5.
Design fatigue curve developed from statistical model for Types 304 and 316 austenitic SS in air

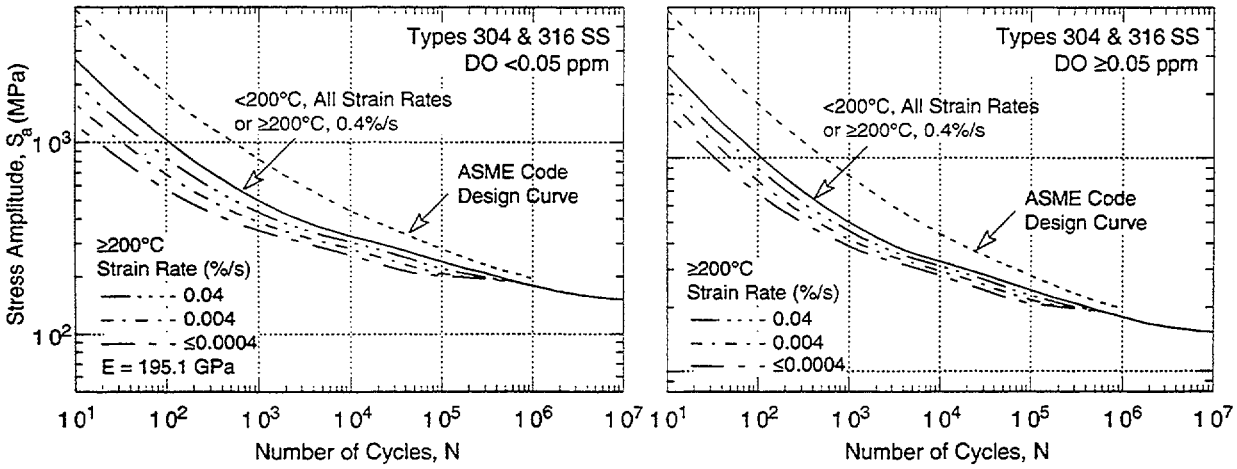

Figure 6. Design fatigue curves developed from statistical models for Types 304 and 316 SS in water with <0.05 and ≥0.05 ppm DO

The best-fit curves were adjusted for the effect of mean stress by using the modified Goodman relationships (Eqs. 2a and 2b), which assume the maximum possible mean stress and typically give a conservative adjustment for mean stress, at least when environmental effects are not significant. To be consistent with the current Code design curves, the mean-stress-adjusted best-fit curves were decreased by the same margins on stress and cycles that are present in the current Code curves. The mean-stress-adjusted best-fit curves were decreased by a factor of 2 on stress for carbon and low-alloy steels and by a factor of 1.5 for austenitic SSs. A factor of 20 on life was used for all curves, although the actual margin on life is ≈10 for austenitic SSs because of the differences between the ASME mean curve and the best-fit curve to existing fatigue data.

For all of the design curves, we define a minimum threshold strain amplitude, below which environmental effects either do not occur or are modest. As discussed earlier, the threshold strain for carbon and low-alloy steels appears to be ≈20% higher than the fatigue limit of the steel. This translates into strain amplitudes of 0.140 and 0.185%, respectively, for CSs and LASs. These values must be adjusted for mean stress effects and variability due to material and experimental scatter. To account for the effects of mean stress, the threshold strain amplitudes are decreased by ≈15% for CSs and by ≈40% for LASs. These decreases

produce a threshold strain amplitude of ≈0.12% for both steels. A factor of 1.7 on strain provides 90% confidence for the variations in fatigue life that are associated with material variability and experimental scatter.[33] Thus, a threshold strain amplitude of 0.07% (or a stress amplitude of 145 MPa) was selected for both carbon and low-alloy steels. The existing fatigue data indicate a threshold strain range of ≈0.32% for austenitic SSs. This value is decreased by ≈10% to account for mean stress effects, and by a factor of 1.5 to account for uncertainties in fatigue life that are associated with material and loading variability. Thus, a threshold strain amplitude of 0.097% (stress amplitude of 189 MPa) was selected for austenitic SSs.

Fatigue Life Correction Factor

The effects of reactor coolant environments on fatigue life have also been expressed in terms of a fatigue life correction factor F_{en}, which is the ratio of the life in air at room temperature to that in water at the service temperature.[11] A similar approach has been proposed by the Electric Power Research Institute,[35] however, they defined F_{en} as the ratio of the life in air to that in water, both at service temperature. A nonmandatory appendix, based on this procedure, is being proposed for inclusion in Section III of the ASME Code. To incorporate environmental effects into the Section III fatigue evaluation, a fatigue usage factor for a specific stress cycle, based on the current Code design fatigue curve is multiplied by the correction factor. A fatigue life correction factor F_{en} can be obtained from the statistical model (Eqs. 3–8), where

$$\ln(F_{en}) = \ln(N_{RTair}) - \ln(N_{water}). \tag{9}$$

The fatigue life correction factor for CSs is given by

$$F_{en} = \exp(0.554 - 0.001515T^* \dot{\varepsilon}^* O^*), \tag{10a}$$

for LASs, by

$$F_{en} = \exp(0.898 - 0.001515T^* \dot{\varepsilon}^* O^*), \tag{10b}$$

and for austenitic SSs, by

$$F_{en} = \exp(0.935 - T' \dot{\varepsilon}' O'), \tag{10c}$$

where the constants T^*, $\dot{\varepsilon}^*$ and O^* are defined in Eqs. 5a–5c, and T', $\dot{\varepsilon}'$ and O' are defined in Eqs. 8a–8c. Because the fatigue life of CSs in high-temperature high-DO water seems to be insensitive to the S content of the steel,* a value of 0.015 wt.% S was assumed in Eq. 5a to obtain the fatigue life correction factors for carbon and low-alloy steels given by Eqs. 10a and 10b.

* M. Higuchi, presented at the Pressure Vessel Research Council Meeting, June, 1995, Milwaukee, WI.

2.1.4 Conservatism in Design Fatigue Curves

The overall conservatism in ASME Code fatigue evaluations has also been demonstrated in fatigue tests on piping welds and components.[44] In air, the margins on the number of cycles to failure for elbows and tees were 118–2500 and 123–1700, respectively, for CSs, and 40–310 and 104–510, respectively, for austenitic SSs. The margins for girth butt welds were significantly lower at 14–128 and 6–77, respectively, for CSs and SSs. In these tests, fatigue life was expressed as the number of cycles for the crack to penetrate through the wall, which ranged in thickness from 6 to 18 mm (0.237 to 0.719 in.). The ASME design fatigue curves represent the number of cycles that are necessary to form a 3–mm–deep crack. Consequently, depending on wall thickness, the actual ASME margins to failure may be lower by a factor of >2.

Deardorff and Smith[45] have also discussed the types and extent of conservatisms that are present in the ASME Section III fatigue evaluations and the effects of LWR environments on fatigue margins. The sources of conservatism include design transients that are considerably more severe than those experienced in service, grouping of transients, and simplified elastic-plastic analysis. Environmental effects on two components, the BWR feedwater nozzle/safe end and the PWR steam generator feedwater nozzle/safe end, both constructed from LAS and known to be affected by severe thermal transients, were also investigated during the study. When environmental effects on fatigue life were not considered, Deardorff and Smith[45] estimated that, for the PWR and BWR nozzles, the ratios of the CUFs computed with the Code design fatigue curve to CUFs computed with the mean experimental curve for test specimen data were ≈60 and 90, respectively. To maintain the factor of 20 on life that was used in the present Code design fatigue curves to account for the uncertainties due to material and loading variability, the margins for the PWR and BWR nozzles are reduced to 3 and 4.5, respectively. The studies by Mayfield et al.[44] and Deardorff and Smith[45] demonstrate the overall conservatism in the current ASME Section III Code fatigue evaluation procedures.

Table 1. Subfactors that may be used to account for effects of various variables on fatigue life

Variable	Factor on Life	Factor on Strain
Material variability and experimental scatter	2.5	1.4–1.7
Size	1.4	1.25
Surface finish	2.0–3.0	1.3
Loading history	1.5–2.5	1.5
Total adjustment	10.5–26.3	1.5–1.7

Data available in the literature have been reviewed to evaluate the conservatism in the ASME Code design fatigue curves. The subfactors that may be used to account for the effects of various material, loading, and environmental variables on the fatigue life of structural materials are summarized in Table 1.[33] The factors on strain primarily account for the variation in the fatigue limit of a material that is caused by material variability, component size and surface finish, and loading history. Because the reduction in fatigue life is associated with the growth of short cracks (<100 μm), the effects of these variables on fatigue limit are typically not cumulative but rather are controlled by the variable that has the largest

effect. The values in Table 1 suggest that a factor of at least 1.5 on strain and 10 on cycles is needed to account for the differences and uncertainties of relating fatigue lives of laboratory test specimens to those of large components. Because carbon and low-alloy steels and austenitic SSs develop a corrosion scale in LWR environments, the effect of surface finish may not be significant, i.e., the effects of surface roughness are included in environmentally assisted decrease in fatigue life in LWR coolant environments. In water, the subfactor on life to account for surface finish effects may be as low as 1.5 or may be eliminated completely; a factor of 1.5 on strain and 7 on cycles is adequate to account for the uncertainties that arise from material and loading variability. Therefore, the factor of 20 on life that is used in developing the design fatigue curves includes, as a safety margin, a factor of 3 or 4 on life that may be used to account for the effects of environment on the fatigue lives of these steels.

These results are consistent with the conclusions of the Pressure Vessel Research Council (PVRC) working group on fatigue S–N data analysis.[46] One of the tasks in the PVRC activity was to define a set of values for material, loading, and environmental variables that lead to "moderate" or "acceptable" effects of environment on fatigue life. A factor of 4 on the ASME mean life was chosen as a working definition of acceptable effects of environment, i.e., up to a factor of 4 decrease in fatigue life due to environment is considered acceptable and does not require further fatigue evaluation. The basis for this criterion is that a factor of 4 on life constitutes normal data scatter and/or at least that much conservatism is included in the design fatigue curves.

2.1.5 Fatigue Evaluations in LWR Environments

Section III, NB–3200– or NB–3600–type analyses of components for service in LWR environments can be performed with either the design fatigue curves or the fatigue life correction factors. Both of these approaches require information about the service conditions, e.g., temperature, strain rate, and DO level.

Fatigue Evaluations Based on Environmentally Corrected Design Fatigue Curves

Fatigue evaluations that are based on the design fatigue curves may be performed as follows:

(a) For each stress cycle or load pair, determine the alternating stress amplitude according to the guidelines of NB 3222.4 (design by analysis) or NB 3650 (analysis of piping products), and the total number of cycles anticipated during the lifetime of the component.

(b) For each stress cycle or load pair, obtain information about the service conditions, e.g., temperature, strain rate, and DO level. The procedure for obtaining these parameters depends on the details of the available information, i.e., whether the elapsed time–vs.–temperature information for the transient is available. Fatigue tests in oxygenated water under combined mechanical and thermal cycling[13,24] indicate that an average temperature may be used if the time–vs.–temperature information is available; the highest temperature may be used for a conservative estimate of life. Because environmental effects on fatigue life are modest at temperatures <150°C and at strains below the threshold value, average temperature may be determined by taking the average of the maximum temperature and either 150°C or the temperature at threshold strain, whichever is higher. An average strain rate is generally used for each load state; it is

obtained from the peak strain and elapsed time for the transient. However, fatigue-monitoring data indicate that actual strain rates may vary significantly during a transient. The slowest strain rate can be used for a conservative estimate of life.

(c) For each alternating stress amplitude and corresponding service condition, obtain a partial usage factor from the appropriate design fatigue curve (Figs. 3, 4, and 6). The design fatigue curves in Fig. 3 are used for carbon and low-alloy steels when any one of the threshold condition is not satisfied, i.e., when any one of the following conditions is true:

Temperature: < 150°C
DO: < 0.05 ppm
Strain Rate: ≥ 1%/s.

The design curves in Fig. 4 are used for carbon and low-alloy steels when all of the threshold conditions are satisfied, i.e., temperature ≥150°C, DO ≥0.05 ppm, and strain rate <1%/s; the curves shown in Fig. 4 are for 200, 250, and 288°C; 0.2 ppm DO level; and 0.1, 0.01, and ≤0.001%/s strain rate.

Similarly, the design curves in Fig. 6 are used for austenitic SSs under various service conditions. The two sets of curves are for <0.05 and ≥0.05 ppm DO in water. In both sets, the solid curve represents the service condition when any one of the two threshold conditions is not satisfied, i.e., when any one of the following conditions is true:

Temperature: < 200°C
Strain Rate: ≥ 0.4%/s.

The design curves shown by the chain dash lines in Fig. 6 are used for austenitic SSs when both of the threshold conditions are satisfied, i.e., temperature ≥200°C and strain rate <0.4%/s; the three curves shown in Fig. 6 are for 0.04, 0.004, and ≤0.0004%/s strain rate, and temperatures between 200 and 320°C.

(d) Calculate the CUF for the component; it is the sum of the partial usage factors. As discussed in the previous section, the design fatigue curves include a factor of 3 or 4 on life that may be used to account for the effects of environment on the fatigue lives of these steels. To avoid additional conservatism, the environmentally adjusted CUF for the component may be decreased by a factor of 3.

Fatigue Evaluations Based on Fatigue Life Correction Factor

Fatigue evaluations that are based on the fatigue life correction factor may be performed as follows:

(a) and (b) are as described above.

(c) For each alternating stress amplitude, obtain a partial usage factor from the current Code design curves in Figs. I-9.1 through I-9.6 of Appendix I to Section III of the Code.

(d) Adjust the partial usage factors for environmental effects by multiplying by F_{en}, which is calculated from Eqs. 10a-10c and the service condition for the stress cycle. The value of

F_{en} is calculated for only those stress cycles that satisfy all of the threshold conditions. For carbon and low-alloy steels, F_{en} is calculated when all of the following conditions are true:

Temperature:	≥ 150°C
DO:	≥ 0.05 ppm
Strain Rate:	< 1%/s.

For austenitic SSs, F_{en} is calculated when the following two conditions are true:

Temperature:	≥ 200°C
Strain Rate:	< 0.4%/s.

Because the design fatigue curves include a margin that may be used to account for the effects of environment, to avoid additional conservatism, F_{en} valves calculated from Eqs. 10a–10c are decreased by this amount. For carbon and low-alloy steels, F_{en} is decreased by a factor of 3 but not less than 1. For austenitic SSs, F_{en} is decreased by a factor of 1.5 because, as discussed earlier, the actual margin on life is ≈10 for austenitic SSs inasmuch as the ASME mean curve and the best-fit curve to existing fatigue data differ.

(e) Finally, calculate the CUF for the component; it is the sum of the partial usage factors.

2.1.6 Conclusions

The design fatigue curve method and the fatigue life correction factor method of evaluating fatigue lives are based on statistical models for estimating fatigue lives of carbon and low-alloy steels and austenitic SSs in LWR environments. The environmentally adjusted design fatigue curves provide allowable cycles for fatigue crack initiation in LWR coolant environments. All of the design curves maintain the margin of 20 on life. However, to be consistent with the current ASME Code curves, the margin on stress is 2 for carbon and low-alloy steels and 1.5 for austenitic SSs.

In the F_{en} method, environmental effects on life are estimated from the statistical models but the correction is applied to fatigue lives estimated from the current Code design curves. Therefore, estimates of fatigue lives that are based on the two methods may differ because of differences in the ASME mean curve and the best-fit curve to existing fatigue data. The current Code design curve for carbon steels (Fig. 2) is comparable to the statistical-model curve for LASs; however, it is somewhat conservative at stress levels <500 MPa when compared with the statistical-model curve for CSs. Consequently, usage factors based on the F_{en} method would be comparable to those based on the environmentally adjusted design fatigue curves for LASs and would be somewhat higher for CSs.

Figure 5 indicates that, for austenitic SSs, the current Code design fatigue curve is nonconservative when compared with the statistical-model curve, i.e., it predicts longer fatigue lives than the best-fit curve to the existing S–N data. Consequently, usage factors that are based on the F_{en} method would be lower than those determined from the environmentally corrected design fatigue curves. However, because the usage factors are decreased by a factor of 1.5 in the F_{en} method and 3 in the design curve method, the values that are obtained from the two methods would be comparable after they are adjusted.

2.2 Crack Initiation in Smooth Fatigue Specimens of Austenitic Stainless Steel in LWR Environments (J. L. Smith and O. K. Chopra)

During the current reporting period, fatigue tests have been conducted on Type 304 SS to determine the crack initiation and crack growth characteristics of this material in air and LWR environments. The results of fatigue tests that examine the influence of the reactor environment on the formation and growth of fatigue cracks in polished smooth specimens of austenitic SSs are presented. The effects of LWR environments on growth of short cracks are discussed.

2.2.1 Experimental

Low-cycle fatigue tests have been conducted on Type 304 austenitic SSs that had been solution annealed at 1050°C for 0.5 h. The composition of the material is given in Table 2. Smooth, cylindrical, 9.5-mm-diam specimens with 19-mm gauge length were used for the fatigue tests. Before testing, the specimen gauge length was given a 1-μm surface finish. The surface finish was applied in the axial direction to prevent circumferential scratches that might act as crack initiation sites.

Table 2. Composition (wt.%) of Type 304 austenitic stainless steel used for fatigue tests

Material	C	P	S	Si	Cr	Ni	Mn	Mo	Cu	N
Type 304[a] (Heat 30956)	0.060	0.019	0.007	0.48	18.99	8.00	1.54	0.44	–	0.100

[a] Solution-annealed at 1050°C for 0.5 h.

All tests were conducted at 288°C with fully reversed axial loading (i.e., R = −1) and a triangular or sawtooth waveform. The strain rate for the triangular wave and the fast-loading half of the sawtooth wave was 0.4%/s. The tests in air were strain controlled by an axial extensometer, and specimen strain was measured at two points outside the gauge region. The data that were obtained were then used to determine the stroke that was required to maintain a constant strain in the specimen gauge section for tests in water environments. Tests in water were conducted in a small autoclave under stroke control, where the specimen strain was controlled between two locations outside the autoclave. The feedwater for the low-DO simulated PWR environment contained <0.01 ppm DO, 2 ppm Li, 1000 ppm B, and ≈2 ppm dissolved H (≈23 cm^3/kg); its pH and conductivity were ≈6.5 and ≈19.2 μS/cm, respectively. The feedwater for the high-DO environment contained ≈0.7 ppm DO; its pH was ≈6.0, conductivity ≈0.09 μS/cm. The chemical analyses of the feed water were conducted at room temperature, and the fatigue tests were performed in both a once-through and a recirculating water system. Details of the test facility and procedure are described elsewhere.[15,17]

Crack growth characteristics during the high-temperature water tests were determined by block loading. The slow/fast sawtooth loading was interrupted at ≈500-cycle intervals, and the specimen was subjected to a block of triangular fast/fast loading cycles at a strain range that was lower than the test strain range. This method has been used successfully to characterize crack growth in A333-Gr 6 CS that was tested at 288°C in water that contained ≈0.8 ppm DO.[12] When carbon and low-alloy steels are tested, the block of fast/fast cycles leaves distinct beach marks on the fracture surface that can be used to characterize crack size as a function of fatigue cycles for the slow/fast test. For SSs, the beach marks are less

prominent, and extensive microscopy is required to reveal the features on the fracture surface associated with the loading blocks.

After an initial microscopic examination, the oxide film was removed from the fracture surface by soaking the specimen in a hot solution of potassium permanganate (80 vol.%) and sodium hydroxide (20 vol.%) for 1 h, rinsing in distilled water, soaking for an additional 1 h in a hot solution of ammonium citrate (20 vol.%) and water, and finally rinsing in an ultrasonic bath of acetone. Once the fracture surface was cleaned, the regions of fast/fast loading blocks could be readily distinguished, as seen in Fig. 7. The regions of fast/fast blocks were then mapped onto a large composite photomicrograph of the fracture surface. Assuming that each striation corresponds to one cycle, the number of striations between the last observed fast/fast block and the onset of ductile (tensile) failure were counted to verify the location of the last block. The remaining visible fast/fast blocks were numbered sequentially toward the initiation site. Figure 8 is a schematic representation of the fracture surfaces and the probable crack fronts as determined by electron microscopy.

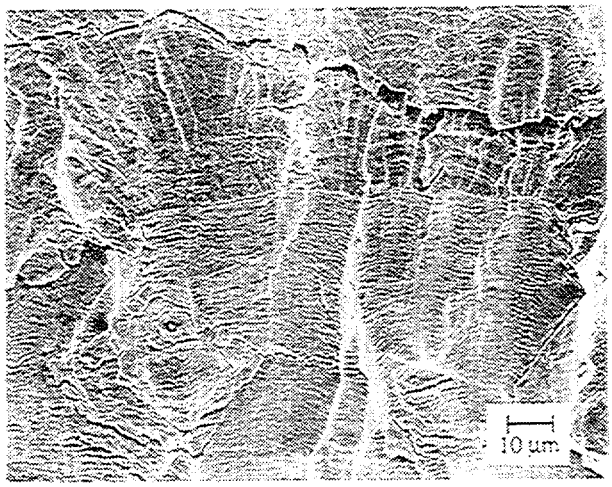

Figure 7. Photomicrograph showing difference in striation spacing formed by fast/fast (top) and slow/fast (bottom) blocks of cycles

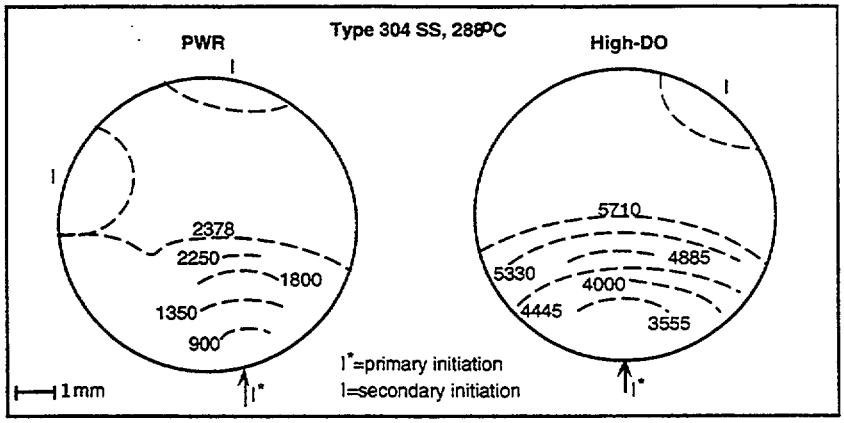

Figure 8. Fracture surface and probable crack front (dashed lines) after various fast/fast loading cycles for PWR and high-DO water environments

Table 3. Fatigue results for Type 304 SS in air and water environments

Test No.	Environment	Strain Range (%)	Strain Rate (%/s) Tensile	Strain Rate (%/s) Comp.	Stress Range (MPa)	Life N_{25} (Cycles)
1801	Air	0.76	0.400	0.40	419.2	24,500
1804	Air	0.50	0.400	0.40	382.8	61,680
1825	Air	0.30	0.040	0.40	394.4	957,160
1805	Air	0.76	0.004	0.40	467.9	14,410
1817	Air	0.50	0.004	0.40	421.7	42,180
1807	PWR	0.51	0.400	0.40	374.6	25,900
1806	PWR	0.73	0.400	0.40	428.9	11,500
1810	PWR	0.77	0.040	0.40	447.6	5,800
1826	PWR	0.29	0.010	0.40	375.8	131,100
1821	PWR	0.76	0.004	0.40	474.3	2,420
1808	PWR	0.77	0.004	0.40	468.3	2,850
1823	PWR	0.51	0.004	0.40	408.2	6,900
1824[a]	PWR	0.75	0.004	0.40	488.5	2,270
1827	High-DO	0.75	0.004	0.40	475.8	3,650
1841[b]	High-DO	0.75	0.004	0.40	483.3	5,657

[a] Every 450 cycles block loaded 500 or 1000 fast/fast cycles at 0.5% strain range and 0.4%/s strain rate.
[b] Every 445 cycles block loaded 700 fast/fast cycles at 0.5% strain range and 0.4%/s strain rate.

2.2.2 Results

Fatigue Life

The fatigue S–N data for Type 304 SS in air and water at 288°C are listed in Table 3; they are plotted in Fig. 9. The ASME mean data curve and the best–fit curves in air, simulated PWR, and high–DO water, based on the statistical model, i.e., Eqs. 6–8, are also shown in Fig. 9. The results indicate a significant decrease in fatigue life in water when compared with fatigue life obtained in air; the reduction in life depends both on strain rate and the DO content of the water. Fatigue life decreases with decreasing strain rate, and the effect is greater in a low–DO PWR environment than in a high–DO environment.

Photomicrographs of the fracture surface of Type 304 SS specimens tested by block loading in water environments are shown in Fig. 10. Both fracture surfaces consist of several cracks that were initiated at differing axial and circumferential locations and did not merge into a single primary crack. The fracture surface of specimens tested at constant strain range typically consist of a single crack or a few cracks that merge to form the final fracture surface.

Fatigue Crack Depth

The depth of the largest crack obtained for the block loading tests in water at 288°C and ≈0.75% strain range is plotted as a function of fatigue cycles in Fig. 11 and as a function of fraction of life in Fig. 12. In these figures, the data for Type 316L SS tested in air at 25°C and ≈0.006–0.02% plastic strain range (which corresponds to ≈0.3–0.32 total strain range) are from Ref. 40. The curve for the uninterrupted test in air at 0.75% strain range and 0.004/0.4%/s tensile/compressive strain rate (shown as a dash–dot line in Fig. 6) was calculated from the best–fit equation of the experimental data for Type 316L SS.[40] Studies on carbon and low–alloy steels[38,47,48] indicate that the fatigue crack size at various life fractions is independent of strain range and strain rate; consequently, the depth of the largest crack at various life fractions is approximately the same at 0.75 and 0.3% strain ranges. The results from this

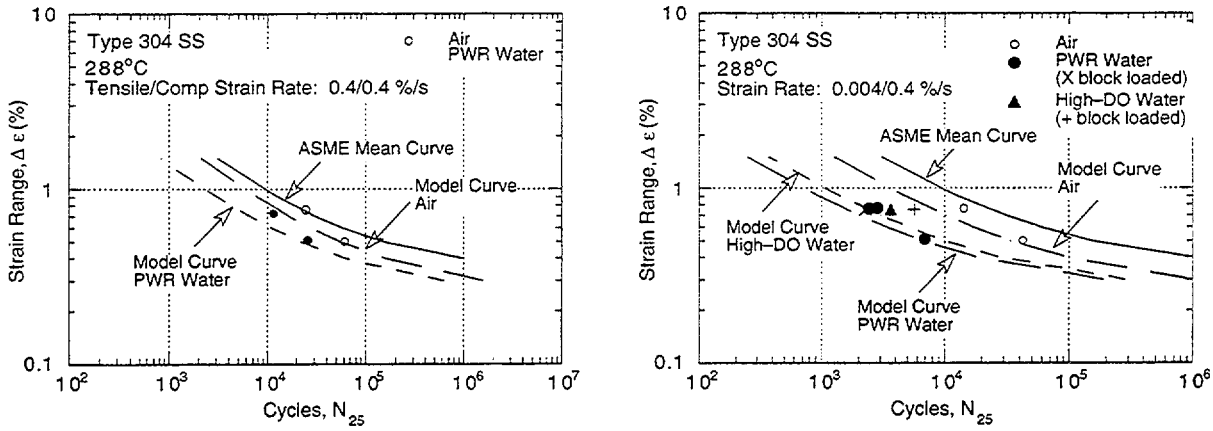

Figure 9. Fatigue strain-vs.-life data for Type 304 SS in air and water environments at 288°C

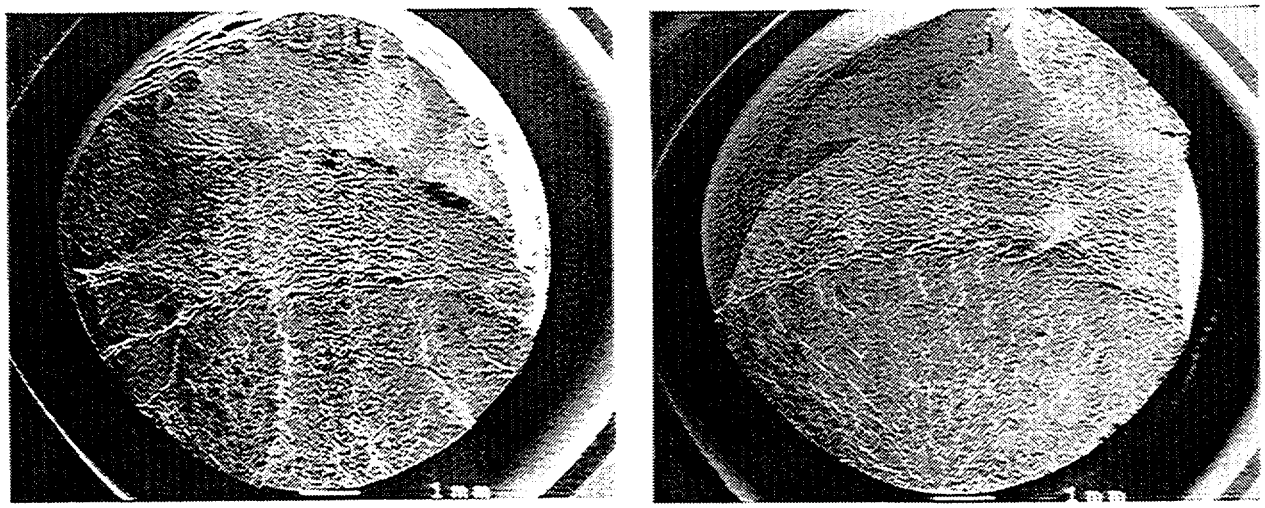

(a) (b)

Figure 10. Photomicrographs of fractured specimens tested with slow/fast and fast/fast block loading in (a) PWR water and (b) high-DO water at 288°C

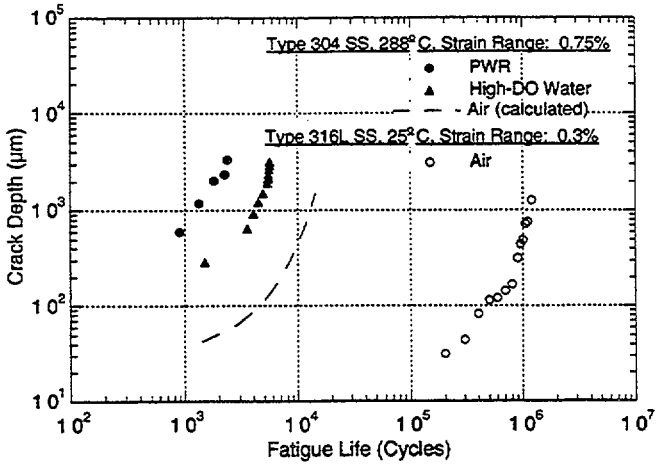

Figure 11. Depth of largest crack plotted as a function of fatigue cycles for austenitic SSs in air and water environments. Data for Type 316L SS taken from Orbtlik et al. (1997).

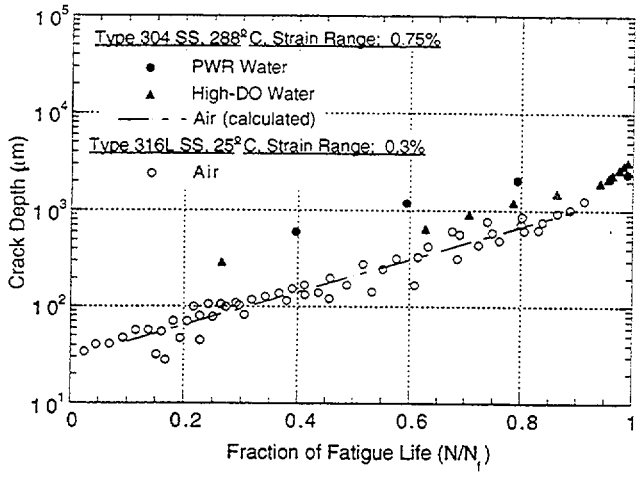

Figure 12.
Depth of largest crack plotted as a function of fraction of life for austenitic SSs in air and water environments. Data for Type 316L SS taken from Orbtlik et al. (1997).

study show that after 1500 cycles the crack lengths in air, high–DO water, and PWR water are ≈40, 300, and 1200 μm, respectively. At the same fraction of life, the crack lengths are longer in water than in air. Furthermore, the crack length in PWR water is greater than in high–DO water.

Crack Growth Rate

The crack growth rates determined from the crack–depth–vs.–cycles data of Fig. 11 are plotted as a function of crack depth in Fig. 13. The CGRs in air are less than those in high–DO water by a factor of 2 and less than those in low–DO PWR water by a factor of 4. The average CGRs at a depth of 1000 μm are 0.28, 0.70, and 1.1 μm/cycle in air, high–DO water, and PWR water, respectively. In Fig. 14 the measured CGRs are shown with the current ASME Section XI reference crack growth curve for austenitic SSs. For cylindrical fatigue specimens, the stress intensity ranges ΔK were determined from the values of ΔJ, which for a small half-circular surface crack[47] are given by

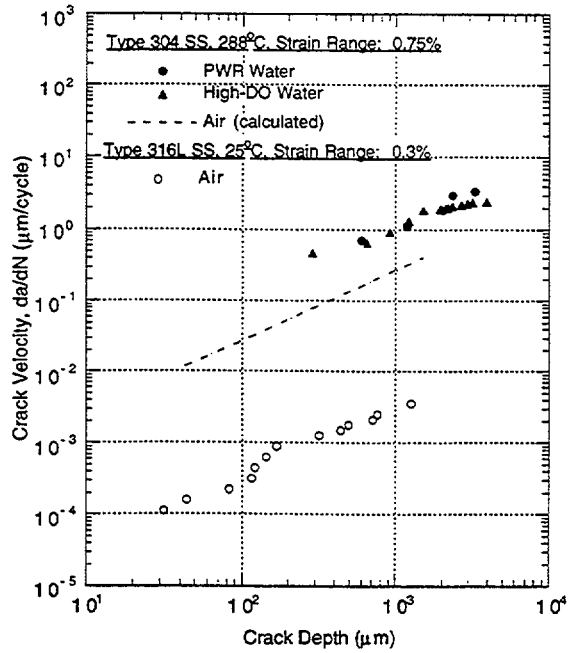

Figure 13.
Crack growth rates, determined from data in Fig. 6, plotted as a function of crack depth for austenitic stainless steels in air and water environments

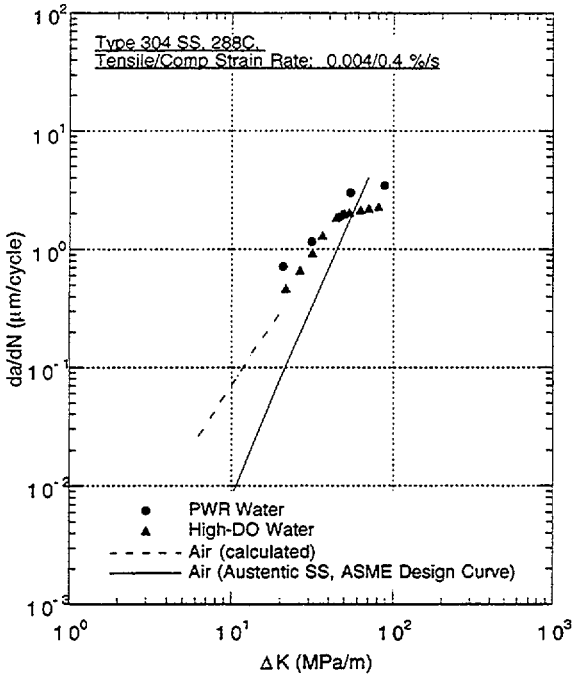

Figure 14.
Crack growth rates, determined from smooth cylindrical fatigue test specimens, and ASME Section XI reference curves for austenitic SSs in air and water environments

$$J = 3.2\left(\frac{\sigma^2}{2E}\right)a + 5.0\left(\frac{\sigma\varepsilon_p}{1+n}\right)a, \qquad (11)$$

where E is the elastic modulus, ε_p is the nominal plastic strain, and a is the crack depth. Modification of the stress intensities associated with conventional cylindrical fatigue specimens was based on rigorous finite-element models.[49] The cyclic stress σ and strain ε are defined as

$$\varepsilon = \frac{\sigma}{E} + \left(\frac{\sigma}{A}\right)^n, \qquad (12)$$

where the constant A and the exponent n were determined from the experimental data.[29] The growth rates in air, shown by the dashed line, were determined from the estimated crack depth-vs.-fatigue life data in air, shown as the dashed curve in Fig. 11.

The results show fair agreement with the ASME Code curve for long cracks. The estimated growth rates in air are greater than those predicted by the Code curve. Fatigue tests are in progress to determine the crack initiation and growth characteristics of austenitic SSs in air. The growth rates in PWR water are marginally greater than those in high-DO water; however, the fatigue life is a factor of ≈2 lower in PWR water. These findings indicate that the decrease in fatigue life in LWR environments is primarily due to the effect of environment during the early stages of crack initiation, i.e., the growth of cracks that are <500 μm deep. The increases in crack growth that are associated with the environment are not consistent with current models, which would generally predict higher environmental CGRs in high-DO environments than in PWR environments.[50,51]

2.2.3 Discussion

The results from the present study indicate that the decrease in fatigue life of austenitic SSs in LWR environments is primarily caused by the effects of the environment on the growth of short cracks. The number of cycles required to produce a 500–μm crack is 300, 8000, and 10,000 for PWR, high–DO, and air, respectively. During the initial stages of fatigue damage (crack sizes of <500 μm), CGRs are more than one order of magnitude higher in low–DO water than in air. Metallographic examination of austenitic SS test specimens indicates that in PWR water, surface cracks grow entirely as tensile cracks, normal to the stress axis (Fig. 15a). In air and high–DO water, surface cracks initially grow as shear cracks that are oriented at an angle of ≈45° to the stress axis and then as tensile cracks normal to the stress axis when slip is no longer confined to shear slip planes (Fig. 15b).

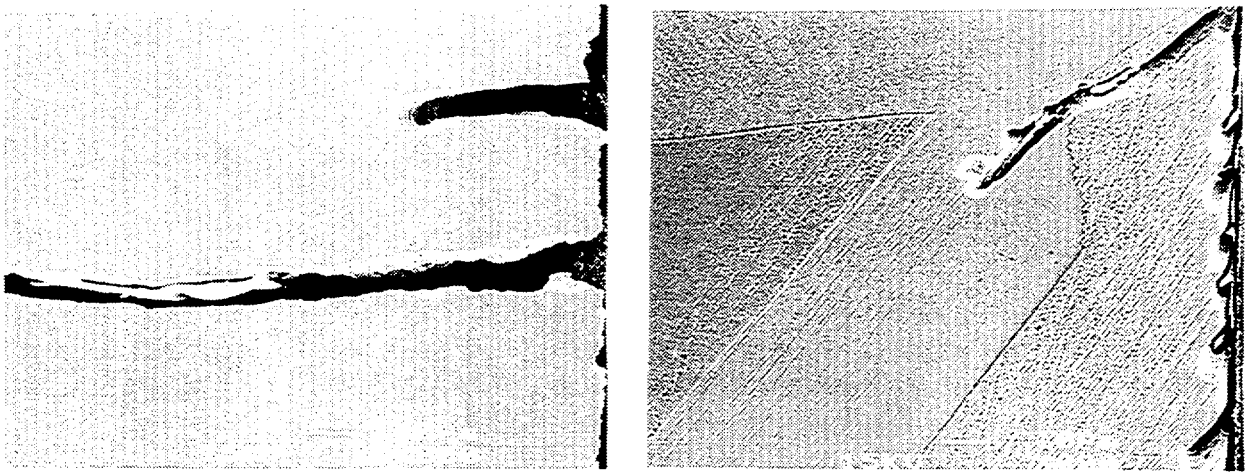

(a) (b)

Figure 15. Photomicrographs of surface cracks along longitudinal sections of Type 316NG SS specimens tested at 288°C in (a) PWR and (b) high–DO water environments

For austenitic SSs, it is difficult to reconcile fatigue lives that are lower in PWR water than in high–DO water in terms of the slip dissolution mechanism despite the absence of Stage I crack growth in low–DO water. Further contradicting the slip dissolution model is the presence of well–defined striations, which are more indicative of H–induced cracking. It is possible that DO has an effect on one of the key elements of corrosion resistance, specifically, the passive oxide film. If DO affects the tenacity of the oxide film, the lower fatigue lives may be attributed to a lower rupture strain for surface oxides in low–DO water than in high–DO water. Work is currently underway to investigate the role of oxide rupture strain in crack growth.

2.2.4 Conclusions

Fatigue tests have been conducted to determine the crack initiation and crack growth characteristics of austenitic SSs in air and LWR environments. Results of fatigue tests that examine the influence of reactor environment on the formation and growth of short cracks in

Type 304 SS are presented. Crack length as a function of fatigue cycles was determined in air and water environments. The significant conclusions are summarized below.

- At the same fraction of life, cracks are longer in water than in air. The CGRs in water are greater than those in air, and the CGRs in PWR water are greater than those in high-DO water.
- The decrease in fatigue life of Type 304 austenitic SS in LWR water is primarily caused by the effects of environment on the growth of short cracks that are <500 μm deep.
- The results from the present study are not consistent with the slip dissolution model for enhanced CGRs in LWR environments. Oxide film rupture strengths and/or H evolution may play a greater role in these environments.

3 Irradiation-Assisted Stress Corrosion Cracking of Austenitic SS

3.1 Introduction

In recent years, failures of reactor-core internal components have increased after accumulating a fluence of >0.5 x 10^{21} n·cm^{-2} (E >1 MeV), or ≈0.7 dpa, in BWRs and at approximately one order of magnitude higher fluences in some PWR components. The general pattern of the observed failures indicates that as nuclear plants age and neutron fluence increases, various nonsensitized austenitic SSs become susceptible to intergranular (IG) failure. Some components are known to have cracked under minimal applied stress. Although most failed components can be replaced (e.g., PWR baffle former bolts), it would be very difficult or impractical to replace some safety-significant structural components (e.g., the BWR top guide, shroud, and core plate). Therefore, the structural integrity of these components at high fluence has been a subject of concern, and extensive research has been conducted to provide an understanding of this type of degradation, which is commonly known as irradiation-assisted stress corrosion cracking (IASCC).[52-72]

Irradiation profoundly affects local coolant water chemistry and component microstructure. Primary material effects of irradiation include alteration of local microchemistry, microstructure, and mechanical properties of the core internal components, which are usually fabricated from ASTM Type 304, 316, or 348 SS. Irradiation produces defects, defect clusters, and defect-impurity complexes in grain matrices and alters the dislocation and dislocation loop structures, leading to radiation-induced hardening, and in many cases, flow localization via dislocation channeling. Irradiation also leads to changes in the stability of second-phase precipitates and the local alloy chemistry near grain boundaries, precipitates, and defect clusters. A grain-boundary microchemistry that significantly differs from the bulk composition can be produced in association with not only radiation-induced segregation but also thermally driven equilibrium and nonequilibrium segregation of alloying and impurity elements.

For many years, irradiation-induced grain-boundary depletion of Cr has been considered to be the primary metallurgical process that causes IASCC. One of the most important factors that has been considered by many investigators to support the Cr-depletion mechanism is the observation that the dependence on water chemistry (i.e., oxidizing potential) of IGSCC of nonirradiated thermally sensitized material and of IASCC of BWR-irradiated solution-

annealed material is similar.[52-54] However, contrary to expectations based on the strong effect of water chemistry implicated in the Cr-depletion mechanism, cracking of control rod cladding and baffle plate bolts has been reported at numerous PWRs (i.e., under nonoxidizing potential). Also, the susceptibility of PWR-irradiated components to IASCC has been shown clearly from expanding-pellet[55] and SSRT[56] tests in PWR water[55] or PWR-simulated water,[56] although PWR water chemistry falls well within the range of the protective electrochemical potential (ECP).[52-54] A direct correlation with grain-boundary Cr concentration and susceptibility of steels to IASCC under BWR conditions does not, however, provide conclusive evidence for the grain-boundary Cr-depletion mechanism.[65]

Other investigators have implicated radiation-induced segregation of ASTM-specified impurities such as Si, P, and S as the primary process that causes IASCC.[55,57,58] The superior resistance of one heat of Type 348 SS that is substantially low in C, Si, P, and S seemed to provide evidence for this implication,[55] and the same rationale was extended to Type 304 SS. However, in direct contradiction, many investigators later reported results that indicated that resistance of high-purity (HP) heats (low in C, Si, S, and P) of Type 304 SS is no better than that of commercial-purity (CP) Type 304 SSs.[59-65] Therefore, it appears that the role of grain-boundary segregation of Si, P, and S is not well established.

Although C significantly increases the yield strength of irradiated SSs, higher C content seems to be either benign or conducive to lower susceptibility to intergranular cracking of irradiated materials.[65] Deleterious effects of O in steels have been reported by Chung et al.[65] and Cookson et al.[66] Indications of the deleterious effect of grain-boundary segregation of N have been reported for BWR neutron absorber tubes.[65] Similar reports suggest that a higher concentration of N is deleterious, at least under BWR conditions.[57,63,67,68] Indications of the deleterious role of N have also been reported for Types 304L and 316L SS that contain C <240 wppm and have been irradiated in BWRs or test reactors at 240-300°C.[62] Kasahara et al.[67] also reported that higher N in Type 316L increased the susceptibility to IASCC, indicating that Type 316LN is a susceptible material. This observation is consistent with the behavior of 316NG reported by Jacobs et al.[57] and Jenssen and Ljungberg.[69] In contrast to this, 316NG irradiated at ≈50°C has been reported to be resistant to intergranular failure at ≈288°C in water that contained 32 ppm DO.[62] Therefore, the role of N appears to be unconvincing, and the optimal range of N concentration is not well defined.

In general, IASCC is characterized by strong heat-to-heat variation in susceptibility, in addition to strong effects of irradiation condition, material type, and grade, even among materials of virtually identical chemical compositions. This indicates that the traditional interpretation based on the role of grain-boundary Cr depletion cannot completely explain the mechanism of IASCC. Thus, although significant grain-boundary Cr depletion is believed by most investigators to play an important role, it has been suspected that other important processes may have been overlooked which could be associated with other minor impurity elements.[65] Therefore, we have initiated a new irradiation testing program to investigate systematically the effects of alloying and impurity elements (Cr, Ni, Si, P, S, Mn, C, and N) on the susceptibility of austenitic SSs to IASCC at several fluence levels.

A test matrix was constructed according to the optimized method of Taguchi.[73,74] Based on the optimized test matrix, eight commercial and 19 laboratory heats of model austenitic SS alloys were, respectively, purchased commercially or fabricated in laboratory.[71] Compositions of the 27 model alloys are given in Table 4. Slow-strain-rate-tensile and 1/4T compact-

tension (CT) specimens were prepared from the alloys and have been irradiated in the Halden reactor at 289°C in He gas to three fluence levels (Table 5).[71] Susceptibility to IASCC was determined by SSRT testing of the irradiated specimens in simulated BWR water and post testing fractographic examination in a scanning electron microscope (SEM). This report summarizes the results obtained to date on 16 model austenitic SS alloys that were irradiated at 288°C in He in the Halden reactor to a fluence of ≈0.3 x 10^{21} n·cm^{-2} (E > 1 MeV) and nine alloys that were irradiated to a fluence of ≈0.9 x 10^{21} n·cm^{-2}.

Table 4. Elemental composition (wt.%) of 27 commercial and laboratory model austenitic stainless steel alloys irradiated in Halden reactor.

ANL ID[a]	Source Heat ID	Ni	Si	P	S	Mn	C	N	Cr	O	B	Mo or Nb
C1	DAN-70378	8.12	0.50	0.038	0.002	1.00	0.060	0.060	18.11	-	<0.001	-
L2	BPC-4-111	10.50	0.82	0.080	0.034	1.58	0.074	0.102	17.02	0.0065	<0.001	-
C3	PNL-C-1	8.91	0.46	0.019	0.004	1.81	0.016	0.083	18.55	-	<0.001	-
L4	BPC-4-88	10.20	0.94	0.031	0.010	1.75	0.110	0.002	15.80	-	<0.001	-
L5	BPC-4-104	9.66	0.90	0.113	0.028	0.47	0.006	0.033	21.00	-	<0.001	-
L6	BPC-4-127	10.00	1.90	0.020	0.005	1.13	0.096	0.087	17.10	0.0058	<0.001	-
L7	BPC-4-112	10.60	0.18	0.040	0.038	1.02	0.007	0.111	15.40	0.0274	<0.001	-
L8	BPC-4-91	10.20	0.15	0.093	0.010	1.85	0.041	0.001	18.30	-	<0.001	-
C9	PNL-C-6	8.75	0.39	0.013	0.013	1.72	0.062	0.065	18.48	-	<0.001	-
C10	DAN-23381	8.13	0.55	0.033	0.002	1.00	0.060	0.086	18.19	-	<0.001	-
L11	BPC-4-93	8.15	0.47	0.097	0.009	1.02	0.014	0.004	17.40	-	<0.001	-
C12	DAN-23805	8.23	0.47	0.018	0.002	1.00	0.060	0.070	18.43	-	<0.001	-
L13	BPC-4-96	8.18	1.18	0.027	0.022	0.36	0.026	0.001	17.40	-	<0.001	-
L14	BPC-4-129	7.93	1.49	0.080	0.002	1.76	0.107	0.028	15.00	0.0045	<0.001	-
L15	BPC-4-126	8.00	1.82	0.010	0.013	1.07	0.020	0.085	17.80	0.0110	<0.001	-
C16	PNL-SS-14	12.90	0.38	0.014	0.002	1.66	0.020	0.011	16.92	-	<0.001	-
L17	BPC-4-128	8.00	0.66	0.090	0.009	0.48	0.061	0.078	15.30	0.0092	<0.001	-
L18	BPC-4-98	8.13	0.14	0.016	0.033	1.13	0.080	0.001	18.00	-	<0.001	-
C19	DAN-74827	8.08	0.45	0.031	0.003	0.99	0.060	0.070	18.21	-	<0.001	-
L20	BPC-4-101	8.91	0.017	0.010	0.004	0.41	0.002	0.002	18.10	-	<0.001	-
C21[b]	DAN-12455	10.24	0.51	0.034	0.001	1.19	0.060	0.020	16.28	-	<0.001	Mo 2.08
L22[c]	BPC-4-100	13.30	0.024	0.015	0.004	0.40	0.003	0.001	16.10	-	<0.001	Mo 2.04
L23[d]	BPC-4-114	12.04	0.68	0.030	0.047	0.96	0.043	0.092	17.30	0.0093	<0.001	Nb 1.06
L24[e]	BPC-4-105	12.30	0.03	0.007	0.005	0.48	0.031	0.002	16.90	0.0129	<0.001	Nb 1.72
L25C3	BPC-4-133	8.93	0.92	0.020	0.008	1.54	0.019	0.095	17.20	0.0085	0.010	-
L26C19	BPC-4-131	8.09	0.79	0.004	0.002	0.91	0.070	0.089	17.20	0.0080	<0.001	-
L27C21	BPC-4-132	10.30	0.96	0.040	0.002	0.97	0.057	0.019	15.30	0.0058	0.030	Mo 2.01

[a]First letters "C" and "L" denote commercial and laboratory heats, respectively.
[b]Commercial-purity Type 316 SS.
[c]High-purity Type 316 SS.
[d]Commercial-purity Type 348 SS.
[e]High-purity Type 348 SS.

Table 5. Summary of specimens per alloy, irradiation fluence, and postirradiation test type.

ANL Alloy ID	SSRT Test			Uniaxial Constant Load Test			J-R or Crack Growth Rate Test		
	high[a]	medium[a]	low[a]	high	medium	low	high	medium	low
C1	1	1	1	–	–	–			
L2	1	1		–	–	–	1	1	
C3	1	1	1	–	–	–	1	1	1
L4	1	1	1	–	–	–	–	–	–
L5	1	1	1	–	–	–	1		
L6	1	1	–	–	–	–	–	–	–
L7	1	1	–	–	–	–	–	–	–
L8	1	1	1	–	–	–	–	–	–
C9	1	1	1	–	–	–	–	–	–
C10	1	1	1	–	–	–	–	–	–
L11	1	1	1	–	–	–	–	–	–
C12	1	1	1	–	–	–	–	–	–
L13	1	1	1	–	–	–	–	–	–
L14	1	1	–	–	–	–	1		
L15	1	1	–	–	–	–	–	–	–
C16	1	1	1	–	–	–	1	1	–
L17	1	1	–	–	–	–	–	–	–
L18	1	1	1	–	–	–	1	1	
C19	5	1	1	4	4	–	1	1	1
L20	5	1	1	4	4	–	1	1	1
C21	1	1	1	–	–	–	1	1	1
L22	1	1	1	–	–	–	1	1	–
L23	1	1	–	–	–	–	1	–	–
L24	1	1	–	–	–	–	1	–	–
L25C3	3	–	–	–	–	–	–	–	–
L26C19	3	–	–	–	–	–	–	–	–
L27C21	2	–	–	–	–	–	–	–	–

[a]Fluence level in 10^{21} n·cm^{-2}, high ≈ 2.5, medium ≈ 0.9, and low ≈ 0.3.

3.2 Slow–Strain–Rate Tensile Testing of Model Austenitic SSs Irradiated in the Halden Reactor (H. M. Chung, W. E. Ruther, and R. V. Strain)

Slow–strain–rate tensile tests and fractographic analysis with a SEM have been completed for the 16 alloys that were irradiated to a fluence of ≈0.3 x 10^{21} n·cm^{-2} (E > 1 MeV) at ≈288°C in a He environment in the Halden reactor. Initial tests were also conducted on nine alloys of the 24 "medium–fluence" alloy specimens irradiated to ≈0.9 x 10^{21} n·cm^{-2} (E > 1 MeV). In addition to the irradiated specimens, unirradiated control specimens were also tested under the same conditions to provide data on baseline properties. Updated test results on unirradiated specimens are summarized in Tables 6 and 7. All SSRT tests were conducted at 289°C in simulated BWR water that contained ≈8 ppm DO. Conductivity and pH of the water were kept at ≈0.07–0.10 and 6.3–6.8, respectively. Strain rate was held constant at 1.65 x 10^{-7} s^{-1}. Electrochemical potential was measured at the effluent side at regular intervals.

3.2.1 SSRT Testing and Fractographic Analysis of Low–Fluence Specimens

Feedwater chemistry (i.e., DO, ECP, conductivity, and pH) and results from SSRT testing (i.e., 0.2%–offset yield strength, maximum strength, uniform plastic strain, and total plastic strain) are summarized in Tables 8 and 9, respectively, for "low–fluence" specimens, i.e., the specimens irradiated to ≈0.3 x 10^{21} n·cm^{-2} (E > 1 MeV). Also shown in these tables are results of SEM fractographic analysis of the failure mode (i.e., ductile, intergranular, and

Table 6. Results of SSRT[a] tests and SEM fractography of nonirradiated control specimens of model austenitic stainless steel alloys.

		Feedwater Chemistry				SSRT Parameters				Fracture Behavior		
Ident. No.	SSRT No.	Oxygen Conc. (ppm)	Average ECP (mV SHE)	Cond. at 25°C ($\mu S \cdot cm^{-1}$)	pH at 25°C	Yield Stress (MPa)	Max. Stress (MPa)	Uniform Elong. (%)	Total Elong. (%)	TGSCC[b] (%)	IGSCC (%)	TGSCC + IGSCC (%)
L23-4	CHR-1	8.6	+228	0.07	6.65	332	480	15.6	17.0	15	0	15
L7-4	CHR-2	8.0	+217	0.07	7.37	195	370	2.5	5.2	20	0	20
L7-B1	CHR-7					282	676	42.3	43.9	0	0	0
L14-4	CHR-3	8.6	+208	0.07	7.37	240	474	41.8	44.2	0	0	0
L17-4	CHR-4	7.5	+262	0.06	7.09	189	412	11.6	13.3	60	0	60
L17-B1	CHR-19	7.8	+166	0.08	6.71	184	447	30.1	31.2	8	0	8
L6-4	CHR-5	7.9	+256	0.08	6.85	227	545	43.0	44.5	0	0	0
L27-4	CHR-6	9.3	+247	0.08	6.96	298	483	20.6	22.9	0	0	0
L26-4	CHR-8	9.4	+223	0.07	6.65	184	596	38.2	40.2	0	0	0
L2-4	CHR-9	8.6	+292	0.06	6.55	193	348	6.6	7.8	57	0	57
L25-4	CHR-10	8.2	+239	0.06	6.42	184	458	25.5	27.0	0	0	0
L15-4	CHR-11	8.2	+195	0.06	6.32	218	512	36.7	37.9	0	0	0
L24-4	CHR-12	8.4	+200	0.07	6.20	352	461	10.4	12.3	10	0	10
C1-15	CHR-13	8.1	+187	0.07	6.33	179	498	49.4	51.7	0	0	0
C19-B1	CHR-14	8.8	+179	0.08	6.29	178	501	47.4	49.2	0	0	0
C9-B1	CHR-15	8.5	+166	0.07	6.83	178	408	17.4	19.4	32	0	32
C12-B1	CHR-16	8.5	+124	0.07	6.18	182	511	46.0	47.6	0	0	0
C10-B1	CHR-17	9.2	+145	0.07	6.26	174	478	30.6	35.1	0	0	0
C21-9	CHR-18	9.2	+187	0.07	6.41	277	455	48.9	59.5	0	0	0

[a]Tested at 289°C at strain rate of 1.65×10^{-7} s^{-1} in simulated BWR water containing ≈8 ppm DO.
[b]TGSCC = transgranular stress corrosion cracking.

Table 7. Composition of nonirradiated control specimens of model austenitic stainless steel alloys, with results of SSRT tests[a] and SEM fractography

Alloy	Composition (wt.%)									O		YS	UTS	UE	TE	TGSCC	IGSCC	TG+IGSCC
ID	Ni	Si	P	S	Mn	C	N	Cr	Mo/Nb	(wppm)	Remarks[b]	(MPa)	(MPa)	(%)	(%)	(%)	(%)	(%)
L23	12.04	0.68	0.030	0.047	0.96	0.043	0.092	17.30	Nb 1.06	93	CP 348	332	480	15.6	17.0	15	0	15
L7	10.60	0.18	0.040	0.038	1.02	0.007	0.111	15.40		274	High N, O; Low Si, C	195	370	2.5	5.2	20	0	20
L14	7.93	1.49	0.080	0.002	1.76	0.107	0.028	15.00		45	High Si, P, C; Low S	240	585	41.8	44.2	0	0	0
L17	8.00	0.66	0.090	0.009	0.48	0.061	0.078	15.30		90	High P; Low Cr, Mn, S	189	412	11.6	13.3	60	0	60
L17	8.00	0.66	0.090	0.009	0.48	0.061	0.078	15.30		90	High P; Low Cr, Mn, S	184	442	30.1	31.2	8	0	8
L6	10.00	1.90	0.020	0.005	1.13	0.096	0.087	17.10		58	High Si, C, Cr; Low S	227	545	43.0	44.5	0	0	0
L27	10.30	0.96	0.040	0.002	0.97	0.057	0.019	15.30	Mo 2.01	-	CP 316; High B (0.03)	298	483	20.6	22.9	0	0	0
L26	8.09	0.79	0.004	0.002	0.91	0.070	0.089	17.20		80	Low P, S	184	596	38.2	40.2	0	0	0
L2	10.50	0.82	0.080	0.034	1.58	0.074	0.102	17.02		66	High P, S, Mn, N	193	348	6.6	7.8	57	0	57
L25	8.93	0.92	0.020	0.008	1.54	0.019	0.095	17.20		85	High B (0.01)	184	458	25.5	27.0	0	0	0
L15	8.00	1.82	0.010	0.013	1.07	0.020	0.085	17.80		110	High N; Low C	218	512	36.7	37.9	0	0	0
L24	12.30	0.03	0.007	0.005	0.48	0.031	0.002	16.90	Nb 1.72	-	HP 348; Low Si, N	352	461	10.4	12.3	10	0	10
C1	8.12	0.50	0.038	0.002	1.00	0.060	0.060	18.11		-	CP 304; Low S	179	498	49.4	51.7	0	0	0
C19	8.08	0.45	0.031	0.003	0.99	0.060	0.070	18.21		-	CP 304; Low Si, S	178	501	47.4	49.2	0	0	0
C9	8.75	0.39	0.013	0.013	1.72	0.062	0.065	18.48		-	High Mn; Low Si	178	408	17.4	19.4	32	0	32
C12	8.23	0.47	0.018	0.002	1.00	0.060	0.070	18.43		-	Low Si, S, P	182	511	46.0	47.6	0	0	0
C10	8.13	0.55	0.033	0.002	1.00	0.060	0.086	18.19		-	High N; Low S	174	478	30.6	35.1	0	0	0
C21	10.24	0.51	0.034	0.001	1.19	0.060	0.020	16.28	Mo 2.08	-	CP 316; Low B (0.01)	277	455	48.9	59.5	0	0	0

[a]Tested at 289°C at strain rate of 1.65×10^{-7} s^{-1} in simulated BWR water.
[b]HP = High purity; CP = Commercial purity.

transgranular fracture surface morphology) of the specimens. In Table 6, the results of SSRT and SEM fractographic analysis (percent IGSCC, and TGSCC, and combined percent IGSCC+TGSCC) are correlated with compositional characteristics of the low-fluence specimens.

Heat-to-heat variations in susceptibility to IGSCC and TGSCC were significant even at the low fluence of $\approx 0.3 \times 10^{21}$ n·cm^{-2} (E > 1 MeV). High-purity Heat L22 of Type 316L SS that

Table 8. Results of SSRT[a] test and SEM fractography for model austenitic stainless steels irradiated in helium at 289°C to fluence of ≈0.3 x 10^{21} n·cm^{-2} (E > 1 MeV)

		Feedwater Chemistry				SSRT Parameters				Fracture Behavior		
Ident. No.	SSRT No.	Oxygen Conc. (ppm)	Average ECP (mV SHE)	Cond. at 25°C (μS·cm^{-1})	pH at 25°C	Yield Stress (MPa)	Max. Stress (MPa)	Uniform Elong. (%)	Total Elong. (%)	TGSCC (%)	IGSCC (%)	TGSCC + IGSCC (%)
C1-1	HR-1	8.3	+184	0.07	7.03	490	680	13.4	16.6	4	0	4
L5-1	HR-2	9.7	+208	0.07	6.89	513	539	29.5	32.7	2	2	4
L22-1	HR-3	8.0	+236	0.07	6.80	360	596	6.6	9.4	50	15	65
C3-1	HR-4	8.7	+161	0.07	6.68	338	491	27.7	31.6	5	0	5
C16-1	HR-5	8.3	+204	0.08	6.74	370	527	17.6	20.6	2	0	2
L4-1	HR-6	9.0	+202	0.08	6.70	367	542	19.7	22.3	46	0	46
L18-1	HR-7	9.0	+203	0.08	6.33	503	572	6.3	8.8	54	0	54
C10-1	HR-8	8.2	+174	0.07	6.35	523	640	17.4	18.9	6	0	6
C21-1	HR-9	8.1	+149	0.08	6.49	480	620	15.9	19.4	4	0	4
L11-1	HR-10	9.0	+157	0.08	6.17	487	599	2.3	3.8	62	0	62
L13-1	HR-11	8.7	+164	0.08	6.17	248	461	22.1	24.8	8	0	8
L20-1	HR-12	8.4	+174	0.07	6.20	454	552	2.9	5.1	32	2	34
C19-1	HR-13	9.5	+132	0.12	6.36	554	682	10.5	14.7	7	0	7
C9-1	HR-14	8.0	+192	0.11	6.30	522	607	13.4	14.6	24	0	24
C12-1	HR-15	9.0	+195	0.08	6.40	404	589	20.4	24.2	5	0	5
L8-1	HR-16	9.0	+215	0.08	6.60	411	571	15.6	17.9	54	0	54

[a]Tested at 289°C at strain rate of 1.65 x 10^{-7} s^{-1} in simulated BWR water containing ≈8 ppm DO.

Table 9. Composition of model austenitic stainless steels irradiated to fluence of ≈0.3 x 10^{21} n·cm^{-2} (E > 1 MeV), with results of SSRT[a] test and SEM fractography

Alloy	Composition (wt.%)										YS	UTS	UE	TE	TGSCC	IGSCC	TG+IGSCC
ID	Ni	Si	P	S	Mn	C	N	Cr	Mo/Nb	Remarks[b]	(MPa)	(MPa)	(%)	(%)	(%)	(%)	(%)
C1	8.12	0.50	0.038	0.002	1.00	0.060	0.060	18.11	-	Low S, CP 304	490	680	13.4	16.6	4	0	4
L5	9.66	0.90	0.113	0.028	0.47	0.006	0.033	21.00	-	High P, Cr; Low C	513	539	29.5	32.7	2	2	4
L22	13.30	0.024	0.015	0.004	0.40	0.003	0.001	16.10	Mo 2.04	HP 316L, low Si, N	360	596	6.6	9.4	50	15	65
C3	8.91	0.46	0.019	0.004	1.81	0.016	0.083	18.55	-	CP 304L, Low Si	338	491	27.7	31.6	5	0	5
C16	12.90	0.38	0.014	0.002	1.66	0.020	0.011	16.92	-	High Ni; Low Si, S	370	527	17.6	20.6	2	0	2
L4	10.20	0.94	0.031	0.010	1.75	0.110	0.002	15.80	-	High Ni, Mn, C; Low N	367	542	19.7	22.3	38	0	38
L18	8.13	0.14	0.016	0.033	1.13	0.080	0.001	18.00	-	Low Si, N	503	572	6.3	8.8	54	0	54
C10	8.13	0.55	0.033	0.002	1.00	0.060	0.086	18.19	-	Low S, CP 304	523	640	17.4	18.9	6	0	6
C21	10.24	0.51	0.034	0.001	1.19	0.060	0.020	16.28	Mo 2.08	CP 316	480	620	15.9	19.4	4	0	4
L11	8.15	0.47	0.097	0.009	1.02	0.014	0.004	17.40	-	High P; Low Si, C, S, N	487	599	2.3	3.8	62	0	62
L13	8.18	1.18	0.027	0.022	0.36	0.026	0.001	17.40	-	High Si; Low Mn, C, N	248	461	22.1	24.8	8	0	8
L20	8.91	0.017	0.010	0.004	0.41	0.002	0.002	18.10	-	HP 304L, Low Si, N	454	552	2.9	5.1	32	2	34
C19	8.08	0.45	0.031	0.003	0.99	0.060	0.070	18.21	-	Low Si, S	554	682	10.5	14.7	7	0	7
C9	8.75	0.39	0.013	0.013	1.72	0.062	0.065	18.48	-	Low Si; High Mn	522	607	13.4	14.6	24	0	24
C12	8.23	0.47	0.018	0.002	1.00	0.060	0.070	18.43	-	Low Si, P, S	404	589	20.4	24.2	5	0	5
L8	10.20	0.15	0.093	0.010	1.85	0.041	0.001	18.30	-	High Ni, P, Mn; Low Si, N	411	571	15.6	17.8	64	0	64

[a]Tested at 289°C at strain rate of 1.65 x 10^{-7} s^{-1} in simulated BWR water; DO ≈8 ppm.
[b]HP = High purity; CP = Commercial purity.

contains a very low Si concentration (≈0.02 wt.%) exhibited relatively low ductility and the highest susceptibility among the specimens to IGSCC (highest percent IGSCC) during the SSRT test. At this low fluence, the susceptibility of all of the other heats to IGSCC was insignificant. Heat L22 also exhibited relatively high susceptibility to IGSCC after irradiation to ≈0.9 x 10^{21}n·cm^{-2} (E > 1 MeV) (as explained later).

The relatively higher susceptibility of the HP heat of Type 316L SS (i.e., Heat L22) when compared with the CP counterpart (i.e., Heat C21), is similar to that observed for BWR neutron absorber tubes fabricated from HP heats of Type 304 SS,[65] and is of particular interest. In an SSRT experiment similar to the present study, Jenssen and Ljunberg[69] irradiated U-notched rod specimens that had been fabricated from two heats of Type 316 SS,

Table 10. Composition and relative susceptibility to IASCC of Type 316 stainless steels irradiated and tested under BWR-like conditions

Heat ID	Steel Type[a]	Source	Ni	Si	P	S	Mn	C	N	B	Cr	Mo	Irradiated in Reactor	Fluence 10^{21} n·cm^{-2}	Type of SCC Test	Relative Susceptibility
L22	HP 316L	ANL	13.30	0.024	0.015	0.004	0.40	0.003	0.001	<0.001	16.10	2.04	Halden, He	0.3 and 0.9	SSRT in hot cell	high
C21	CP 316	ANL	10.24	0.51	0.034	0.001	1.19	0.060	0.020	<0.001	16.28	2.08	Halden, He	0.3	SSRT in hot cell	low
F	HP 316L	ABB	11.60	0.26	0.021	0.001	1.44	0.009	0.062	0.001	16.69	2.65	BWR	0.3-9.0	SSRT in BWR loop	high
K	CP 316	ABB	12.40	0.64	0.016	0.006	1.73	0.055	0.029	<0.0004	16.51	2.25	BWR	0.3-9.0	SSRT in BWR loop	low

[a]HP = high purity; CP = commercial purity.

then performed postirradiation SSRT tests in a BWR loop under normal oxidizing-water chemistry. As shown in Table 10, one CP heat of Type 316 SS (Heat K) was resistant to IASCC, whereas one HP heat of Type 316L SS (Heat F) was susceptible. Table 10 also presents the composition, irradiation and test conditions, and test results of two heats of Type 316 SS that were tested in our laboratory. The two relatively more susceptible heats in the table (i.e., Heats L22 and F) are characterized by an unusually low Si concentration of <0.26 wt.%, whereas the two relatively more resistant heats (i.e., Heats C21 and K) contain a higher concentration of Si, i.e., >0.5 wt.%.

An observation from a further evaluation of the results in Table 9 was the effect of Si content on irradiation-induced hardening that is manifested by yield strengths of the alloys after irradiation. Maximum strengths of the 16 low-fluence alloys tested in ≈8-ppm-DO water were correlated with concentrations of Si, C, and N. Of the 16 alloys listed in Table 9, three (L22, L11, and L20) contain low concentrations of Si, C, and N, whereas one (L13) contains low concentrations of C and N but a high concentration of Si. Therefore, these four alloys were considered an ideal combination that could provide information on the effect of Si on irradiation-induced hardening. The three alloys that contained low concentrations of Si (0.17-0.47 wt.%) exhibited consistently higher irradiation-induced hardening than the alloy that contained the high Si concentration of ≈1.18 wt.% (see Fig. 16). Consistent with this hardening behavior, the three low-Si alloys exhibited significantly lower ductility than the alloy that contained the high concentration of Si, i.e., 3.8-9.4 vs. 24.8%. This is also shown in Fig. 16.

Susceptibilities of the 16 alloys to TGSCC and IGSCC at the low fluence of ≈0.3 x 10^{21} n·cm^{-2} (E > 1 MeV) are shown in Figs. 17 and 18, respectively. At this relatively low fluence, susceptibility to IGSCC was insignificant except for Type 316L SS HP Alloy L22. In contrast to IGSCC, susceptibility to TGSCC was significant for seven alloys, whereas for the other nine alloys, susceptibility was insignificant. Compositional characteristics of the seven alloys, given in Fig. 17 and Table 9, indicate that Si and N play a role in TGSCC. In Fig. 19, susceptibilities of all 16 alloys to TGSCC are classified and replotted in terms of N and Si concentrations. All alloys that contain <0.01 wt.% N and <1.0 wt.% Si were susceptible, whereas all alloys that contain >0.01 wt.% N or >1.0 wt.% Si were relatively resistant to TGSCC. This result indicates that to delay the onset of and reduce the susceptibility to IASCC, it is helpful to ensure an alloy N concentration >0.01 wt.% and Si concentration >1.0 wt.%. Because practically all commercial heats of Types 304 or 304L SS contain >0.01 wt.% N, to delay onset of and increase resistance to IASCC at low fluence, it seems helpful to ensure a certain minimum concentration of Si in the steels. However, the optimal range of Si concentration is not known at this time, and, from the point of view of other considerations such as welding, corrosion, creep, fatigue, and overall irradiation performance at high fluence, an expanded data base will be needed to evaluate the integral performance of steels that contain high concentrations of Si.

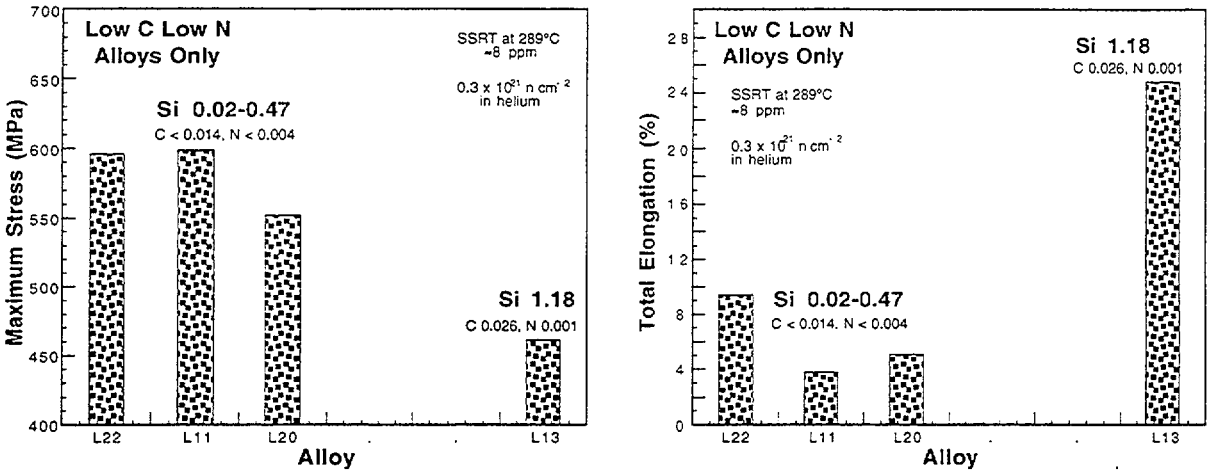

Figure 16. Effects of Si on maximum strength (left) and total elongation (right) of model stainless steel alloys that contain low C (<0.03 wt.%) and low N (<0.004 wt.%) and were irradiated to ≈0.3 x 10^{21} n·cm^{-2} (E > 1 MeV)

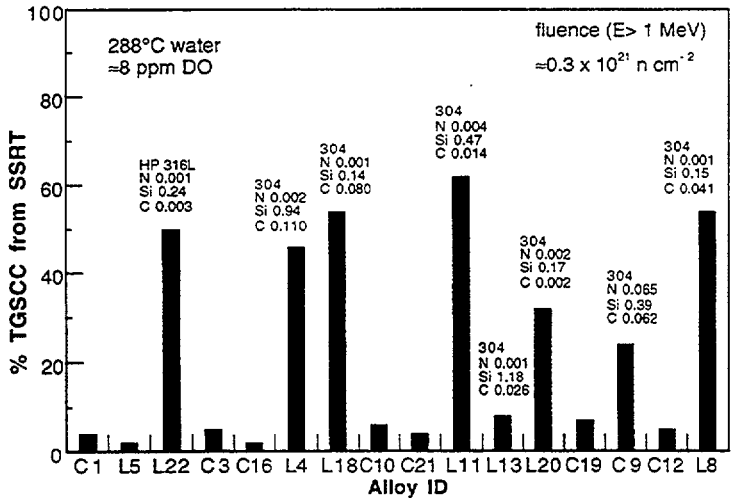

Figure 17.
Percent TGSCC of model stainless steel alloys irradiated in He in Halden reactor to fluence of ≈0.3 x 10^{21} n·cm^{-2} (E > 1 MeV) and tested at 288°C in simulated BWR water

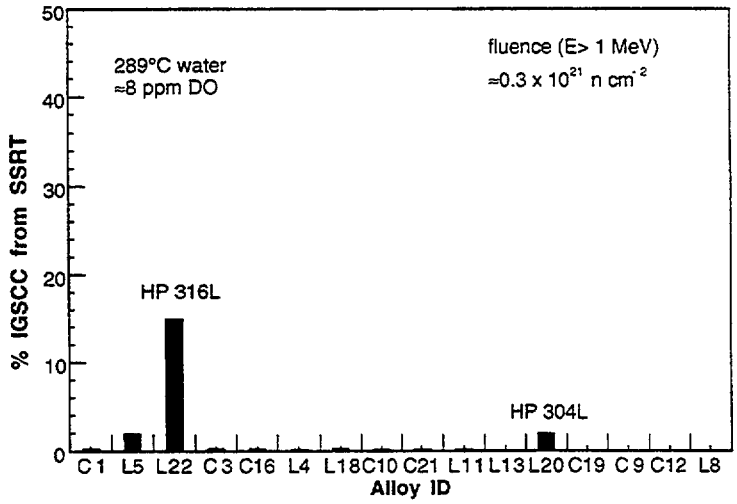

Figure 18.
Percent IGSCC of model stainless steel alloys irradiated in He in Halden reactor to fluence of ≈0.3 x 10^{21} n·cm^{-2} (E > 1 MeV) and tested at 288°C in simulated BWR water containing DO ≈8 ppm

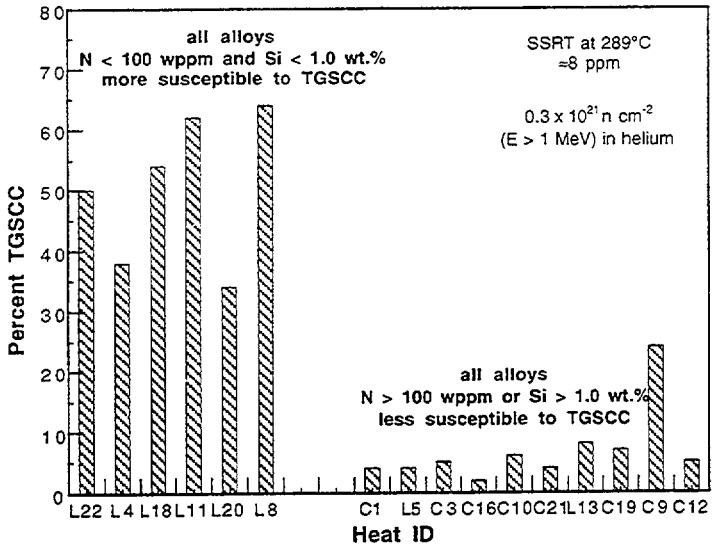

Figure 19.
Susceptibility to TGSCC of model stainless steel alloys, irradiated in He in Halden reactor to fluence of ≈0.3 x 10^{21} n·cm^{-2} (E > 1 MeV) and tested at 288°C in simulated BWR water containing ≈8 ppm DO, classified as a function of N and Si contents of the alloys

Tsukada et al.[63] and Miwa et al.[70] irradiated sheet SSRT specimens of HP Type 304L SS (C 0.003, Si 0.01, Mn 1.36, P 0.001, S 0.0014, and N 0.0014 wt.%), one specimen with and the other without doped ≈0.69 wt.% Si, in He at 240°C in the JRR-3 reactor to a fluence of ≈0.67 x 10^{21} n·cm^{-2} (E > 1 MeV). After SSRT testing of the specimens at 300°C in HP water that contained ≈32 ppm DO, these authors that their high-Si (Si 0.69 wt.%) specimen exhibited significantly higher ductility than their low-Si (Si 0.01 wt.%) specimen, namely, total elongation of ≈21% vs. 11%. At the same time, they observed that the number density of Frank loops was significantly lower in the high-Si specimen than in the low-Si specimen, although the number densities of the "black-dot" defect clusters appeared similar.[73] Because the SSRT test temperature was ≈60°C higher than the irradiation temperature, some fraction of the defect clusters and loops probably annealed out during the test, and various types of interaction could have occurred at ≈240 and ≈300°C between irradiation-induced defect clusters and impurities. Susceptibilities to IGSCC of the two specimens were similar, whereas the high-Si specimen was more susceptible to TGSCC than the low-Si specimen, which is the opposite of the trend that was observed in this study and is summarized in Fig. 19.

These observations, combined with the results in Fig. 16, are a strong indication that Si atoms exert profound effects on irradiation-induced hardening in Types 304 and 304L SSs. That is, Si content <0.5 wt.% is conducive to higher irradiation-induced hardening and lower ductility in BWR-like water after irradiation. In contrast, Si content >1.0 wt.% is conducive to lower irradiation-induced hardening and higher ductility in simulated BWR water after irradiation.

3.2.2 SSRT Testing and Fractographic Analysis of Medium-Fluence Specimens

Initial tests were conducted on nine "medium-fluence" specimens irradiated to ≈0.9 x 10^{21} n·cm^{-2} (E > 1 MeV) (see Tables 11 and 12). For all medium-fluence specimens that were tested, effects of the higher fluence on yield stress, maximum stress, uniform strain, total strain, percent IGSCC, and percent TGSCC were significant; this is shown in Figs. 20A-G. Preliminary results from the tests also indicate that when fluence increased from ≈0.3 x 10^{21} n·cm^{-2} (E > 1 MeV) to ≈0.9 x 10^{21} n·cm^{-2} in the low-N and low-Si alloys (e.g., Heats L22, L18, and L11), susceptibility to TGSCC decreased, and at the same time, susceptibility to IGSCC

increased at the expense of percent TGSCC (Figs. 20E and F). This trend is consistent with that observed for field-cracked BWR components. However, the threshold fluence for the transition from TGSCC to IGSCC appears to differ from alloy to alloy. For example, susceptibility to TGSCC of Alloy C9, a commercial heat of Type 304 SS, still increased when fluence increased from ≈0.3 x 10^{21} n·cm^{-2} (E > 1 MeV) to ≈0.9 x 10^{21} n·cm^{-2}.

Table 11. Results of SSRT[a] test and SEM fractography for model austenitic stainless steels irradiated in He at 289°C to fluence of ≈0.9 x 10^{21} n·cm^{-2} (E > 1 MeV)

		Feedwater Chemistry				SSRT Parameters				Fracture Behavior		
Ident. No.	SSRT No.	Oxygen Conc. (ppm)	Average ECP (mV SHE)	Cond. at 25°C (μS·cm^{-1})	pH at 25°C	Yield Stress (MPa)	Max. Stress (MPa)	Uniform Elong. (%)	Total Elong. (%)	TGSCC (%)	IGSCC (%)	TGSCC + IGSCC (%)
L22-02	HR-17	8.0	+181	0.08	6.77	475	549	4.20	5.82	30	35	65
L11-02	HR-18	8.0	+191	0.08	6.55	820	856	0.43	1.65	50	14	64
L18-02	HR-19	8.0	+193	0.10	6.07	710	755	3.98	5.05	38	14	52
L20-04	HR-20	8.0	+225	0.07	6.75	515	574	1.85	3.36	erratic press., test invalid		
L20-05	HR-26	9.0	+182	0.09	3.62	670	743	0.37	1.03	0	0	0
C9-02	HR-21	8.0	+240	0.07	6.47	651	679	1.42	2.50	62	22	84
L17-02	HR-22	8.0	+198	0.07	6.42	574	654	2.02	3.08	44	41	85
L7-02	HR-23	8.0	+215	0.07	6.03	490	531	0.24	2.44	38	54	92
C10-02	HR-24	7.0	+221	0.07	5.26	651	706	6.35	9.25	14	0	14
C3-02	HR-25	8.0	+240	0.07	6.34	632	668	16.72	19.74	9	4	13

[a]Tested at 289°C at strain rate of 1.65 x 10^{-7} s^{-1} in simulated BWR water containing ≈8 ppm DO.

Table 12. Composition of model austenitic stainless steels irradiated to fluence of ≈0.9 x 10^{21} n·cm^{-2} (E > 1 MeV) and results of SSRT[a] test and SEM fractography

Alloy	Composition (wt.%)										YS	UTS	UE	TE	TGSCC	IGSCC	TG+IGSCC
ID	Ni	Si	P	S	Mn	C	N	Cr	Mo/Nb	Remarks[b]	(MPa)	(MPa)	(%)	(%)	(%)	(%)	(%)
L22-02	13.30	0.024	0.015	0.004	0.40	0.003	0.001	16.10	Mo 2.04	HP 316L; Low Si, N	475	549	4.20	5.82	30	35	65
L11-02	8.15	0.47	0.097	0.009	1.02	0.014	0.004	17.40	-	high P; low Si, C, S, N	820	856	0.43	1.65	50	14	64
L18-02	8.13	0.14	0.016	0.033	1.13	0.080	0.001	18.00	-	low Si, N	710	755	3.98	5.05	38	14	52
L20-04	8.91	0.017	0.010	0.004	0.41	0.002	0.002	18.10	-	HP 304L; low Si, N, Mn	515	574	1.85	3.36	erratic pressure, test invalid		
L20-05	8.91	0.017	0.010	0.004	0.41	0.002	0.002	18.10	-	HP 304L; low Si, N, Mn	670	743	0.37	1.03	0	0	0
C9-02	8.75	0.39	0.013	0.013	1.72	0.062	0.065	18.48	-	low Si; high Mn	651	679	1.42	2.50	62	22	84
L17-02	8.00	0.66	0.090	0.009	0.48	0.061	0.078	15.30	-	high P; low Cr, Mn, S	574	654	2.02	3.08	44	41	85
L7-02	10.60	0.18	0.040	0.038	1.02	0.007	0.111	15.40	O 0.0274	high N, O; low Si, C	490	531	0.24	2.44	38	54	92
C10-02	8.13	0.55	0.033	0.002	1.00	0.060	0.086	18.19	-	CP 304; low S; high N	651	706	6.35	9.25	14	0	14
C3-02	8.91	0.46	0.019	0.004	1.81	0.016	0.083	18.55	-	CP 304L; high Mn, N; low S	632	668	16.72	19.74	9	4	13

[a]Tested at 289°C at strain rate of 1.65 x 10^{-7} s^{-1} in simulated BWR water containing ≈8 ppm DO.
[b]HP = High purity; CP = Commercial purity.

Susceptibility to IGSCC of all alloys that contain <0.5 wt.% Si (i.e., L22, L18, L11, C9, and L7) increased significantly when fluence increased from ≈0.3 x 10^{21} n·cm^{-2} (E > 1 MeV) to ≈0.9 x 10^{21} n·cm^{-2} (Fig. 20F), indicating deleterious effect of low concentration of Si. That is, under otherwise similar conditions, a low concentration of Si appears to promote susceptibility to TGSCC and IGSCC at relatively low fluences.

There was also a strong indication that a low concentration of Cr (<15.5 wt.%) promotes susceptibility of Type 304 SS to IASCC. For the same fluence level of ≈0.9 x 10^{21} n·cm^{-2} (E > 1 MeV), the susceptibilities to IGSCC of L17 (Cr ≈15.3 wt.%) and L7 (Cr ≈15.4 wt.%) were significantly higher than those of other alloys that contain normal Cr concentrations of ≈18 wt.% (Fig. 20F). Consistent with this observation, Alloy L5, which contains an unusually high Cr concentration of ≈21.0 wt.% was resistant to both TGSCC and IGSCC at ≈0.3 x 10^{21} n·cm^{-2} (E > 1 MeV) (Figs. 20E and F, respectively). This alloy also contains a relatively high Si concentration of ≈0.90 wt.%. The relatively good performance of alloy L5 is also manifested

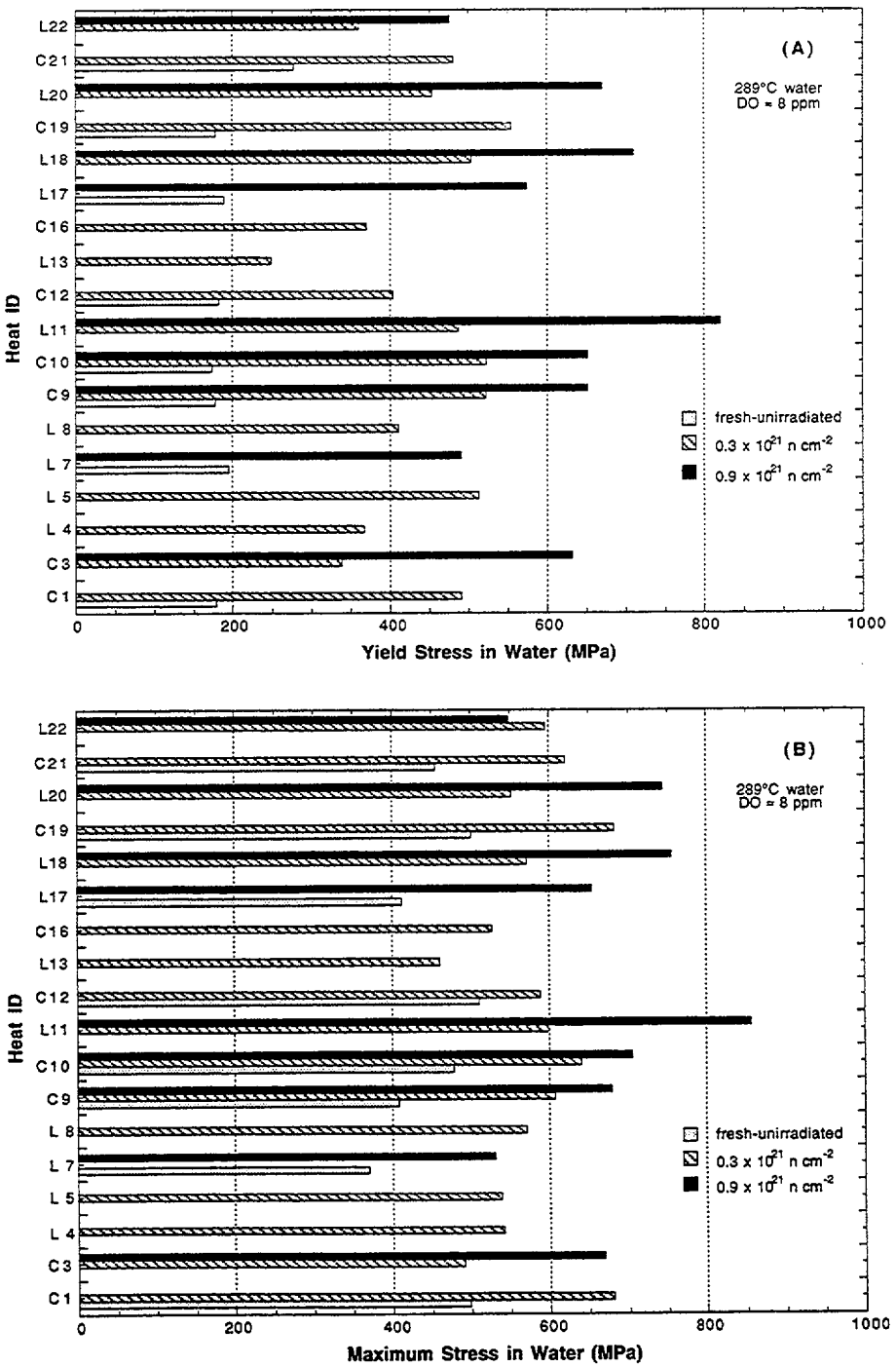

Figure 20. Effects of fluence on (A) yield strength, (B) maximum strength, (C) uniform elongation, (D) total elongation, (E) percent TGSCC, (F) percent IGSCC, and (G) percent TGSCC + IGSCC measured in 289°C water containing ≈8 ppm DO

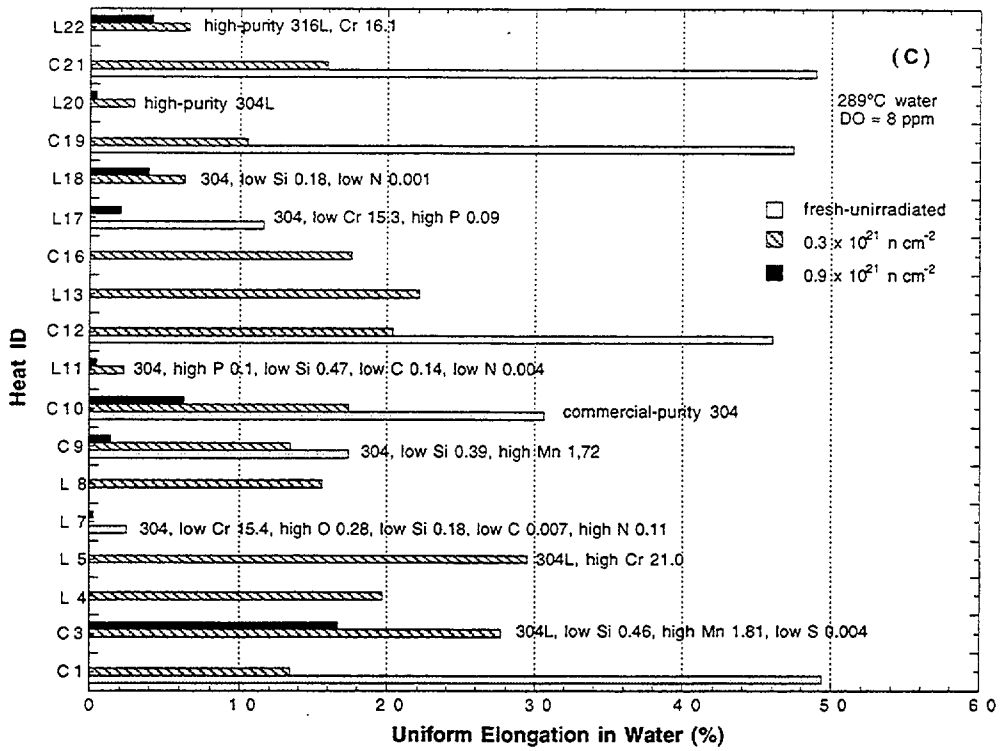

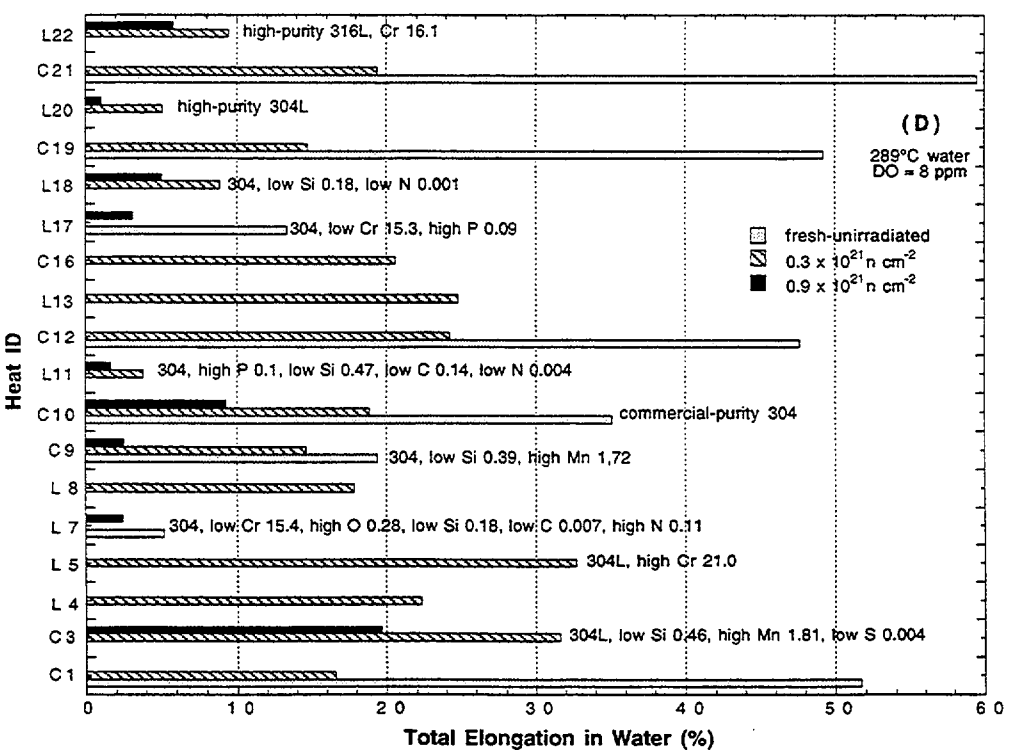

Figure 20. Continued.

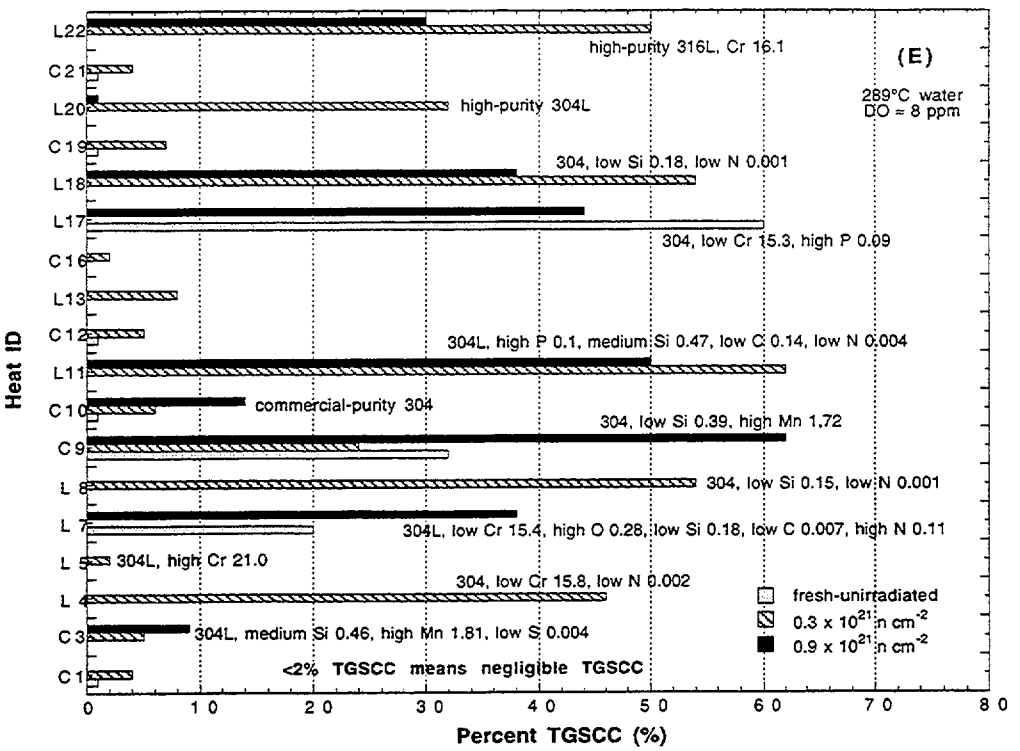

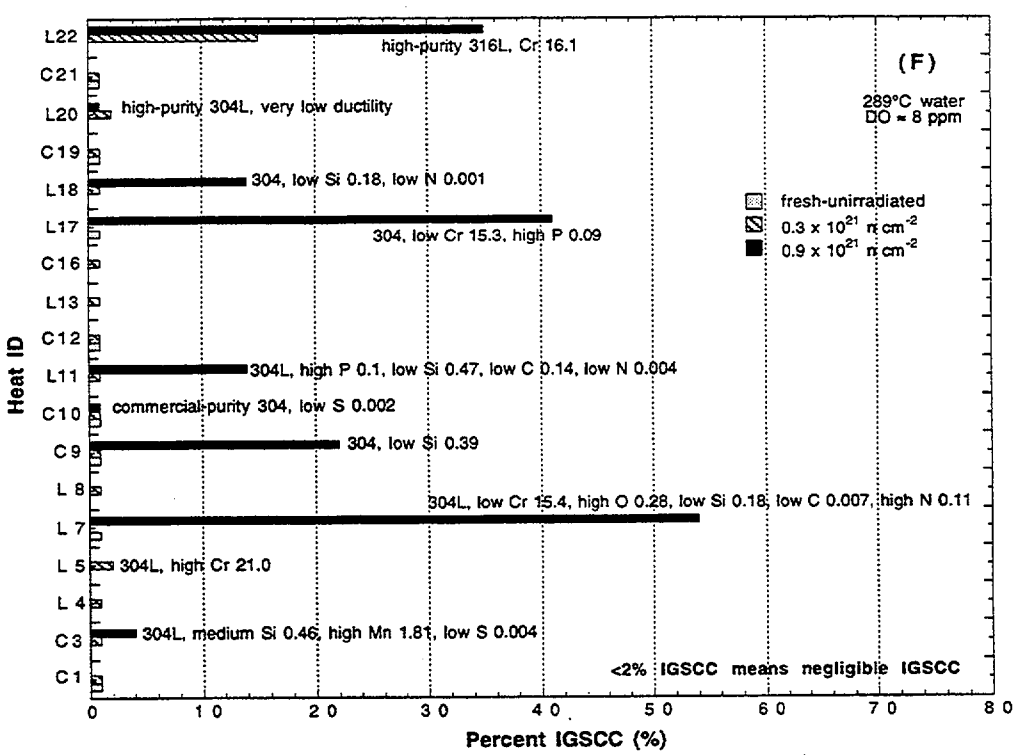

Figure 20. Continued.

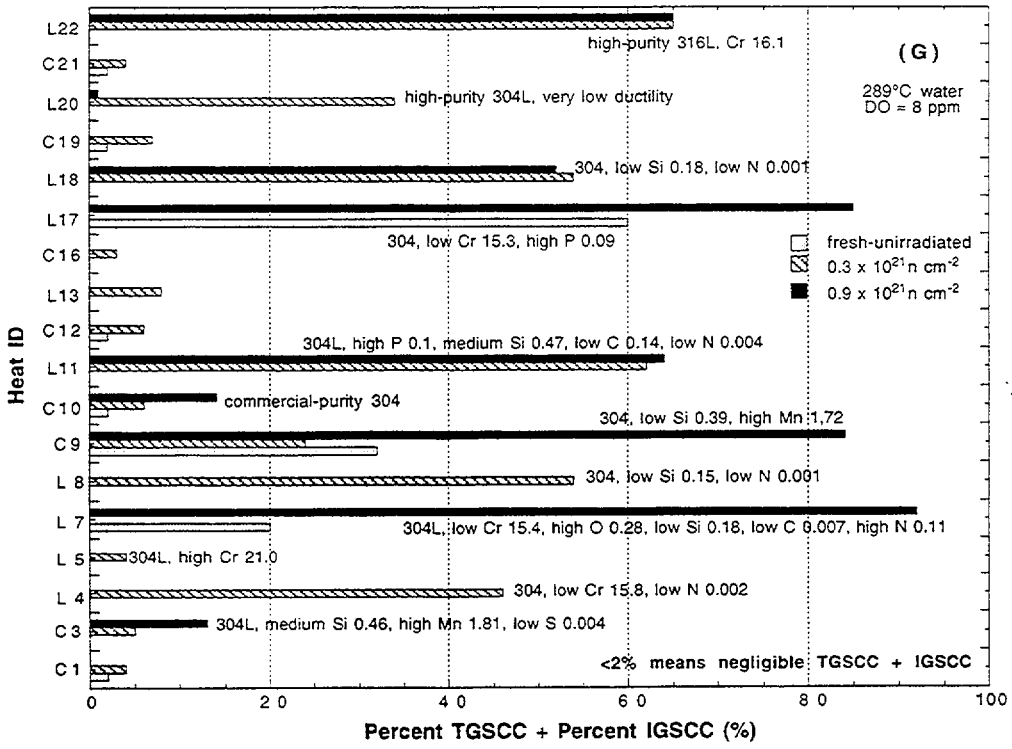

Figure 20. Continued.

by the fact that its ductility is the highest among all of the alloys that were irradiated to ≈0.3 x 10^{21} n·cm^{-2} (E > 1 MeV) (Fig. 20D).

Alloy L7, a laboratory heat of Type 304L SS, exhibited significant susceptibility to TGSCC in the nonirradiated state and the highest susceptibility to IGSCC after irradiation to ≈0.9 x 10^{21} n·cm^{-2} (E > 1 MeV). It appears that the high susceptibility to IASCC of this alloy is related to several deleterious compositional characteristics, i.e., an unusually low concentration of Cr (≈15.3 wt.%), unusually high concentration of O (≈0.027 wt.%),[61,65,71,74] unusually low concentration of Si (≈0.18 wt.%), and unusually low concentration of C (≈0.007 wt.%). This finding lends support to a view that IASCC is influenced by many alloying and impurity elements in a complex manner rather than by a single process of grain-boundary Cr depletion.[65]

There are also indications that a combination of a high concentration of Mn and a low concentration of S is beneficial. For example, Alloy C3, a CP heat of Type 304L SS that contains ≈1.81 wt.% Mn and ≈0.004 wt.% S exhibited unusually high ductility (>20%), low percent TGSCC (<9%), and low percent IGSCC (<4%) after irradiation to ≈0.3 x 10^{21} n·cm^{-2} and ≈0.9 x 10^{21} n·cm^{-2} (E > 1 MeV) (Figs. 20D, E, and F, respectively). However, conclusive evidences for the effect of Mn and S must be established on the basis of more comprehensive data that must be obtained on the whole test matrix after it is irradiated to higher fluences of ≈0.9 x 10^{21} n·cm^{-2} (E > 1 MeV) and ≈2.5 x 10^{21} n·cm^{-2}.

3.3 Fracture Toughness J–R Test of Austenitic Stainless Steels Irradiated in the Halden Reactor (E. E. Gruber and O. K. Chopra)

Austenitic stainless steels are used extensively as structural alloys in reactor pressure vessel internal components because of their high strength, ductility, and fracture toughness. Fracture of these steels occurs by stable tearing at stresses well above the yield stress, and tearing instabilities require extensive plastic deformation. However, exposure to high levels of neutron irradiation for extended periods changes the microstructure and degrades the fracture properties of these steels. Irradiation leads to a significant increase in yield strength and reduction in ductility and fracture resistance of austenitic SSs.[75–77]

Neutron irradiation of austenitic SSs at temperatures below 400°C leads to the formation of a substructure with very fine defects that consist of small (<5 nm) vacancy and interstitial loops or "black spots" and larger (>5 nm) faulted interstitial loops.[78–80] The latter are obstacles to dislocation motion and lead to matrix strengthening and increase in tensile strength. Also, irradiation-induced defects cause loss of ductility and reduced strain hardening capacity of the material. The effects of radiation on various austenitic SSs vary significantly and appear to be related to minor differences in the composition of the steels; the composition can influence the stacking fault energy and/or irradiation-induced microstructure. As the yield strength approaches ultimate strength, planar slip or dislocation channeling is promoted and leads to pronounced degradation in the fracture resistance of these steels.[77] In general, higher stacking-fault energy enhances and cold working inhibits dislocation channeling.

The effect of neutron exposure on the fracture toughness J_{ic} of austenitic SSs irradiated at 350–450°C is shown in Fig. 21.[81–89] The effects of irradiation may be divided into three regimes: little or no loss of toughness below a threshold exposure of ≈1 dpa, substantial decrease in toughness at exposures of 1–10 dpa, and no effect on toughness above a saturation exposure of 10 dpa. The effect is largest in high-toughness steels. The degradation in fracture properties saturates at a J_{ic} value of ≈30 kJ/m^2 (or equivalent critical stress

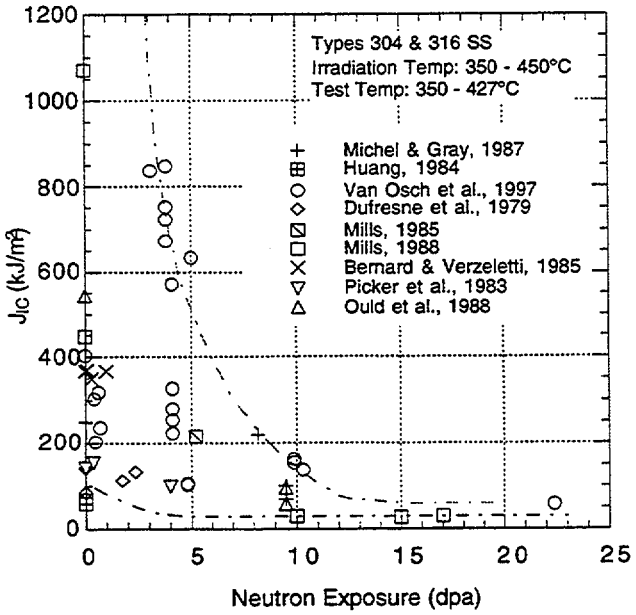

Figure 21.
Fracture toughness J_{IC} as a function of neutron exposure for austenitic Types 304 and 316 stainless steel

intensity factor K_{jc} of 70 MPa $m^{0.5}$). Also, the failure mechanism changes from dimple fracture to channel fracture.

The existing fracture toughness test data have been obtained at temperatures above 350°C; fracture toughness results that are relevant to LWRs are very limited.[76] This paper presents fracture toughness J–R curves for several heats of Type 304 SS that were irradiated to fluence levels of ≈0.3 x 10^{21} n·cm^{-2} (E > 1 MeV) at ≈288°C in a He environment in the Halden boiling heavy–water reactor.

3.3.1 Experimental

Fracture toughness J–R curve tests have been conducted on several heats of Type 304 SS that were irradiated to fluence levels of ≈0.3 x 10^{21} n·cm^{-2} (E > 1 MeV) at ≈288°C in a He environment in the Halden boiling heavy–water reactor. The tests were performed on 1/4–T CT specimens in air at 288°C according to the requirements of ASTM Specification E 1737 for "J–Integral Characterization of Fracture Toughness." The composition of the various heats of Type 304 SS is presented in Table 13. Figure 22 shows the configuration of the CT specimens that were irradiated in the Halden reactor. Although the Halden specimens are rectangular, their dimensions are similar to those of disk–shaped compact tension DC(T) specimens. Calculations of crack length and J–integral were performed with the correlations recommended for DC(T) specimens in ASTM Specification E 1737.

Table 13. Composition (wt.%) of Type 304 SS alloys irradiated in the Halden Reactor

Alloy ID[a]	Vendor Heat ID	Analysis	Ni	Si	P	S	Mn	C	N	Cr	O[b]
L2	BPC–4–111	Vendor	10.50	0.82	0.080	0.034	1.58	0.074	0.102	17.02	66
		ANL									
C16	PNL–SS–14	Vendor	12.90	0.38	0.014	0.002	1.66	0.020	0.011	16.92	–
		ANL	12.32	0.42	0.026	0.003	1.65	0.029	0.011	16.91	157
C19	DAN–74827	Vendor	8.08	0.45	0.031	0.003	0.99	0.060	0.070	18.21	–
		ANL	8.13	0.51	0.028	0.008	1.00	0.060	0.068	18.05	200
L20	BPC–4–101	Vendor	8.91	0.17	0.010	0.004	0.41	0.002	0.002	18.10	–
		ANL	8.88	0.10	0.020	0.005	0.47	0.009	0.036	18.06	940

[a]First letters "C" and "L" denote commercial and laboratory heats, respectively.
[b]In wppm.

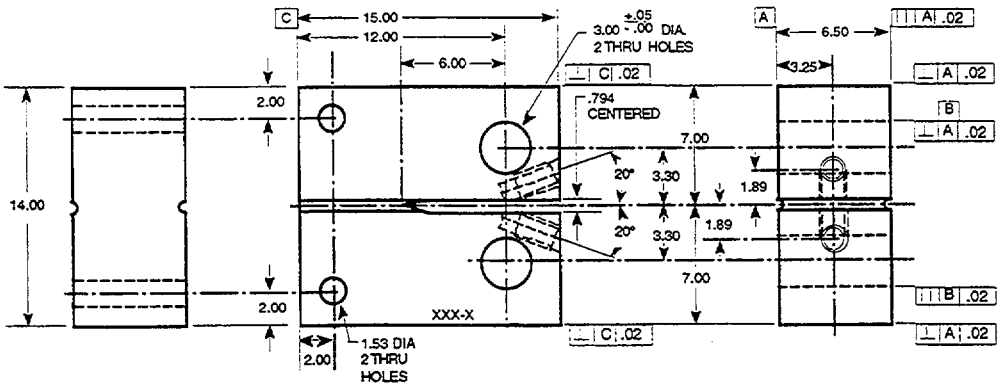

Figure 22. Configuration of compact-tension specimen for this study. Dimensions in mm.

The fracture toughness test facility is designed for in-cell testing, with the hydraulic actuator, test train, furnace, and other required equipment mounted on top of a portable, wheeled cart that can be easily rolled into the cell. The detailed description of the test facility and procedures have been presented elsewhere.[90] Specimen extension is monitored and controlled outside of the high-temperature zone. The displacement of load points (center of the loading pins) is determined by subtracting the machine compliance from the measured extension.

The fatigue precracked specimens were loaded at a constant extension rate and the tests were interrupted periodically to determine the crack length. The specimen was held at constant extension to measure crack length by both the DC potential drop and elastic unloading compliance techniques. For most steels, load relaxation occurs during the hold period or unloading, which causes a time-dependent nonlinearity in the unloading curve. Consequently, before unloading, the specimen was held for ≈1 min to allow load relaxation.

The final crack size was marked by heat tinting and/or by fatigue cycling at room temperature. The specimens were then fractured and the initial (i.e., fatigue precrack) and final (test) crack lengths of both halves of the fractured specimen were measured optically. The crack lengths were determined by the 9/8 averaging technique, i.e., the two near-surface measurements were averaged and the resultant value was averaged with the remaining seven measurements.

Several fracture toughness J-R curve tests were conducted at room temperature and 288°C on two heats of thermally aged CF-8M cast SS and on a 50% cold-worked Type 316NG SS to develop correlations for estimating crack lengths by the two techniques and to validate the test procedure. For the room-temperature tests, actual displacement of load points was measured optically and compared with the estimated loadline displacement. The measured and estimated values of loadline displacement were in very good agreement (Gruber and Chopra, 1998); for loadline displacements up to 2 mm, the error in the estimated values was <0.02 mm. The J-integral was calculated from the load-vs.-loadline displacement curves according to the correlations for DC(T) specimens in ASTM Specification E 1737.

The following correlation, obtained from the best-fit of the experimental data, was used to determine crack lengths by the unloading compliance method.

$$a_i/W = 1.2011 - 7.1572u_x + 16.874u_x^2 - 13.527u_x^3, \tag{13}$$

where

$$u_x = \frac{1}{\left[(B_{ef}E_{ef}C_{ci})^{1/2} + 1\right]}, \tag{14}$$

$$B_{ef} = B - (B - B_N)^2 / B, \tag{15a}$$

$$E_{ef} = E / (1 - \upsilon^2), \tag{15b}$$

W is the specimen width, B is the specimen thickness, B_N is the net specimen thickness, E is the elastic modulus, υ is Poisson's ratio, and C_{ci} is the specimen elastic compliance corrected

for rotation of the crack centerline. The effective elastic modulus E_{ef} was adjusted with the measured initial crack length a_i, i.e., E_{ef} was determined from Eqs. 13 and 14 by using the measured fatigue precrack length a_i and the corresponding corrected specimen elastic compliance C_{ci}.

The following correlation, obtained from the best-fit of the experimental data for normalized crack length and normalized DC potential, was used to determine crack lengths by the DC potential method.

$$\frac{a_i}{W} = \left[0.28887 \left(\frac{U}{U_o} - 0.5 \right) \right]^{0.34775}, \tag{16}$$

where W is the specimen width, and U and U_o are the current and initial potentials. Equation 16 is comparable to the ASTM E 1737 correlation for a CT specimen with current inputs at the W/4 position and DC potential lead connections at the W/3 position.

The DC potential data were corrected for the effects of plasticity on the measured potential, i.e., large crack-tip plasticity can increase measured potentials due to resistivity increases without crack extension. As per ASTM E 1737, the change in potential before crack initiation was ignored and the remainder of the potential change was used to establish the J–R curve. A plot of normalized potential vs. loadline displacement generally remains linear until the onset of crack extension. For all data within the linear portion of the curve, crack extension was calculated from the blunting-line relationship $\Delta a = J/(4\sigma_f)$. For high-strain-hardening materials, e.g., austenitic SSs, a slope that is four times the flow stress ($4\sigma_f$) represents the blunting line better than a slope of $2\sigma_f$, as defined in ASTM E 1737.[77]

Unlike the elastic unloading compliance measurements, which were adjusted only with the measured initial crack length, crack length measurements obtained by the DC potential-drop technique were adjusted with both the initial and final crack lengths. The two-point pinning method was used to correct the measured potentials from the test data. The corrected normalized potentials $\overline{NP}$ are expressed in terms of the measured normalized potentials NP (or U/U_o in Eq. 16) by the relationship

$$\overline{NP} = \frac{NP - P_1}{P_2 - P_1}. \tag{17}$$

The variables P_1 and P_2 are solutions of the expressions

$$\overline{NP_i} = \frac{NP_i - P_1}{P_2 - P_1} \tag{18a}$$

and

$$\overline{NP_f} = \frac{NP_f - P_1}{P_2 - P_1}, \tag{18b}$$

where $\overline{NP_i}$ and $\overline{NP_f}$ are normalized potentials that correspond to initial and final crack lengths determined from Eq. 16, and NP_i and NP_f are the measured values.

3.3.2 Results

Nonirradiated Type 304 Stainless Steel

Fracture toughness J–R curve tests on nonirradiated specimens were conducted on only one of the model austenitic SS alloys, e.g., Heat L2. The load-vs.-loadline displacement and fracture toughness J–R curves for the material are shown in Figs. 23 and 24, respectively. The curve obtained by the unloading compliance method shows good agreement with that obtained by the DC potential method. However, the fracture toughness of Heat L2 is poor. The J–R curve is significantly lower than that observed for Type 304 SSs, Fig. 25.[86,92–94] For wrought austenitic SSs, the J_{ic} values at temperatures up to 550°C are typically >400 kJ/m^2;[77] experimental J_{ic} for Heat L2 is ≈210 kJ/m^2.

Irradiated Type 304 Stainless Steels

Fracture toughness J–R curve tests were conducted at 288°C on Heats C19 and L20 of Type 304 SS irradiated in He at 288°C to 0.3 x 10^{21} n·cm^{-2} (E > 1 MeV) in the Halden reactor. The load-vs.-loadline displacement and fracture toughness J–R curves for the steels are shown in Figs. 26–29. For all tests, the J–R curves obtained by the unloading compliance method show very good agreement with those obtained by the DC potential method.

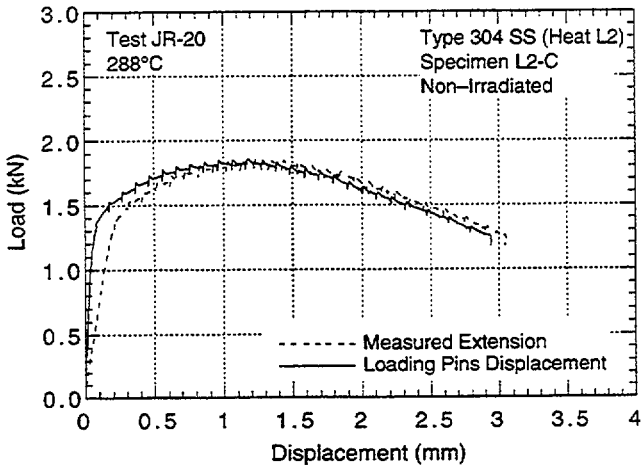

Figure 23. Load-vs.-loadline displacement for nonirradiated Type 304 SS specimen of Heat L2 tested at 288°C

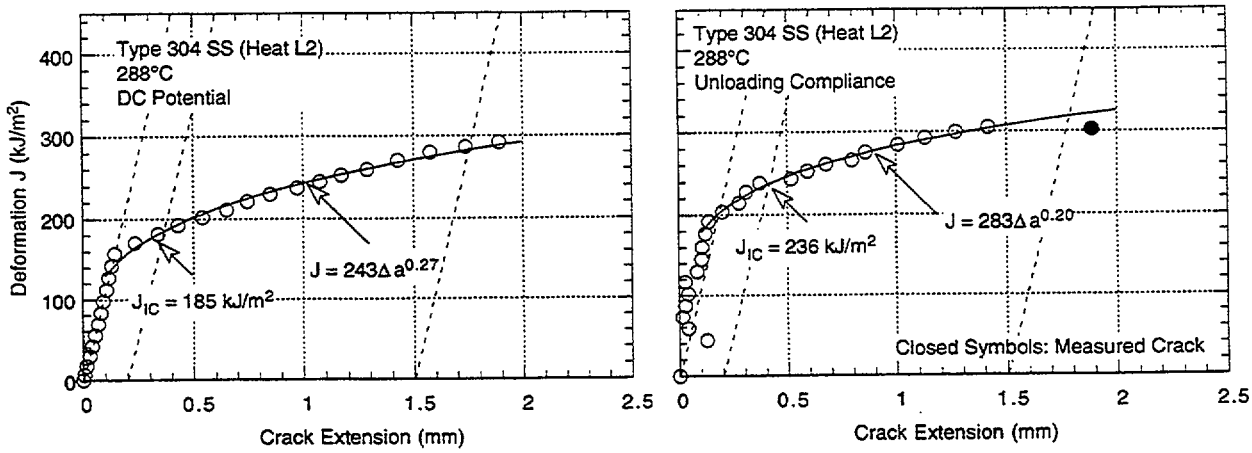

Figure 24. Fracture toughness J–R curve for nonirradiated Type 304 SS specimen of Heat L2 at 288°C determined by DC potential drop and unloading compliance methods

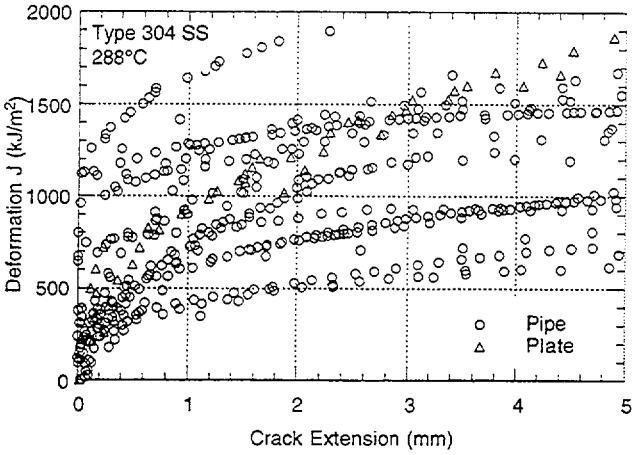

Figure 25.
Fracture toughness J–R curves for Type 304 stainless steels at 288°C

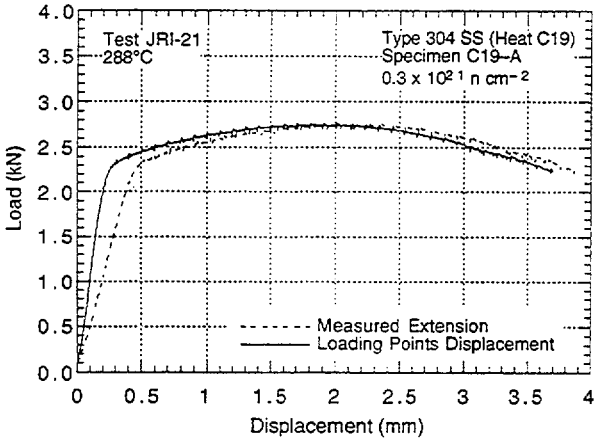

Figure 26.
Load–vs.–loadline displacement curve for Heat C19 of Type 304 SS irradiated to 0.3 x 10^{21} n·cm^{-2} in the Halden reactor at 288°C

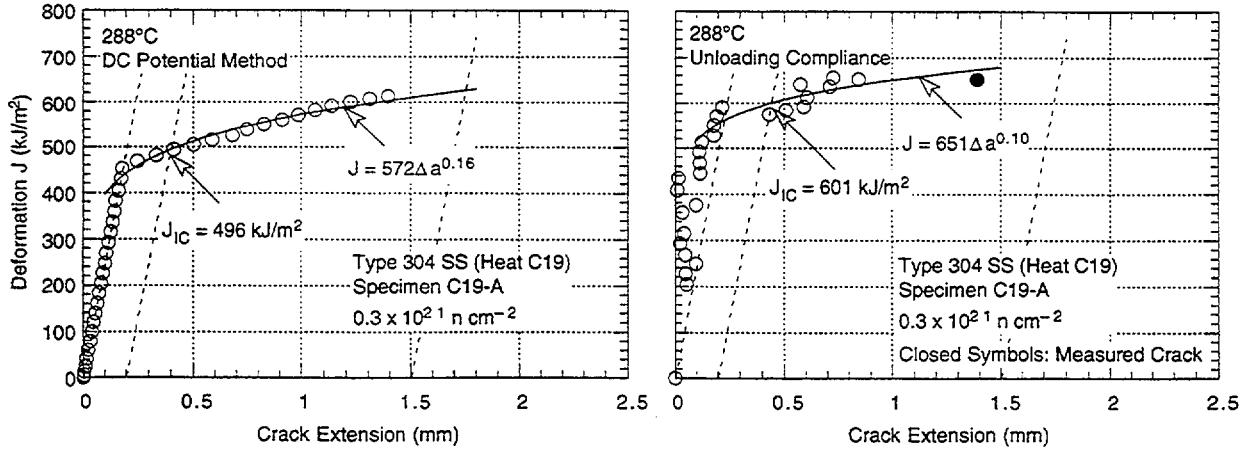

Figure 27. Fracture toughness J–R curves determined by DC potential drop and unloading compliance methods for Heat C19 of Type 304 SS irradiated to 0.3 x 10^{21} n·cm^{-2}

The fracture toughness of the commercial Heat C19 is superior to that of the laboratory Heat L20. The values of fracture toughness J_{ic} are ≥500 kJ/m^2 for C19 and ≈60 kJ/m^2 for L20. Although J–R curve tests were conducted on these heats in the nonirradiated condition, the differences between the fracture toughness of the irradiated commercial and laboratory heats most likely arise from differences in toughness of the nonirradiated steels. Fracture toughness J–R curve tests are in progress on nonirradiated steels.

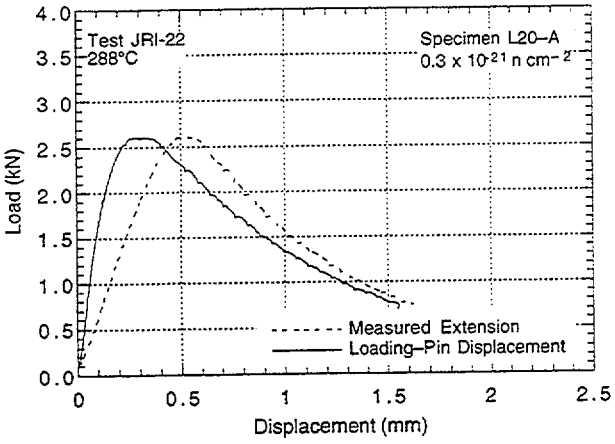

Figure 28.
Load–vs.–loadline displacement curve for Heat L20 of Type 304 SS irradiated to 0.3 x 10^{21} n·cm^{-2} in the Halden reactor at 288°C

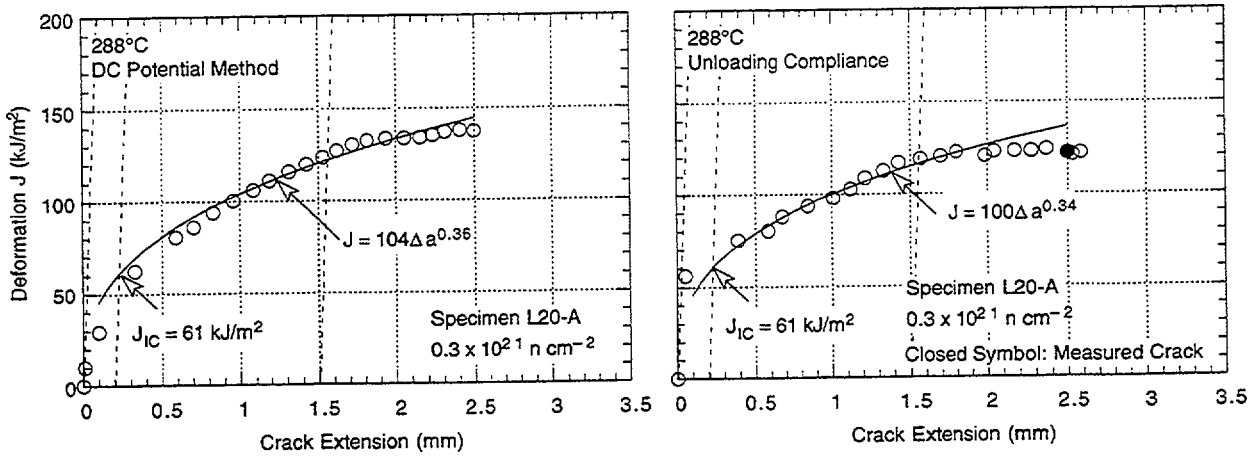

Figure 29. Fracture toughness J–R curves determined by DC potential drop and unloading compliance methods for Heat L20 of Type 304 SS irradiated to 0.3 x 10^{21} n·cm^{-2}

4 Environmentally Assisted Cracking of Alloys 600 and 690 in Simulated LWR Water (W. E. Ruther, W. K. Soppet, T. F. Kassner, and W. J. Shack)

The objective of this work is to evaluate the resistance of Alloys 600 and 690 to EAC in simulated LWR coolant environments. High–Ni alloys have experienced general corrosion (tube wall thinning), localized IGA, and SCC in LWRs. Secondary–side IGA* and axial and circumferential SCC** have occurred in Alloy 600 tubes at tube support plates in many steam generators. Primary–water SCC of Alloy 600 steam generator tubes in PWRs at roll transitions and U–bends and in tube plugs*** is a widespread problem that has been studied intensively.

*USNRC Information Notice No. 91–67, "Problems with the Reliable Detection of Intergranular Attack (IGA) of Steam Generator Tubing," Oct. 1991.

**USNRC Information Notice No. 90–49, "Stress Corrosion Cracking in PWR Steam Generator Tubes," Aug. 1990; Notice No. 91–43, "Recent Incidents Involving Rapid Increases in Primary–to–Secondary Leak Rate," July 1991; Notice No. 92–80, "Operation with Steam Generator Tubes Seriously Degraded," Dec. 1992; Notice No. 94–05, "Potential Failure of Steam Generator Tubes with Kinetically Welded Sleeves," Jan. 1994.

***USNRC Information Notice No. 89–33, "Potential Failure of Westinghouse Steam Generator Tube Mechanical Plugs," March 1989; Notice No. 89–65, "Potential for Stress Corrosion Cracking in Steam Generator Tube Plugs Supplied by Babcock and Wilcox," Sept. 1989; Notice No. 94–87, "Unanticipated Crack in a Particular Heat of Alloy 600 Used for Westinghouse Mechanical Plugs for Steam Generator Tubes," Dec. 1994.

Cracking has also occurred in Alloy 600 and other high-Ni alloys (e.g., Inconel-82 and -182 and Alloy X750) that are used in applications such as instrument nozzles and heater thermal sleeves in the pressurizer† and the penetrations for control-rod drive mechanisms in reactor vessel closure heads in the primary system of PWRs;†† in dissimilar-metal welds between SS piping and LAS nozzles, in jet pump hold-down beams,††† and in shroud-support-access-hole covers§ in BWRs. Alloy 600, in general, undergoes differing thermomechanical processing for applications other than steam generator tubes. Because environmental degradation of the alloys in many cases is very sensitive to processing, further evaluation of even SCC is needed. In addition, experience strongly suggests that materials that are susceptible to SCC are also susceptible to environmental degradation of fatigue life and fatigue-crack growth properties. In this investigation, we have obtained information on the effect of temperature, load ratio R, and stress intensity (K) on EAC of Alloys 600 and 690 in simulated BWR and PWR water. Correlations for the CGRs were developed on the basis of the best fit of the data to equations that incorporate relevant loading parameters and the DO level in water.

4.1 Crack Growth Rates of Alloys 600 and 690 in Air and Water

Crack growth experiments have been performed on Alloys 600 and 690 to explore the effects of temperature, load ratio, stress intensity, and water chemistry on CGRs. These data have been summarized in Ref. 95. Baseline CGR tests were also performed in air at several temperatures between 35 and 320°C. Correlations for the CGRs of Alloys 600 and 690 as a function of stress intensity, load ratio, and DO level have also been developed.[95] Although these correlations provide excellent fits to the available experimental data, because these data were obtained only for a single rise time, alternate forms for the correlations were also chosen to extrapolate the results to other rise times, i.e., frequencies.[96]

The CGRs of Alloys 600 and 690 in air can be expressed by the equation

$$CGR_{air} = \left(\frac{1}{t_r}\right)\frac{da}{dN} = \left(\frac{1}{t_r}\right)D(1 - bR)^p \Delta K^n , \qquad (19)$$

where $R = K_{min}/K_{max}$, $\Delta K = K_{max}(1-R)$, t_r is the rise time of the loading waveform, and D, b, p, and n are empirical parameters. The values of these parameters for Alloys 600 and 690 are listed in Table 14. For temperatures below 289°C, the effect of temperature on the CGR in air is modest, thus, the values in Table 14 can be used for temperatures between 35 and 289°C.

Ford and Andresen[97,98] argue that there are fundamental reasons to expect that the CGRs for these alloys in LWR environments should be of the form

$$CGR_{env} = CGR_{air} + A(\dot{\varepsilon}_T)^m, \qquad (20)$$

---

†USNRC Information Notice No. 90-10, "Primary Water Stress Corrosion Cracking (PWSCC) of Inconel 600," Feb. 1990.

††USNRC Generic Letter 97-01: "Degradation of Control Rod Drive Mechanism and Other Vessel Closure Head Penetrations," Apr. 1, 1997; USNRC Information Notice No. 96-11, "Ingress of Demineralizer Resins Increases Potential for Stress Corrosion Cracking of Control Rod Drive Mechanism Penetrations," Feb. 1996; INPO Document SER 20-93 "Intergranular Stress Corrosion Cracking of Control Rod Drive Mechanism Penetrations," Sept. 1993.

†††USNRC Information Notice 93-101, "Jet Pump Hold-Down Beam Failure," Dec. 1993.

§USNRC Information Notice 92-57, "Radial Cracking of Shroud Support Access Hole Cover Welds," Aug. 1992.

Table 14. Constants in CGR equations in air ($T \leq 289°C$)

Alloy	D ($m \cdot s^{-1}$)	b	p	n
600	1.64×10^{-13}	0.82	-1.74	3.80
690	2.23×10^{-13}	0.83	-1.51	3.80
600 and 690	1.92×10^{-13}	0.83	-1.62	3.80

Table 15. "Best fit" values for parameters A and m in Eq. 21 for Alloys 600 and 690

Alloy	Environment	A	m
600 Low C	High and low DO	1.5×10^{-5}	0.48
600	Low DO	2.1×10^{-8}	0.33
600	300 ppb DO	4.4×10^{-7}	0.33
600	300 ppb DO + impurities	1.9×10^{-6}	0.33
600	6 ppm DO	7.7×10^{-7}	0.33
690	Low DO	2.1×10^{-7}	0.33
690	6 ppm DO	4.4×10^{-7}	0.33

where CGR_{env} is the CGR in the environment, CGR_{air} is the CGR in air (a relatively inert environment), and $\dot{\varepsilon}_T$ is the crack tip strain rate. The parameters A and m depend on the material and the environment. Shoji has argued that under cyclic loading, $\dot{\varepsilon}_T$ is proportional to CGR_{air}.[99] Thus, Eq. 20 can be written as

$$CGR_{env} = CGR_{air} + A(CGR_{air})^m, \quad (21)$$

which is a convenient form for comparisons with experimental data and which has been widely used to correlate CGR data.[100–102] The best-fit values of parameters A and m in Eq. 21 for Alloys 600 and 690 in various environments are summarized in Table 15.

The CGRs in the low-C heat of Alloy 600 do not appear to be sensitive to either heat treatment or DO level, and the entire data set was fit with a single set of parameters. The three heats of Alloy 600 with ≈0.06 wt.% C in either a solution-annealed or mill-annealed condition, show strong environmental enhancement in high-DO environments. The situation is less clear in low-DO environments. Some tests under loading conditions that would produce CGRs in air of $\approx 10^{-11}$–10^{-10} $m \cdot s^{-1}$ show enhancement, others do not. Fewer tests of these materials have been performed in low-DO environments at the very low CGRs that might be expected to show a greater degree of environmental enhancement.

Alloy 690 in either the solution-annealed condition or after thermal treatment, shows only a modest enhancement in low-DO environments (which include both HP water and water with H_3BO_3 and LiOH additions); the enhancement appears to be independent of the loading conditions as long as $CGR_{air} \geq 10^{-11}$ s^{-1}. The CGRs in Alloy 690 in high-DO seem to be consistent with the CGR_{air} model, although the data are sparse. Some environmental enhancement occurs under loading conditions that correspond to low CGRs in air.

The experimental effort during the current reporting period has focused on SCC of Alloys 600 and 690 in simulated LWR environments under constant applied load. Crack growth tests have been conducted on CT specimens of Alloys 600 and 690 under constant load in high-DO water at temperatures between 200 and 320°C. Crack growth tests were also conducted on these alloys under cyclic loading conditions in air at 380°C. The heat numbers, heat and heat-treatment identification code, product form, and source of materials for fabrication of 1T CT specimens are presented in Table 16. The composition and tensile properties of the alloys are listed in Tables 17 and 18, respectively.

Table 16. Product form and source of Alloys 600 and 690

Alloy	Heat No.	Material Condition	Heat/Heat Treat. Code	Product Form	Source
600	NX8197	Mill Annealed	1	1.0-in.-thick plate	A. M. Castle & Co.
600	NX8844J-26	Annealed 1038°C/1 h	2	1.0-in.-thick plate	EPRI[a]
600	NX8844B-33	Annealed 872°C/1 h	8	1.0-in.-thick plate	EPRI[a]
600	NX8844G-3	Hot Worked 982°C, 20% Reduction	9	1.0-in.-thick plate	EPRI[a]
690	NX8244HK-1A	Annealed 982°C/1 h	10	1.0-in.-thick plate	EPRI[a]
690	NX8244HK-1B	Annealed 1093°C/1 h	11	1.0-in.-thick plate	EPRI[a]
690	NX8244HG-33	Annealed + 715°C/5 h	12	1.34-in.-thick plate	INCO Alloys Intl.

[a]INCO Alloys Intl., Inc. of Huntington, WV, produced numerous heats of Alloys 600 and 690 for the Electric Power Research Institute, Palo Alto, CA, which provided material for this study.

Table 17. Composition (wt.%) of Alloys 600 and 690 for corrosion fatigue tests

Heat	Cr	Mo	Ni	Fe	Mn	Si	C	N	P	S	Cu	Ti	Al	Co	Nb+Ta
NX8197	15.43	0.58	73.82	9.20	0.20	0.27	0.080	0.010	0.016	0.002	0.11	0.18	0.24	0.06	0.05
NX8844B-33	15.03	0.17	75.16	7.93	0.24	0.27	0.080	0.015	0.019	0.001	0.22	0.21	0.28	0.04	0.04
NX8844J-26	15.00	0.16	74.94	8.14	0.23	0.32	0.060	0.016	0.014	0.002	0.22	0.24	0.24	0.03	0.03
NX8844G-3	15.14	0.16	74.78	8.28	0.23	0.35	0.070	0.015	0.015	0.002	0.22	0.25	0.25	0.04	0.04
NX8244HK-1A	30.66	<0.01	59.09	9.22	0.20	0.18	0.024	0.010	0.004	0.002	<0.01	0.20	0.31	<0.01	<0.01
NX8244HK-1B	30.64	<0.01	59.20	9.19	0.21	0.18	0.023	0.011	0.005	0.002	<0.01	0.19	0.32	<0.01	<0.01
NX8244HG-33	30.46	0.04	58.88	9.22	0.11	0.16	0.030	0.047	0.017	0.001	0.05	0.25	0.32	0.02	0.01

Table 18. Tensile properties[a] of Alloys 600 and 690 in various heat-treated conditions

Heat No.	Material Condition	Temp. (°C)	σ_y (MPa)	σ_u (MPa)	ε_t (%)	RA (%)	Hardness (R_B)	ASTM Grain Size
Alloy 600								
NX8197	Mill Annealed	25[b]	256.5	683.3	42.0	–	81	–
		25	373.6	683.9	42.2	64.4	91	6
		25	392.8	685.4	41.6	64.9	–	–
		290	316.9	668.1	46.8	62.2	–	–
NX8844J-26	Annealed 1038°C/1 h	25[b]	298.6	694.3	41.0	–	86	4
		25	245.5	653.5	49.2	61.1	87	4
		290	234.0	637.8	45.2	53.3	–	–
		290	218.0	626.5	48.7	57.2	–	–
		320	246.8	639.4	45.8	48.9	–	–
NX8844B-33	Annealed 872°C/1 h	25[b]	339.9	748.8	35.5	–	90	7.5
		25	333.2	714.9	39.6	66.9	91	8
		290	282.6	686.1	38.6	61.1	–	–
		320	282.6	680.6	39.1	55.5	–	–
NX8844G-3	Hot Worked 982°C, 20%	25[b]	355.1	697.8	38.5	–	85	2.5
		25	335.3	666.4	43.5	56.9	88	2
		290	292.2	630.1	44.1	53.5	–	–
		320	297.0	630.3	44.9	54.9	–	–
Alloy 690								
NX8244HK-1A	Annealed 982°C/1 h	25[b]	245.2	665.0	51.0	–	78	–
		25	256.3	647.7	56.9	75.2	83	5
		290	195.4	569.8	58.5	71.8	–	–
		320	196.4	572.2	58.2	71.7	–	–
NX8244HK-1B	Annealed 1093°C/1 h	25b	212.3	602.8	59.0	–	70	–
		25	215.6	592.2	70.5	71.6	78	2
		290	145.2	504.9	70.6	68.1	–	–
		320	150.9	499.4	67.1	67.3	–	–
NX8662HG-33	Annealed + 715°C/5 h	25b	291.7	670.2	43.5	–	82	5
		25	292.1	683.8	48.7	63.2	96	5
		290	237.1	601.2	49.7	61.6	–	–
		320	232.3	598.8	50.7	62.8	–	–

aTensile tests conducted in air at a strain rate of 1.0 x 10–4 s–1.
bResults from vendor documents.

4.1.1 Crack Growth Rates in Air

The results of the CGR tests on Alloys 600 and 690 in air under cyclic loading conditions at 380°C and data obtained earlier[95] at 35–320°C are listed in Table 19. The experimental CGRs and those predicted from Eq. 19 are plotted in Fig. 30. The results indicate that in the range of 35–289°C, temperature has little or no apparent effect on CGRs. However, for the tests at 320 and 380°C, the observed CGRs are greater than those predicted by Eq. 19. Based on these data, the effect of temperature on CGR, i.e., an increase in growth rate with an increase in temperature, could be greater than that observed for austenitic SSs in air.[103] Because the tests at differing temperatures were conducted on differing heats and under differing heat–treatment conditions, it is likely that the differences in CGRs of Alloys 600 and 690 are not due to the effect of temperature but rather to differences in material conditions.

Table 19. Crack growth rate data for Alloys 600 and 690 in air

Specimen Number	Temp. °C	Load Ratio	Kmax MPa.m1/2	ΔK MPa.m1/2	CGR[a] (m/s)
Alloy 600 (Heat NX8844J-26) Solution Annealed 1038°C/1h					
J26-03	35	0.50	30.60	15.30	9.34E-10
J26-03	35	0.45	30.90	17.00	1.14E-09
J26-03	35	0.40	31.30	18.78	1.64E-09
J26-03	35	0.35	31.60	20.54	2.19E-09
J26-03	35	0.30	32.30	22.61	2.84E-09
J26-03	35	0.25	32.80	24.60	3.65E-09
J26-03	35	0.20	33.00	26.40	4.08E-09
J26-03	35	0.55	33.40	15.03	9.97E-10
J26-03	35	0.70	34.10	10.23	3.58E-10
J26-03	35	0.80	34.30	6.86	1.38E-10
J26-03	35	0.65	34.60	12.11	5.68E-10
J26-03	35	0.90	34.70	3.47	1.60E-11
J26-03	35	0.85	34.80	5.22	5.60E-11
J26-03	130	0.60	35.30	14.12	1.06E-09
J26-03	130	0.70	35.50	10.65	4.60E-10
J26-03	130	0.80	35.50	7.10	1.29E-10
J26-03	130	0.90	35.60	3.56	1.10E-11
J26-03	130	0.50	35.90	17.95	1.76E-09
J26-03	130	0.40	36.30	21.78	2.96E-09
J26-03	130	0.30	36.80	25.76	4.88E-09
J26-03	130	0.20	37.20	29.76	6.83E-09
J26-03	130	0.85	37.50	5.63	9.90E-11
Alloy 600 (Heat NX8197) Mill Annealed					
197-10	289	0.20	31.40	25.12	5.88E-09
197-10	289	0.80	31.50	6.30	1.99E-10
197-10	289	0.40	32.20	19.32	3.30E-09
197-10	289	0.90	32.30	3.23	5.00E-12
197-10	289	0.60	40.10	16.04	1.86E-09
197-10	289	0.40	41.40	24.84	7.68E-09
197-10	289	0.20	42.60	34.08	1.88E-08
197-10	289	0.90	42.70	4.27	3.40E-11
197-10	289	0.40	46.80	28.08	1.15E-08
197-10	289	0.60	47.70	19.08	3.21E-09
197-10	289	0.90	47.80	4.78	5.20E-11
197-10	289	0.30	55.60	38.92	1.37E-08
197-10	289	0.90	55.80	5.58	1.12E-10
197-10	289	0.95	55.90	2.80	7.00E-12

Table 19. (Continued)

Specimen Number	Temp. °C	Load Ratio	Kmax MPa.m1/2	ΔK MPa.m1/2	CGR[a] (m/s)
Alloy 600 (Heat NX8844B-33) Solution Annealed 872°C/1h					
B33-01	320	0.20	26.32	21.06	3.68E-09
B33-01	320	0.25	26.80	20.10	4.05E-09
B33-01	320	0.30	27.55	19.29	3.98E-09
B33-01	320	0.35	28.18	18.32	3.37E-09
B33-01	320	0.40	28.53	17.12	2.76E-09
B33-01	320	0.50	28.72	14.36	1.66E-09
B33-01	320	0.60	28.80	11.52	8.44E-10
B33-01	320	0.70	28.99	8.70	4.59E-10
B33-01	320	0.75	29.13	7.28	3.26E-10
B33-01	320	0.80	29.37	5.87	2.76E-10
B33-01	320	0.83	29.59	5.03	1.38E-10
B33-01	320	0.86	29.65	4.15	6.60E-11
B33-01	320	0.90	29.70	2.97	1.60E-11
B33-01	380	0.80	30.78	6.16	7.02E-10
B33-01	380	0.83	31.15	5.29	1.70E-10
B33-01	380	0.86	31.27	4.38	3.50E-11
B33-01	380	0.90	31.52	3.15	3.40E-11
B33-01	380	0.75	31.90	7.98	7.07E-10
B33-01	380	0.70	32.24	9.67	9.22E-10
B33-01	380	0.60	32.77	13.11	1.94E-09
B33-01	380	0.50	34.03	17.02	4.39E-09
B33-01	380	0.40	35.18	21.11	9.03E-09
B33-01	380	0.30	37.22	26.05	1.52E-08
B33-01	380	0.20	40.07	32.06	2.40E-08
Alloy 690 (Heat NX8244HK-1B) Solution Annealed 1093°C/1h					
K1B-03	35	0.50	30.50	15.25	1.05E-09
K1B-03	35	0.45	30.90	17.00	1.34E-09
K1B-03	35	0.40	31.30	18.78	1.55E-09
K1B-03	35	0.35	31.60	20.54	2.18E-09
K1B-03	35	0.30	32.50	22.75	3.81E-09
K1B-03	35	0.25	33.30	24.98	5.67E-09
K1B-03	35	0.20	33.70	26.96	8.30E-09
K1B-03	35	0.55	34.50	15.53	1.53E-09
K1B-03	35	0.70	35.40	10.62	4.90E-10
K1B-03	35	0.80	35.60	7.12	2.05E-10
K1B-03	35	0.65	36.10	12.63	8.04E-10
K1B-03	35	0.90	36.10	3.61	1.20E-11
K1B-03	35	0.85	36.90	5.53	6.90E-11
K1B-03	130	0.60	37.80	15.14	1.58E-09
K1B-03	130	0.70	38.10	11.42	7.06E-10
K1B-03	130	0.80	38.20	7.65	2.39E-10
K1B-03	130	0.90	38.30	3.83	1.70E-11
K1B-03	130	0.50	38.70	19.37	1.99E-09
K1B-03	130	0.40	39.40	23.63	4.32E-09
K1B-03	130	0.30	40.40	28.26	8.29E-09
K1B-03	130	0.20	41.20	32.97	1.34E-08
K1B-03	130	0.85	41.80	6.27	1.72E-10
Alloy 690 (Heat NX8662HG-33) MA+ Thermally Treated 715°C/5h					
HG-10	289	0.20	31.70	25.36	8.39E-09
HG-10	289	0.80	31.90	6.38	2.74E-10
HG-10	289	0.40	32.90	19.74	4.68E-09
HG-10	289	0.90	32.90	3.29	2.00E-12
HG-10	289	0.60	41.30	16.52	2.85E-09
HG-10	289	0.40	43.10	25.86	1.07E-08
HG-10	289	0.20	45.30	36.24	2.81E-08

Table 19. (Continued)

Specimen Number	Temp. °C	Load Ratio	Kmax MPa.m1/2	ΔK MPa.m1/2	CGR[a] (m/s)
HG-10	289	0.90	45.40	4.54	5.50E-11
HG-10	289	0.40	53.00	31.80	1.94E-08
HG-10	289	0.60	55.00	22.00	6.16E-09
HG-10	289	0.90	55.20	5.52	1.21E-10
HG-10	289	0.30	67.90	47.53	5.53E-08
HG-10	289	0.90	68.60	6.86	2.02E-10
HG-10	289	0.95	68.60	3.43	8.00E-12
Alloy 690 (Heat NX8244HK-1A) Solution Annealed 982°C/1h					
K1A-02	320	0.20	26.86	21.49	5.07E-09
K1A-02	320	0.25	27.55	20.66	5.75E-09
K1A-02	320	0.30	28.78	20.15	5.70E-09
K1A-02	320	0.35	29.80	19.37	5.58E-09
K1A-02	320	0.40	30.54	18.32	5.07E-09
K1A-02	320	0.50	30.87	15.44	3.21E-09
K1A-02	320	0.60	31.10	12.44	1.69E-09
K1A-02	320	0.70	31.47	9.44	8.82E-10
K1A-02	320	0.75	31.73	7.93	4.86E-10
K1A-02	320	0.80	32.02	6.48	2.93E-10
K1A-02	320	0.83	32.18	5.47	8.90E-11
K1A-02	320	0.86	32.18	4.50	5.00E-12
K1A-02	320	0.90	32.18	3.22	2.00E-12
K1A-02	380	0.80	34.19	6.84	4.45E-10
K1A-02	380	0.83	34.84	5.92	2.39E-10
K1A-02	380	0.86	35.11	4.92	5.30E-11
K1A-02	380	0.90	35.29	3.53	4.20E-11
K1A-02	380	0.75	36.00	9.00	1.10E-09
K1A-02	380	0.70	36.67	11.00	1.64E-09
K1A-02	380	0.60	37.71	15.08	3.06E-09
K1A-02	380	0.50	40.31	20.16	7.00E-09
K1A-02	380	0.40	43.25	25.95	1.35E-08
K1A-02	380	0.30	48.27	33.79	2.62E-08
K1A-02	380	0.20	62.10	49.68	6.83E-08

[a]Crack length measured by DC potential drop method.

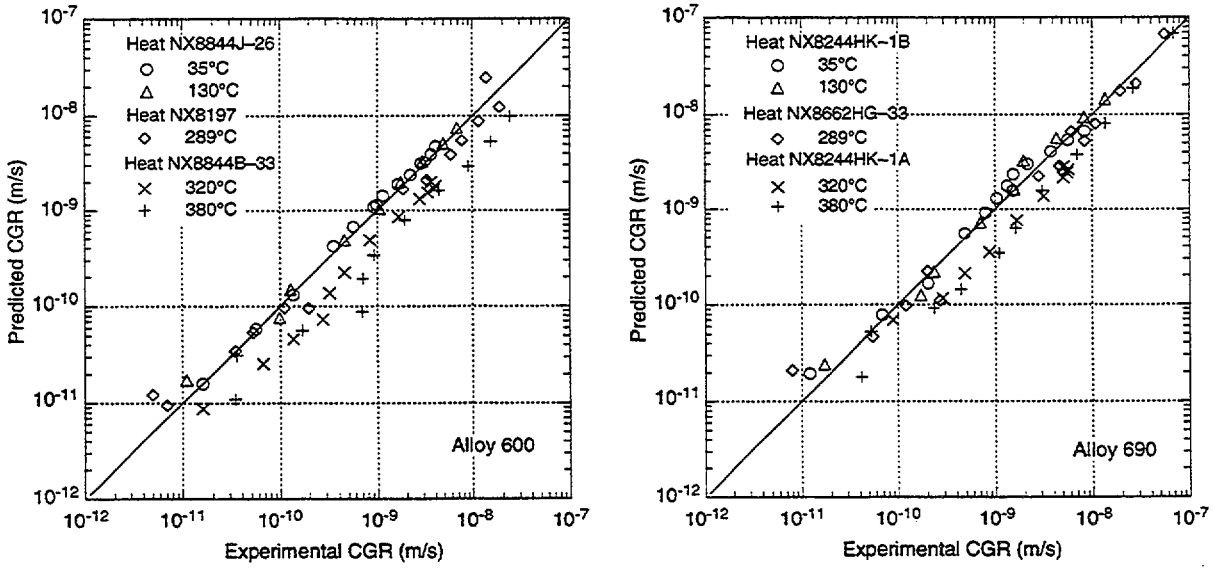

Figure 30. Predicted vs. experimental values of crack growth rate of Alloys 600 and 690 in air at temperatures between 35 and 380°C

4.1.2 Crack Growth Rates under Constant Load in High–DO Water

The crack growth data for Alloy 600 and 690 specimens under constant load in high–DO water (i.e., ≈300 ppb DO) between 200 and 320°C are listed in Table 20. The effect of the stress intensity factor K on growth rates is shown in Fig. 31 for Alloys 600 and 690 at 289°C, and the effect of temperature is shown in Fig. 32 for Alloy 600 at K values of 27–30 MPa·$m^{1/2}$. The results indicate that the CGRs for the hot–worked Alloy 600 are a factor of ≈5 greater than those for the hot–worked + thermally treated Alloy 600. For both alloys, growth rates increase slightly with increasing K; values of the power–law exponent n are 0.40 and 0.54.

Table 20. Crack growth rate data for Alloys 600 and 690 specimens under constant load in high–purity water between 200 and 320°C

Specimen Number	Test Environment[a]	DO (ppb)	Temp. (°C)	K MPa.$m^{1/2}$	CGR[b] (m/s)
Alloy 600 (Heat NX8844J–26) Solution Annealed 1038°C/1h					
J26-04	HP	≈300	200	26.70	5.00E-11
J26-04	HP	≈300	240	26.60	6.50E-11
J26-04	HP	≈300	289	26.50	9.40E-11
J26-04	HP	6200	289	26.90	3.20E-11
J26-04	HP	≈300	289	27.20	7.00E-12
J26-04	HP	≈300	320	29.30	6.20E-11
J26-04	HP + 150 ppb sulfate	≈300	320	29.80	6.60E-11
J26-04	HP + 1000 ppb sulfate	≈300	320	39.20	1.22E-10
Alloy 600 (Heat NX8844B–33) Solution Annealed 872°C/1h					
B33-02	HP	≈300	200	28.20	2.40E-11
B33-02	HP	≈300	240	28.20	2.20E-11
B33-02	HP	≈300	289	28.10	5.40E-11
B33-02	HP	≈300	289	28.40	2.20E-11
B33-02	HP	≈300	289	28.60	2.20E-11
B33-02	HP	≈300	320	30.00	7.00E-12
B33-02	HP + 1000 ppb sulfate	≈300	320	38.20	5.80E-11
Alloy 600 (NX8844G–3) Hot–Worked 982°C, 20% Reduction					
G3-04	HP	≈300	289	26.50	8.60E-11
G3-04	HP + 1000 ppb sulfate	≈300	289	28.30	5.70E-10
G3-04	HP + 3000 ppb sulfate	≈300	289	28.80	5.50E-10
G3-04	HP + 100 ppb sulfate	≈300	289	30.60	3.32E-10
G3-04	HP + 30 ppb sulfate	≈300	289	31.90	3.26E-10
G3-04	HP	≈300	289	33.40	1.52E-10
G3-04	HP	≈300	289	42.10	9.20E-11
G3-04	HP	≈300	289	51.00	1.37E-10
G3-03	HP	≈300	289	26.70	2.40E-11
G3-03	HP + 1000 ppb sulfate	≈300	289	27.20	1.48E-10
G3-03	HP + 3000 ppb sulfate	≈300	289	27.30	1.40E-10
G3-03	HP + 100 ppb sulfate	≈300	289	27.80	6.70E-11
G3-03	HP + 30 ppb sulfate	≈300	289	27.90	3.80E-11
G3-03	HP	≈300	289	28.10	1.60E-11
G3-03	HP	≈300	289	33.80	2.00E-11
G3-03	HP	≈300	289	40.60	2.60E-11
G3-02	HP	≈300	200	27.80	1.95E-10
G3-02	HP	≈300	240	27.30	1.38E-10
G3-02	HP	≈300	289	26.90	5.30E-11
G3-02	HP	≈300	289	28.20	2.25E-10
G3-02	HP	≈300	289	29.30	4.80E-11
G3-02	HP	≈300	320	31.30	6.00E-12
G3-02	HP + 150 ppb sulfate	≈300	320	31.80	2.70E-11
G3-02	HP + 1000 ppb sulfate	≈300	320	40.20	3.40E-11

Table 20. (Continued)

Specimen Number	Test Environment[a]	DO (ppb)	Temp. (°C)	K MPa.m$^{1/2}$	CGR[b] (m/s)
Alloy 690 (Heat NX8244HK-1B) Solution Annealed 1093°C/1h					
K1B-04	HP	≈300	289	26.10	2.00E-12
K1B-04	HP + 1000 ppb sulfate	≈300	289	26.20	4.00E-12
K1B-04	HP + 3000 ppb sulfate	≈300	289	26.20	2.00E-12
K1B-04	HP + 100 ppb sulfate	≈300	289	26.20	2.00E-12
K1B-04	HP + 30 ppb sulfate	≈300	289	26.20	3.00E-12
K1B-04	HP	≈300	289	26.20	6.00E-12
K1B-04	HP	≈300	289	31.40	4.00E-12
K1B-04	HP	≈300	289	40.60	5.00E-12

[a]HP = High-purity water. Sulfate added as H_2SO_4.
[b]Crack length measured by DC potential drop method.

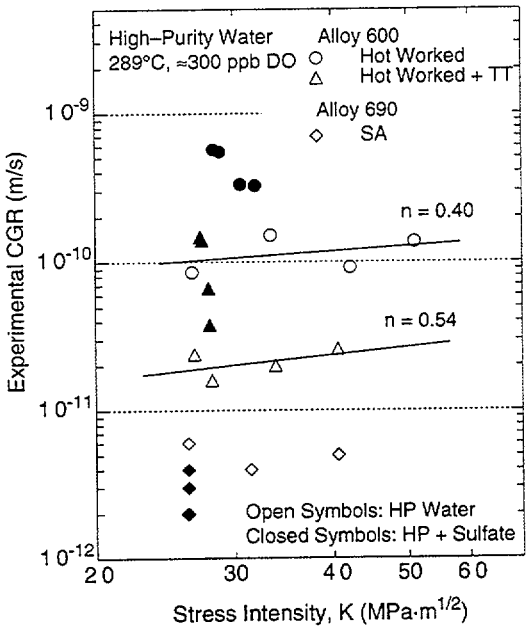

Figure 31.
Effect of stress intensity factor K on crack growth rates of Alloys 600 and 690 in high-purity water at 289°C

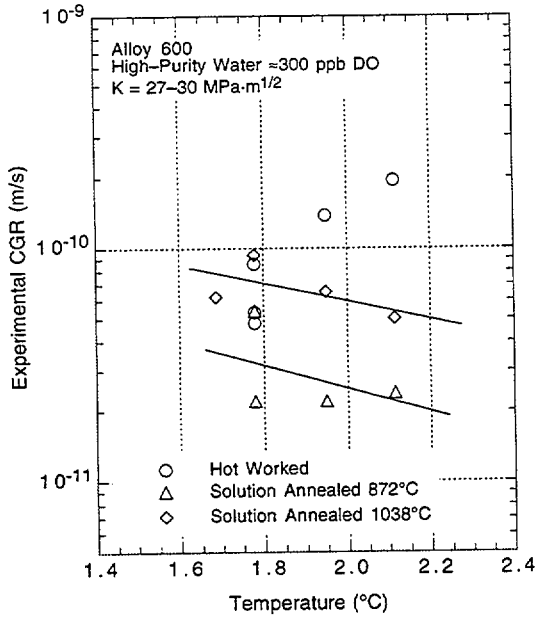

Figure 32.
Effect of temperature on crack growth rates of Alloy 600 in high-purity water

respectively, for the hot-worked and hot-worked + thermally treated Alloy 600. The addition of sulfate increased the CGRs of both alloys by a factor of 3–7. The Alloy 690 specimens show little dependence of K on growth rates. The CGRs for Alloy 690 range between $\approx 2 \times 10^{-12}$ and 6×10^{-12} m/s; however, these values may be below the sensitivity of the crack-length monitoring system. Also, the addition of sulfates exerted no effect on the growth rates of Alloy 690.

Between 200 and 320°C, the CGRs in solution-annealed Alloy 600 are weakly dependent on temperature. Although there is considerable uncertainty because the data set is small and the data are scattered, these CGRs appear to increase slightly with increasing temperature. However, the growth rates in hot-worked Alloy 600 (20% reduction) decrease significantly with temperature and become comparable to those in the solution-annealed materials. A decrease in the CGRs of SCC in simulated BWR environments at temperatures above 288°C has been observed in austenitic SSs.[104,105] In that case, however, the decrease was much greater and produced CGRs $<10^{-11}$ m/s in the SS.

5 Summary of Results

5.1 Environmental Effects on Fatigue S–N Behavior of Primary Pressure Boundary Materials

The existing fatigue S–N data on the effects of various material, loading, and environmental parameters on the fatigue lives of carbon and low-alloy steels and austenitic SSs have been summarized. Two approaches have been proposed for incorporating the effects of LWR environments into ASME Section III fatigue evaluations: (a) develop new design fatigue curves for LWR applications, and (b) use a fatigue life correction factor to account for environmental effects. Both methods of evaluating fatigue lives are based on statistical models for estimating fatigue lives of carbon and low-alloy steels and austenitic SSs in LWR environments. The environmentally adjusted design fatigue curves provide allowable cycles for fatigue crack initiation in LWR coolant environments. The design curves for carbon and low-alloy steels as well as for austenitic SSs maintain the margin of 20 on life. However, to be consistent with the current ASME Code curves, the margin on stress is 2 for carbon and low-alloy steels and 1.5 for austenitic SSs.

In the F_{en} method, environmental effects on life are estimated from the statistical models but the correction is applied to fatigue lives estimated from the current Code design curves. Therefore, estimates of fatigue lives that are based on the two methods may differ because of differences in the ASME mean curve and the best-fit curve to existing fatigue data. The existing fatigue S–N data indicate that the current Code design curve for CSs is comparable to the statistical-model curve for LASs, whereas, it is somewhat conservative at stress levels <500 MPa when compared with the statistical-model curve for CSs. Consequently, usage factors based on the F_{en} method would be comparable to those based on the environmentally adjusted design fatigue curves for LASs and would be somewhat higher for CSs.

For austenitic SSs, the ASME mean curve and consequently the current Code design fatigue curve are nonconservative in air when compared with the statistical-model curve and a

corresponding design curve, i.e., it predicts longer fatigue lives than the best–fit curve to the existing S–N data. Consequently, before adjusting for the conservatism in the design curves, usage factors that are based on the F_{en} method would be lower than those determined from design fatigue curves based on the Argonne results.

Fatigue tests have also been conducted to determine the crack initiation and growth characteristics of austenitic SSs in air and LWR environments. Results of fatigue tests that examine the influence of the reactor environment on the formation and growth of short cracks in Types 304 SS are presented. Crack lengths as a function of fatigue cycles were determined in air and water environments. The significant conclusions are summarized below.

- At the same fraction of life, the crack lengths are longer in water than in air. The crack growth rates in water are greater than those in air, and the CGRs in PWR water are greater than those in high-DO water.

- The decrease in fatigue life of Type 304 austenitic SS in LWR water is primarily caused by the effects of environment on the growth of short cracks that are <500 μm deep.

- The results from the present study are not consistent with the slip dissolution model for enhanced CGRs in LWR environments. Oxide film rupture strengths and/or H_2 evolution may play a greater role in these environments.

5.2 Irradiation–Assisted Stress Corrosion Cracking of Austenitic Stainless Steels

Sixteen austenitic SS alloys that were irradiated at 289°C in He to a fluence of ≈0.3 x 10^{21} n·cm^{-2} (E > 1 MeV) and nine alloys that were irradiated to a fluence of ≈0.9 x 10^{21} n·cm^{-2} (E > 1 MeV) were subjected to SSRT tests and posttest fractographic analyses by SEM. After irradiation to ≈0.3 x 10^{21} n·cm^{-2} or ≈0.9 x 10^{21} n·cm^{-2} (E > 1 MeV), strong heat-to-heat variation in irradiation-induced hardening was observed. Heat-to-heat variations in susceptibilities to IGSCC and TGSCC were very significant among steels of the same grade that contain nominally similar concentrations of alloying and impurity elements, as defined in the ASTM specifications. After irradiation to a fluence of ≈0.3 x 10^{21} n·cm^{-2} (E > 1 MeV), an HP laboratory heat of Type 316L SS that contains a very low concentration of Si exhibited the highest susceptibility to IGSCC. All of the other 15 alloys exhibited negligible susceptibility to IGSCC at this low fluence.

Silicon atoms profoundly affect irradiation–induced hardening of and irradiation–induced microstructural evolution in Type 304 SSs. A high concentration of Si is conducive to less irradiation-induced hardening and a lower number density of Frank loops. Susceptibilities to TGSCC of 16 alloys at ≈0.3 x 10^{21} n·cm^{-2} (E > 1 MeV) could be correlated in terms of N and Si concentrations. All alloys that contained <0.01 wt.% N and <1.0 wt.% Si were susceptible, whereas all alloys that contained >0.01 wt.% N or >1.0 wt.% Si were relatively resistant. Because practically all commercial heats of Type 304 or 304L SSs contain >100 wppm N, this means that, to delay onset of and increase resistance to IASCC, it is helpful to ensure a certain minimum concentration of Si. Results of initial tests on alloys irradiated to a fluence of ≈0.9 x 10^{21} n·cm^{-2} (E > 1 MeV) were consistent with the finding that a low level of Si (<0.5 wt.%) is conducive to relatively higher susceptibility to IASCC. Consistent with the effect in Type 304 SSs, a low concentration of Si (e.g., <0.26 wt.%) appears to promote higher

susceptibility of HP heats of Type 316 SS to IASCC when compared with CP heats that contain high concentration of Si.

At $\approx 0.3 \times 10^{21}$ n·cm^{-2} to $\approx 0.9 \times 10^{2}$ n·cm^{-2} (E > 1 MeV), the beneficial effect of a high concentration of Cr was significant. Alloys that contain <15.8 wt.% Cr exhibited higher susceptibilities to TGSCC and IGSCC, compared to an alloy that contains >21 wt.% Cr.

Fracture toughness J–R curve tests have been conducted on two heats of Type 304 SS that were irradiated to a fluence of $\approx 0.3 \times 10^{21}$ n·cm^{-2} (E > 1 MeV) at ≈288°C in a He environment in the Halden boiling heavy–water reactor. The tests were performed on 1/4–T CT specimens in air at 288°C; crack extensions were determined by both DC potential and elastic unloading compliance techniques. Neutron irradiation at 288°C to 0.3×10^{21} n·cm^{-2} decreased the fracture toughness of both heats. The commercial heat C19 exhibited fracture toughness that is superior to the fracture toughness of the laboratory heat L20. The values of fracture toughness J_{ic} are ≥500 kJ/m^2 for C19 and ≈60 kJ/m^2 for L20.

5.3 Environmentally Assisted Cracking of Low–Carbon Alloys 600 and 690 in Simulated LWR Water

Fracture–mechanics CGR tests have been conducted on CT specimens of several heats of Alloys 600 and 690 in annealed, and in annealed and thermally treated, conditions in HP water with DO levels between 1 and 7500 ppb and in low–DO water that contained boric acid, lithium hydroxide, and low concentrations of dissolved H at 200–320°C. Fracture–mechanics CGR tests were also conducted on CT specimens of several of these alloys in air at temperatures between 35 and 320°C. Correlations have been developed for estimating the CGRs of Alloys 600 and 690 as a function of stress intensity, load ratio, and DO level. However, because the experimental data were obtained for only a single rise time, alternate forms for the correlations have also been developed to extrapolate the results to other rise times, i.e., frequencies. Experiments are planned to verify the predictions of the correlation for the effect of rise time/frequency.

The CGRs in the low–C heat of Alloy 600 do not appear to be sensitive to either heat treatment or DO level, whereas the CGRs in the high–C heats show a strong environmental enhancement in high–DO environments. The results are inconclusive for the high–C Alloy 600 in low–DO environments. Alloy 690 shows only a modest environmental enhancement in low–DO environments; environmental effects appear to be independent of the loading conditions as long as $CGR_{air} \geq 10^{-11}$ s^{-1}. The CGRs in Alloy 690 in high–DO water show some environmental enhancement for loading conditions that correspond to low CGRs in air.

During the current reporting period crack growth tests have been performed on Alloys 600 and 690 under cyclic loading conditions in air at 380°C. The results indicate that in the range of 35–289°C, temperature has little or no apparent effect on CGRs. The observed CGRs at 320 and 380°C are greater than those at 35–289°C. However, because the tests at differing temperatures were conducted on differing heats and under differing heat–treatment conditions, it is likely that the differences in CGRs are not due to the effect of temperature but rather to the differences in material conditions.

Constant load crack growth tests have also been conducted on CT specimens of Alloys 600 and 690 in high–DO water at 200–320°C. The growth rates for the hot–worked Alloy 600

are a factor of ≈5 higher than those for the hot-worked + thermally treated Alloy 600. The addition of sulfate increased the CGRs of both alloys by a factor of 3–7. The Alloy 690 specimens show little dependence of K on growth rates; the CGRs range between ≈2 x 10^{-12} and 6 x 10^{-12} m/s, values that may be below the sensitivity of the crack-monitoring system. The results indicate that for Alloy 600, the CGRs increase slightly with increasing stress intensity factor K.

References

1. K. Iida, *A Review of Fatigue Failures in LWR Plants in Japan*, Nucl. Eng. Des. **138**, 297–312 (1992).

2. K. Kussmaul, R. Rintamaa, J. Jansky, M. Kemppainen, and K. Törrönen, *On the Mechanism of Environmental Cracking Introduced by Cyclic Thermal Loading*, in IAEA Specialists Meeting Corrosion and Stress Corrosion of Steel Pressure Boundary Components and Steam Turbines, VTT Symp. 43, Espoo, Finland, pp. 195–243 (1983).

3. K. Kussmaul, D. Blind, and J. Jansky, *Formation and Growth of Cracking in Feed Water Pipes and RPV Nozzles*, Nucl. Eng. Des. **81**, 105–119 (1984).

4. E. Lenz, B. Stellwag, and N. Wieling, *The Influence of Strain Induced Corrosion Cracking on the Crack Initiation in Low Alloy Steels in HT–Water – A Relation Between Monotonic and Cyclic Crack Initiation Behavior*, in IAEA Specialists Meeting Corrosion and Stress Corrosion of Steel Pressure Boundary Components and Steam Turbines, VTT Symp. 43, Espoo, Finland, pp. 243–267 (1983).

5. *ASME Boiler and Pressure Vessel Code Section III – Rules for Construction of Nuclear Power Plant Components*, The American Society of Mechanical Engineers, New York, 1992 Ed.

6. B. F. Langer, *Design of Pressure Vessels for Low–Cycle Fatigue*, ASME J. Basic Eng. **84**, 389–402 (1962).

7. *Tentative Structural Design Basis for Reactor Pressure Vessels and Directly Associated Components (Pressurized, Water Cooled Systems)*, PB 151987, U.S. Dept. of Commerce, Office of Technical Service, 1 Dec. 1958 Revision.

8. S. Ranganath, J. N. Kass, and J. D. Heald, *Fatigue Behavior of Carbon steel Components in High–Temperature Water Environments*, in BWR Environmental Cracking Margins for Carbon Steel Piping, EPRI NP–2406, Electric Power Research Institute, Palo Alto, CA, Appendix 3 (May 1982).

9. W. A. Van Der Sluys, *Evaluation of the Available Data on the Effect of the Environment on the Low Cycle Fatigue Properties in Light Water Reactor Environments*, in Proc. 6th Intl. Symp. on Environmental Degradation of Materials in Nuclear Power Systems – Water Reactors, R. E. Gold and E. P. Simonen, eds., The Metallurgical Society, Warrendale, PA, pp. 1–4 (1993).

10. N. Nagata, S. Sato, and Y. Katada, *Low–Cycle Fatigue Behavior of Pressure Vessel Steels in High–Temperature Pressurized Water*, ISIJ Intl. **31** (1), 106–114 (1991).

11. M. Higuchi and K. Iida, *Fatigue Strength Correction Factors for Carbon and Low–Alloy Steels in Oxygen–Containing High–Temperature Water*, Nucl. Eng. Des. **129**, 293–306 (1991).

12. M. Higuchi, K. Iida, and Y. Asada, *Effects of Strain Rate Change on Fatigue Life of Carbon Steel in High-Temperature Water*, in Fatigue and Crack Growth: Environmental Effects, Modeling Studies, and Design Considerations, PVP Vol. 306, S. Yukawa, ed., American Society of Mechanical Engineers, New York, pp. 111–116 (1995); also in Proc. Symp. on Effects of the Environment on the Initiation of Crack Growth, ASTM STP 1298, American Society for Testing and Materials, Philadelphia (1997).

13. H. Kanasaki, M. Hayashi, K. Iida, and Y. Asada, *Effects of Temperature Change on Fatigue Life of Carbon Steel in High Temperature Water*, in Fatigue and Crack Growth: Environmental Effects, Modeling Studies, and Design Considerations, PVP Vol. 306, S. Yukawa, ed., American Society of Mechanical Engineers, New York, pp. 117–122 (1995).

14. G. Nakao, H. Kanasaki, M. Higuchi, K. Iida, and Y. Asada, *Effects of Temperature and Dissolved Oxygen Content on Fatigue Life of Carbon and Low-Alloy Steels in LWR Water Environment*, in Fatigue and Crack Growth: Environmental Effects, Modeling Studies, and Design Considerations, PVP Vol. 306, S. Yukawa, ed., American Society of Mechanical Engineers, New York, pp. 123–128 (1995).

15. O. K. Chopra and W. J. Shack, *Effects of LWR Environments on Fatigue Life of Carbon and Low-Alloy Steels*, in Fatigue and Crack Growth: Environmental Effects, Modeling Studies, and Design Considerations, PVP Vol. 306, S. Yukawa, ed., American Society of Mechanical Engineers, New York, pp. 95–109 (1995).

16. O. K. Chopra and W. J. Shack, *Evaluation of Effects of LWR Coolant Environments on Fatigue Life of Carbon and Low-Alloy Steels*, in Effects of the Environment on the Initiation of Crack Growth, ASTM STP 1298, W. A. Van Der Sluys, R. S. Piascik, and R. Zawierucha, eds., American Society for Testing and Materials, Philadelphia, pp. 247–266 (1997).

17. O. K. Chopra and W. J. Shack, *Low-Cycle Fatigue of Piping and Pressure Vessel Steels in LWR Environments*, Nucl. Eng. Des. **184**, 49–76 (1998).

18. O. K. Chopra and W. J. Shack, *Effects of LWR coolant environments on fatigue design curves of carbon and low-alloy steels*, NUREG/CR-6583, ANL-97/18 (March 1998).

19. O. K. Chopra and W. J. Shack, *Fatigue Crack Initiation in Carbon and Low-Alloy Steels in Light Water Reactor Environments – Mechanism and Prediction*, in Fatigue, Environmental Factors, and New Materials, PVP Vol. 374, H. S. Mehta, R. W. Swindeman, J. A. Todd, S. Yukawa, M. Zako, W. H. Bamford, M. Higuchi, E. Jones, H. Nickel, and S. Rahman, eds., American Society of Mechanical Engineers, New York, pp. 155–168 (1998).

20. O. K. Chopra and W. J. Shack, *Overview of Fatigue Crack Initiation in Carbon and Low-Alloy Steels in Light Water Reactor Environments*, J. Pressure Vessel Technol. **121**, 49–60 (1999).

21. M. Fujiwara, T. Endo, and H. Kanasaki, *Strain Rate Effects on the Low Cycle Fatigue Strength of 304 Stainless Steel in High-Temperature Water Environment, Fatigue Life: Analysis and Prediction*, in Proc. Intl. Conf. and Exposition on Fatigue, Corrosion Cracking, Fracture Mechanics, and Failure Analysis, ASM, Metals Park, OH, pp. 309–313 (1986).

22. H. Mimaki, H. Kanasaki, I. Suzuki, M. Koyama, M. Akiyama, T. Okubo, and Y. Mishima, *Material Aging Research Program for PWR Plants*, in Aging Management Through Maintenance Management, PVP Vol. 332, I. T. Kisisel, ed., American Society of Mechanical Engineers, New York, pp. 97–105 (1996).

23. H. Kanasaki, R. Umehara, H. Mizuta, and T. Suyama, *Fatigue Lives of Stainless Steels in PWR Primary Water*, Trans. 14th Intl. Conf. on Structural Mechanics in Reactor Technology (SMiRT 14), Lyon, France, pp. 473–483 (1997).

24. H. Kanasaki, R. Umehara, H. Mizuta, and T. Suyama, *Effects of Strain Rate and Temperature Change on the Fatigue Life of Stainless Steel in PWR Primary Water*, Trans. 14th Intl. Conf. on Structural Mechanics in Reactor Technology (SMiRT 14), Lyon, France, pp. 485–493 (1997).

25. M. Higuchi and K. Iida, *Reduction in Low-Cycle Fatigue Life of Austenitic Stainless Steels in High-Temperature Water*, in Pressure Vessel and Piping Codes and Standards, PVP Vol. 353, D. P. Jones, B. R. Newton, W. J. O'Donnell, R. Vecchio, G. A. Antaki, D. Bhavani, N. G. Cofie, and G. L. Hollinger, eds., American Society of Mechanical Engineers, New York, pp. 79–86 (1997).

26. M. Hayashi, *Thermal Fatigue Strength of Type 304 Stainless Steel in Simulated BWR Environment*, Nucl. Eng. Des. **184**, 135–144 (1998).

27. M. Hayashi, K. Enomoto, T. Saito, and T. Miyagawa, *Development of Thermal Fatigue Testing with BWR Water Environment and Thermal Fatigue Strength of Austenitic Stainless Steels*, Nucl. Eng. Des. **184**, 113–122 (1998).

28. O. K. Chopra and D. J. Gavenda, *Effects of LWR Coolant Environments on Fatigue Lives of Austenitic Stainless Steels*, in Pressure Vessel and Piping Codes and Standards, PVP Vol. 353, D. P. Jones, B. R. Newton, W. J. O'Donnell, R. Vecchio, G. A. Antaki, D. Bhavani, N. G. Cofie, and G. L. Hollinger, eds., American Society of Mechanical Engineers, New York, pp. 87–97 (1997).

29. O. K. Chopra and D. J. Gavenda, *Effects of LWR Coolant Environments on Fatigue Lives of Austenitic Stainless Steels*, J. Pressure Vessel Technol. **120**, 116–121 (1998).

30. O. K. Chopra and J. L. Smith, *Estimation of Fatigue Strain-Life Curves for Austenitic Stainless Steels in Light Water Reactor Environments*, in Fatigue, Environmental Factors, and New Materials, PVP Vol. 374, H. S. Mehta, R. W. Swindeman, J. A. Todd, S. Yukawa, M. Zako, W. H. Bamford, M. Higuchi, E. Jones, H. Nickel, and S. Rahman, eds., American Society of Mechanical Engineers, New York, pp. 249–259 (1998).

31. O. K. Chopra, *Effects of LWR coolant environments on fatigue design curves of Austenitic Stainless steels*, NUREG/CR-5704, ANL-98/31 (April 1999).

32. S. Majumdar, O. K. Chopra, and W. J. Shack, *Interim Fatigue Design Curves for Carbon, Low-Alloy, and Austenitic Stainless Steels in LWR Environments*, NUREG/CR-5999, ANL-93/3 (April 1993).

33. J. Keisler, O. K. Chopra, and W. J. Shack, *Fatigue Strain-Life Behavior of Carbon and Low-Alloy Steels, Austenitic Stainless Steels, and Alloy 600 in LWR Environments*, NUREG/CR-6335, ANL-95/15 (Aug. 1995).

34. J. Keisler, O. K. Chopra, and W. J. Shack, *Statistical Models for Estimating Fatigue Strain-Life Behavior of Pressure Boundary Materials in Light Water Reactor Environments*, Nucl. Eng. Des. **167**, 129-154 (1996).

35. H. S. Mehta and S. R. Gosselin, *An Environmental Factor Approach to Account for Reactor Water Effects in Light Water Reactor Pressure Vessel and Piping Fatigue Evaluations*, in Fatigue and Fracture Volume 1, PVP Vol. 323, H. S. Mehta, ed., American Society of Mechanical Engineers, New York, pp. 171-185 (1996).

36. K. J. Miller, *Damage in Fatigue: A New Outlook*, in International Pressure Vessels and Piping Codes and Standards: Volume 1 - Current Applications, PVP Vol. 313-1, K. R. Rao and Y. Asada, eds., American Society of Mechanical Engineers, New York, pp. 191-192 (1995).

37. K. J. Miller, *Initiation and Growth Rates of Short Fatigue Cracks*, in Fundamentals of Deformation and Fracture, Eshelby Memorial Symposium, Cambridge University Press, Cambridge, pp. 477-500 (1985).

38. K. Tokaji, T. Ogawa, and S. Osaka, *The Growth of Microstructurally Small Fatigue Cracks in a Ferrite-Pearlite Steel*, in Fatigue Fracture Eng. Mater. Struct. **11**, 311-342 (1988).

39. D. J. Gavenda, P. R. Luebbers, and O. K. Chopra, *Crack Initiation and Crack Growth Behavior of Carbon and Low-Alloy Steels*, in Fatigue and Fracture 1, Vol. 350, S. Rahman, K. K. Yoon, S. Bhandari, R. Warke, and J. M. Bloom, eds., American Society of Mechanical Engineers, New York, pp. 243-255 (1997).

40. K. Obrtlik, J. Polák, M. Hájek, and A. Vasek, *Short Fatigue Crack Behaviour in 316L Stainless Steel*, Int. J. Fatigue **19**, 471-475 (1997).

41. S. G. Sundara Raman, D. Argence, and A. Pineau, *High Temperature Short Fatigue Crack Behaviour in a Stainless Steel*, Fatigue Fracture Eng. Mater. Struct. **20**, 1015-1031 (1997).

42. F. P. Ford, *Overview of Collaborative Research into the Mechanisms of Environmentally Controlled Cracking in the Low Alloy Pressure Vessel Steel/Water System*, in Proc. 2nd Int. Atomic Energy Agency Specialists' Meeting on Subcritical Crack Growth, NUREG/CP-0067, MEA-2090, Vol. 2, pp. 3-71 (1986).

43. H. Hänninen, K. Törrönen, and W. H. Cullen, *Comparison of Proposed Cyclic Crack Growth Mechanisms of Low Alloy Steels in LWR Environments*, in Proc. 2nd Int. Atomic Energy Agency Specialists' Meeting on Subcritical Crack Growth, NUREG/CP-0067, MEA-2090, Vol. 2, pp. 73-97 (1986).

44. M. E. Mayfield, E. C. Rodabaugh, and R. J. Eiber, *A Comparison of Fatigue Test Data on Piping with the ASME Code Fatigue Evaluation Procedure*, ASME paper 79-PVP-92, American Society of Mechanical Engineers, New York (1979).

45. A. F. Deardorff and J. K. Smith, *Evaluation of Conservatisms and Environmental Effects in ASME Code, Section III, Class 1 Fatigue Analysis*, SAND94-0187, prepared by Structural Integrity Associates, San Jose, CA, under contract to Sandia National Laboratories, Albuquerque, NM (1994).

46. W. A. Van Der Sluys, and S. Yukawa, *Status of PVRC Evaluation of LWR Coolant Environmental Effects on the S-N Fatigue Properties of Pressure Boundary Materials*, in Fatigue and Crack Growth: Environmental Effects, Modeling Studies, and Design Considerations, PVP Vol. 306, S. Yukawa, ed., American Society of Mechanical Engineers, New York, pp. 47-58 (1995).

47. N. E. Dowling, *Crack Growth During Low-Cycle Fatigue of Smooth Axial Specimens*, in Cyclic Stress-Strain and Plastic Deformation Aspects of Fatigue Crack Growth, ASTM STP 637, American Society for Testing and Materials, Philadelphia, PA, pp. 97-121 (1977).

48. C. M. Suh, R. Yuuki, and H. Kitagawa, *Fatigue Microcracks in a Low Carbon Steel*, Fatigue Fracture Eng. Mater. Struct. **8**, 193-203 (1985).

49. T. P. O'Donnell and W. J. O'Donnell, *Stress Intensity Values in Conventional S-N Fatigue Specimens*, in Fatigue and Crack Growth: International Pressure Vessels and Piping Codes and Standards: Volume 1 - Current Applications, PVP Vol. 313-1, K. R. Rao and Y. Asada, eds., American Society of Mechanical Engineers, New York, pp. 195-197 (1995).

50. W. J. Shack and T. F. Kassner, *Review of Environmental Effects on Fatigue Crack Growth of Austenitic Stainless Steels*, NUREG/CR-6176, ANL-94/1 (1994).

51. J. D. Gilman, R. Rungta, P. Hinds, and H. Mindlan, *Corrosion-Fatigue Crack Growth Rates in Austenitic Stainless Steels in Light Water Reactor Environments*, Int. J. Pressure Vessel Piping **31**, 55-68 (1988).

52. M. E. Indig, J. L. Nelson, and G. P. Wozadlo, *Investigation of the Protection Potential Against IASCC*, in Proc. 5th Intl. Symp. on Environmental Degradation of Materials in Nuclear Power Systems - Water Reactors, D. Cubicciotti, E. P. Simonen, and R. Gold, eds., American Nuclear Society, La Grange Park, IL, pp. 941-947 (1992).

53. M. Kodama, S. Nishimura, J. Morisawa, S. Shima, S. Suzuki, and M. Yamamoto, *Effects of Fluence and Dissolved Oxygen on IASCC in Austenitic Stainless Steels*, in Proc. 5th Intl. Symp. on Environmental Degradation of Materials in Nuclear Power Systems – Water Reactors, D. Cubicciotti, E. P. Simonen, and R. Gold, eds., American Nuclear Society, La Grange Park, IL, pp. 948-954 (1992).

54. H. M. Chung, W. E. Ruther, J. E. Sanecki, A. G. Hins, and T. F. Kassner, *Effect of Water Chemistry on Intergranular Cracking of Irradiated Austenitic Stainless Steels*, in Proc. 7th Intl. Symp. on Environmental Degradation of Materials in Nuclear Power Systems - Water Reactors, NACE International, Houston, pp. 1133-1143 (1995),

55. F. Garzarolli, P. Dewes, R. Hahn, and J. L. Nelson, *Deformability of High-Purity Stainless Steels and Ni-Based Alloys in the Core of a PWR*, in Proc. 6th Intl. Symp. on Environmental Degradation of Materials in Nuclear Power Systems - Water Reactors, R. E. Gold and E. P. Simonen, eds., The Minerals, Metals, and Materials Society, Warrendale, PA, pp. 607-613 (1993).

56. I. Suzuki, M. Koyama, H. Kanasaki, H. Mimaki, M. Akiyama, T. Okubo, Y. Mishima, and T. R. Mager, *Stress Corrosion Cracking of Irradiated Stainless Steels in Simulated PWR Primary Water*, in Proc. ASME–JSME 4th Intl. Conf. on Nuclear Engineering, March 10–14, 1996, New Orleans, American Society of Mechanical Engineers, Vol. 5, pp. 205–213 (1996).

57. A. J. Jacobs, G. P. Wozadlo, K. Nakata, T. Yoshida, and I. Masaoka, *Radiation Effects on the Stress Corrosion and Other Selected Properties of Type-304 and Type-316 Stainless Steels*, in Proc. 3rd Int. Symp. Environmental Degradation of Materials in Nuclear Power Systems – Water Reactors, G. J. Theus and J. R. Weeks, eds., The Metallurgical Society, Warrendale, PA, p. 673 (1988).

58. K. Fukuya, K. Nakata, and A. Horie, *An IASCC Study Using High Energy Ion Irradiation*, in Proc. 5th Intl. Symp. on Environmental Degradation of Materials in Nuclear Power Systems – Water Reactors, D. Cubicciotti, E. P. Simonen, and R. Gold, eds., American Nuclear Society, La Grange Park, IL, pp. 814–820 (1992).

59. H. M. Chung, W. E. Ruther, J. E. Sanecki, A. G. Hins, and T. F. Kassner, *Stress Corrosion Cracking Susceptibility of Irradiated Type 304 Stainless Steels*, in Effects of Radiation on Materials: 16th Int. Symp., ASTM STP 1175, A. S. Kumar, D. S. Gelles, R. K. Nanstad, and T. A. Little, eds., American Society for Testing and Materials, Philadelphia, pp. 851-869 (1993).

60. H. M. Chung, W. E. Ruther, J. E. Sanecki, and T. F. Kassner, *Grain Boundary Microchemistry and Intergranular Cracking of Irradiated Austenitic Stainless Steels*, in Proc. 6th Intl. Symp. on Environmental Degradation of Materials in Nuclear Power Systems - Water Reactors, R. E. Gold and E. P. Simonen, eds., The Minerals, Metals, and Materials Society, Warrendale, PA, pp. 511-519 (1993).

61. J. M. Cookson, D. L. Damcott, G. S. Was, and P. L. Anderson, *The Role of Microchemical and Microstructural Effects in the IASCC of High Purity Austenitic Stainless Steels*, in Proc. 6th Intl. Symp. on Environmental Degradation of Materials in Nuclear Power Systems - Water Reactors, R. E. Gold and E. P. Simonen, eds., The Minerals, Metals, and Materials Society, Warrendale, PA, pp. 573-580 (1993).

62. M. Kodama, J. Morisawa, S. Nishimura, K. Asano, S. Shima, and K. Nakata, *Stress Corrosion Cracking and Intergranular Corrosion of Austenitic Stainless Steels Irradiated at 323K*, J. Nucl. Mater. **212–215**, 1509 (1994).

63. T. Tsukada, Y. Miwa, and H. Nakajima, *Stress Corrosion Cracking of Neutron Irradiated Type 304 Stainless Steels*, in Proc. 7th Intl. Symp. on Environmental Degradation of Materials in Nuclear Power Systems - Water Reactors, NACE International, Houston, pp. 1009–1018 (1995).

64. F. Garzarolli, P. Dewes, R. Hahn, and J. L. Nelson, *In-Reactor Testing of IASCC Resistant Stainless Steels*, in Proc. 7th Intl. Symp. on Environmental Degradation of Materials in Nuclear Power Systems - Water Reactors, NACE International, Houston, pp.1055–1065 (1995).

65. H. M. Chung, W. E. Ruther, J. E. Sanecki, A. G. Hins, N. J. Zaluzec, and T. F. Kassner, *Irradiation–Assisted Stress Corrosion Cracking of Austenitic Stainless Steels: Recent Progress and New Approaches*, J. Nucl. Mater. **239**, 61 (1996).

66. J. M. Cookson, G. S. Was, and P. L. Anderson, *Oxide-Induced Initiation of Stress Corrosion Cracking in Irradiated Stainless Steel*, Corrosion **54**, 299 (1998).

67. S. Kasahara, K. Nakata, K. Fukuya, S. Shima, A. J. Jacobs, G. P. Wozadlo, and S. Suzuki, *Effects of Minor Elements on IASCC Susceptibility in Austenitic Stainless Steels Irradiated with Neutrons*, in Proc. 6th Intl. Symp. on Environmental Degradation of Materials in Nuclear Power Systems - Water Reactors, R. E. Gold and E. P. Simonen, eds., The Minerals, Metals, and Materials Society, Warrendale, PA, pp. 615-623 (1993).

68. A. J. Jacobs, G. P. Wozadlo, K. Nakata, S. Kasahara, T. Okada, S. Kawano, and S. Suzuki, *The Correlation of Grain Boundary Composition in Irradiated Stainless Steel with IASCC Resistance*, in Proc. 6th Intl. Symp. on Environmental Degradation of Materials in Nuclear Power Systems - Water Reactors, R. E. Gold and E. P. Simonen, eds., The Minerals, Metals, and Materials Society, Warrendale, PA, pp. 597-606 (1993).

69. A. Jenssen and L. G. Ljungberg, *Irradiation Assisted Stress Corrosion Cracking Postirradiation CERT Tests of Stainless Steels in a BWR Loop*, in Proc. 7th Intl. Symp. on Environmental Degradation of Materials in Nuclear Power Systems - Water Reactors, NACE International, Houston, pp. 1043–1052 (1995).

70. Y. Miwa, T. Tsukada, S. Jitsukawa, S. Kita, S. Hamada, Y. Matsui, and M. Shindo, *Effect of Minor Elements on Irradiation Assisted Stress Corrosion Cracking of Model Stainless Steels*, J. Nucl. Mater. **233-237**, 1393 (1996).

71. T. Tsukada, Y. Miwa, and H. Nakajima, *Effects of Minor Elements on IASCC of Type 316 Model Stainless Steels*, in Proc. 8th Intl. Symp. on Environmental Degradation of Materials in Nuclear Power Systems - Water Reactors, S. M. Bruemmer, ed., American Nuclear Society, La Grange Park, pp. 795-802 (1997).

72. H. M. Chung, J.-H. Park, W. E. Ruther, J. E. Sanecki, R. V. Strain, and N. J. Zaluzec, *Fabrication-Related Impurity Contamination and Stress Corrosion Cracking of Austenitic Stainless Steel Core-Internal Components*, in Proc. 8th Intl. Symp. on Environmental Degradation of Materials in Nuclear Power Systems - Water Reactors, S. M. Bruemmer, ed., American Nuclear Society, La Grange Park, pp. 846-856 (1997).

73. G. Taguchi, *Quality Engineering Using Robust Design*, M. S. Phadke, Ed., Prentice Hall, Engelwood Cliffs, NJ (1989).

74. H. M. Chung, W. E. Ruther, R. V. Strain, and T. M. Karlsen, *Slow Strain Rate Tensile Testing of Model Austenitic Stainless Steels Irradiated in the Halden Reactor*, in Environmentally Assisted Cracking in Light Water Reactors, Semiannual Report, January-June 1998, NUREG/CR-4667, Vol. 26, ANL-98/30, pp. 10-21 (March 1999).

75. S. M. Bruemmer et al., *Critical Issue Reviews for the Understanding and Evaluation of Irradiation-Assisted Stress Corrosion Cracking*, EPRI TR-107159, Electric Power Research Institute, Palo Alto, CA (1996).

76. M. L. Herrera, et al., *Evaluation of the Effects of Irradiation on the Fracture Toughness of BWR Internal Components*, in Proc. ASME/JSME 4th Intl. Conf. on Nucl. Eng. (ICONE-4) Vol. 5, A. S. Rao, R. M. Duffey, and D. Elias, Eds., American Society of Mechanical Engineers, New York, pp. 245–251 (1996)

77. W. J. Mills, *Fracture Toughness of Type 304 and 316 Stainless Steels and their Welds*, Intl. Mater. Rev. **42**, 45–82 (1997).

78. P. J. Maziasz and C. J. McHargue, *Microstructural Evolution in Annealed Austenitic Steels during Neutron Irradiation*, Int. Met. Rev. **32**, 190 (1987).

79. P. J. Maziasz, *Overview of Microstructural Evolution in Neutron-Irradiated Austenitic Stainless Steels*, J. Nucl. Mater. **205**, 118–145 (1993).

80. F. A. Garner, *Evolution of Microstructures in Face-Centered Cubic Metals during Neutron Irradiation*, J. Nucl. Mater. **205**, 98–111 (1993).

81. J. Dufresne, B. Henry, and H. Larsson, *Fracture Toughness of Irradiated AISI 304 and 316L Stainless Steels*, in Effects of Radiation on Structural Materials, ASTM STP 683, J. A. Sprague and D. Kramer, Eds., American Society for Testing and Materials, Philadelphia, pp. 511–528 (1979).

82. C. Picker, A. L. Stott, and H. Cocks, H., *Effects of Low-Dose Fast Neutron Irradiation on the Fracture Toughness of Type 316 Stainless Steel and Weld Metal*, in Proc. Specialists Meeting on Mechanical Properties of Fast Reactor Structural Materials, Chester, UK, Paper IWGFR 49/440–4 (1983).

83. F. H. Huang, *The Fracture Characterization of Highly Irradiated Type 316 Stainless Steel*, Int. J. Fracture **25**, 181–193 (1984).

84. J. Bernard and G. Verzeletti, *Elasto-Plastic Fracture Mechanics Characterization of Type 316H Irradiated Stainless Steel up to 1 dpa*, IN Effects of Radiation on Materials: Twelfth Intl. Symp., ASTM STP 870, F. A. Garner and J. S. Perrin, Eds., American Society for Testing and Materials, Philadelphia, pp. 619–641 (1985).

85. W. J. Mills, *Irradiation Effects on the Fracture Toughness of Austenitic Fe–Cr–Ni Alloys*, HEDL–TME–82–17, Hanford Engineering Development Laboratory (1985).

86. W. J. Mills, *Fracture Toughness of Irradiated Stainless Steel Alloys*, Nucl. Technol. **82**, 290–303 (1988).

87. D. J. Michel and R. A. Gray, 1987, *Effects of Irradiation on the Fracture Toughness of FBR Structural Materials*, J. Nucl. Mater. **148**, 194–203 (1987).

88. P. Ould, P. Balladon, and Y. Meyzaud, *Bull. Cercle Etud. Metaux* **15**, 31.1–31.12 (1988).

89. E. V. Van Osch, M. G. Horsten, and M. I. De Vries, *Fracture Toughness PWR Internals*, ECN Contribution to CEC Contract on PWR Internals–Part 2 (ETNU/CT/94/0136–F), ECN–I–97–010 (71747/NUC/EvO/mh/006274), Netherland Energy Research Foundation ECN, Petten, the Netherlands (1997).

90. T. H. Hughes and E. E. Gruber, *Development of Hot–Cell J–R Test Facility*, in Environmentally Assisted Cracking in Light Water Reactors Semiannual Report July 1996–December 1996, NUREG/CR–4667, Vol. 23, ANL–97/10, pp. 42–52 (1997).

91. E. E. Gruber and O. K. Chopra, *Fracture Toughness J–R Test of Austenitic Stainless Steels Irradiated in Halden Reactor*, in Environmentally Assisted Cracking in Light Water Reactors Semiannual Report January 1997–June 1997, NUREG/CR–4667, Vol. 24, ANL–98/6, pp. 54–65 (1998).

92. A. L. Hiser, *Fracture Toughness Chracterization of Nuclear Piping Steels*, NUREG/CR–5118, MEA–2325, Materials Engineering Associates, Inc., Lanham, MD (1989).

93. G. M. Wilkowski, et al, *Degraded Piping Program – Phase II, Semiannual Report*, NUREG/CR–4082, Vol. 2, (1985).

94. M. G. Vassilaros, R. A. Hays, and J. P. Gudas, *Investigation of the Ductile Fracture Properties of Type 304 Stainless Steel Plate, Welds, and 4–Inch Pipe*, in Proc. 12th Water Reactor Safety Information Meeting, NUREG/CP–0058, Vol. 4, U.S. Nuclear Regulatory Commission, pp. 176–189 (1985).

95. W. E. Ruther, W. K. Soppet, and T. F. Kassner, *Environmentally Assisted Cracking of Alloys 600 and 690 in Simulated LWR Water*, in Environmentally Assisted Cracking in Light Water Reactors, Semiannual Report, July 1997–December 1997, NUREG/CR–4667 Vol. 25, ANL–98/18, pp. 42–75 (Sept. 1998).

96. W. E. Ruther, W. K. Soppet, T. F. Kassner, and W. J. Shack, *Environmentally Assisted Cracking of Alloys 600 and 690 in Simulated LWR Water*, in Environmentally Assisted Cracking in Light Water Reactors, Semiannual Report, January 1998–June 1998, NUREG/CR–4667 Vol. 26, ANL–98/18, pp. 25–32 (March 1999).

97. F. P. Ford, *Quantitative Prediction of Environmentally Assisted Cracking*, Corrosion, **52**, 375–395 (1997).

98. F. P. Ford, D. F. Taylor, P. L. Andresen, and R. Ballinger, *Corrosion–Assisted Cracking of Stainless and Low–alloy Steels*, EPRI NP–5064s, Electric Power Research Institute, Palo Alto, CA (Feb. 1987).

99. T. Shoji, *Quantitative Prediction of Environmentally Assisted Cracking Based on Crack Tip Strain Rate*, in Proc. Conf. on Predictive Capabilities in Environmentally–Assisted Cracking, R. Rungta, ed., PVP Vol. 99, American Society of Mechanical Engineers, New York, pp. 127–142 (1985).

100. W. J. Shack and T. F. Kassner, *Review of Environmental Effects on Fatigue Crack Growth of Austenitic Stainless Steels*, NUREG/CR–6176, ANL–94/1 (May 1994).

101. J. D. Gilman, R. Rungta, P. Hinds, and H. Mindlin, *Corrosion–fatigue Crack–growth Rates in Austenitic Stainless Steels in Light Water Reactor Environments*, Int. J. Pressures Vessels and Piping, **31**, 55–68 (1988).

102. E. D. Eason, E. E. Nelson, and J. D. Gilman, *Technical Basis for a Revised Fatigue Crack Growth Rate Reference Curve for Ferritic Steels in Light Water Reactor Environments*, in Welding Research Council Bulletin 404, Report No. 3, pp 38–51 (1995).

103. L. A. James and D. P. Jones, *Fatigue Crack Growth Correlation for Austenitic Stainless Steels in Air*, in Proc. Conf. on Predictive Capabilities in Environmentally–Assisted Cracking, R. Rungta, ed., PVP Vol. 99, American Society of Mechanical Engineers, New York, pp. 363–414 (1985).

104. W. E. Ruther, W. K. Soppet, and T. F. Kassner, *Effect of Temperature and Ionic Impurities at Very Low Concentrations on Stress Corrosion Cracking of AISI 304 Stainless Steel*, Corrosion **44**, 791-799 (1988).

105. W. E. Ruther, W. K. Soppet, and T. F. Kassner, *Influence of Environment and Temperature on Crack Growth of Type 304 SS under Cyclic Loading in Simulated BWR–Quality Water*, in Environmentally Assisted Cracking in Light Water Reactors, Annual Report, October 1983–September 1984, NUREG/CR–4287 ANL–85–33, pp. 110–114 (1985).

NRC FORM 335 (2–89) NRCM 1102, 3201, 3202

U. S. NUCLEAR REGULATORY COMMISSION

BIBLIOGRAPHIC DATA SHEET

(See instructions on the reverse)

1. REPORT NUMBER *(Assigned by NRC. Add Vol., Supp., Rev., and Addendum Numbers, if any.)*
NUREG/CR–4667, Vol. 27
ANL–99/11

2. TITLE AND SUBTITLE
Environmentally Assisted Cracking in Light Water Reactors.
Semiannual Report July 1998—December 1998

3. DATE REPORT PUBLISHED
MONTH: October
YEAR: 1999

4. FIN OR GRANT NUMBER
W6610

5. AUTHOR(S)
O. K. Chopra, H. M. Chung, E. E. Gruber,
T. F. Kassner, W. E. Ruther, W. J. Shack,
J. L. Smith, W. K. Soppet, and R. V. Strain

6. TYPE OF REPORT
Technical; Semiannual

7. PERIOD COVERED *(Inclusive Dates)*
July 1998–December 1998

8. PERFORMING ORGANIZATION – NAME AND ADDRESS *(If NRC, provide Division, Office or Region, U.S. Nuclear Regulatory Commission, and mailing address; if contractor, provide name and mailing address.)*

Argonne National Laboratory
9700 South Cass Avenue
Argonne, IL 60439

9. SPONSORING ORGANIZATION – NAME AND ADDRESS *(If NRC, type "Same as above": if contractor, provide NRC Division, Office or Region, U.S. Nuclear Regulatory Commission, and mailing address.)*

Division of Engineering Technology
Office of Nuclear Regulatory Research
U.S. Nuclear Regulatory Commission
Washington, DC 20555–0001

10. SUPPLEMENTARY NOTES
M. B. McNeil, NRC Project Manager

11. ABSTRACT (200 words or less)

This report summarizes work performed by Argonne National Laboratory on fatigue and environmentally assisted cracking (EAC) in light water reactors from July 1998 to December 1998. Topics that have been investigated include (a) environmental effects on fatigue S–N behavior of primary pressure boundary materials, (b) irradiation–assisted stress corrosion cracking of austenitic stainless steels (SSs), and (c) EAC of Alloys 600 and 690. Fatigue tests have been conducted to determine the crack initiation and crack growth characteristics of austenitic SSs in LWR environments. Procedures are presented for incorporating the effects of reactor coolant environments on the fatigue life of pressure vessel and piping steels. Slow-strain-rate tensile tests and posttest fractographic analyses were conducted on several model SS alloys that were irradiated to ≈0.3 and 0.9 x 10^{21} n·cm^{-2} (E > 1 MeV) in helium at 289°C in the Halden reactor. The results have been used to determine the influence of alloying and impurity elements on the susceptibility of these steels to irradiation assisted stress corrosion cracking. Fracture toughness J–R curve tests were also conducted on two heats of Type 304 SS that were irradiated to ≈0.3 x 10^{21} n·cm^{-2} in the Halden reactor. Crack–growth–rate tests have been conducted on compact–tension specimens of Alloys 600 and 690 under constant load to evaluate the resistance of these alloys to stress corrosion cracking in LWR environments.

12. KEY WORDS/DESCRIPTORS *(List words or phrases that will assist researchers in locating this report.)*
Corrosion Fatigue
Crack Growth
Irradiation–Assisted Stress Corrosion Cracking
Radiation–Induced Segregation
Stress Corrosion Cracking
Types 304, 304L, 316, and 316NG Stainless Steel
Alloys 600 and 690

13. AVAILABILITY STATEMENT
Unlimited

14. SECURITY CLASSIFICATION
(This Page)
Unclassified
(This Report)
Unclassified

15. NUMBER OF PAGES

16. PRICE

NRC FORM 335 (2–89)

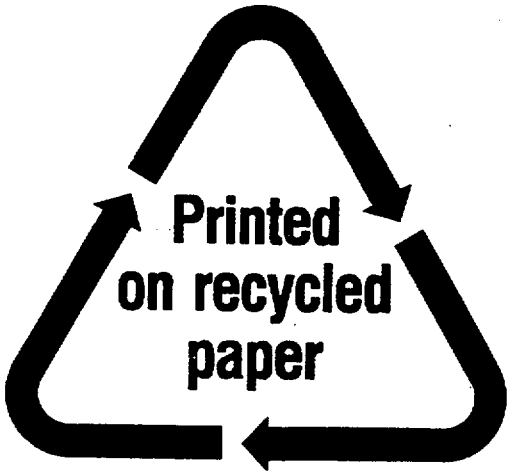

Federal Recycling Program